

The Pennsylvania State University

The Graduate School

**THE CONTRIBUTION OF DYNAMIC NEUROINFLAMMATORY  
STATES IN ALZHEIMER'S DISEASE**

A Dissertation in

Biomedical Engineering

by

Madison Kathryn Kuhn

© 2023 Madison Kathryn Kuhn

Submitted in Partial Fulfillment  
of the Requirements  
for the Degree of

Doctor of Philosophy

December 2023

The dissertation of Madison Kathryn Kuhn was reviewed and approved by the following:

Elizabeth A. Proctor

Assistant Professor of Neurosurgery and Pharmacology  
Dissertation Advisor and Chair of Committee

James R. Connor

Distinguished Professor of Neuroscience and Anatomy  
Vice Chair for Research, Department of Neurosurgery

Irina Elcheva

Assistant Professor of Pediatrics Division Hematology and Oncology

Bruce J. Gluckman

Director of the Center for Neural Engineering  
Professor of Engineering Science and Mechanics, of Neurosurgery, and of Biomedical Engineering

Xiaojun Lian

Associate Professor of Biomedical Engineering

Justin R. Pritchard

Associate Professor of Biomedical Engineering

Yuguo Lei

Associate Professor of Biomedical Engineering  
Graduate Program Coordinator

## ABSTRACT

It is well appreciated that neuroinflammation is a driver of Alzheimer's disease (AD) pathology, but its complex contribution has been difficult to untangle. Immune activation, particularly by microglia, is needed to restore brain homeostasis, but under chronic immune insult, immune signaling becomes dysregulated in a variety of ways. The diverse collection of cellular immune activation states that underly the overall neuroinflammatory milieu of the brain uniquely contributes to pathology spread and the vulnerability of neurons. Contradictory activation states, such as an under-reactive response with loss of beneficial function and a detrimental, overreactive one, complicate efforts to restore beneficial function, both in the identification of therapeutic targets and treatment timelines. This dissertation was designed to dissect the contribution of the brain's dynamic neuroinflammatory state from different levels of view. I first used an AD mouse model for tissue-level characterization of dysregulated immune cues to identify how diverse immune states collectively present in progressing disease and converge to affect neuron health. I identified a disease-predictive cytokine signature that, when applied to healthy neurons in the absence of pathology, reduced neuronal mitochondrial respiration, supporting the existence of pathology-independent neuroinflammatory effects on neuronal vulnerability. I then applied an AD cerebral organoid model to dissect microglia-specific function related to the immune milieu and its corresponding changes in pathology. AD organoids derived from human iPSCs carrying the N141I PSEN2 mutation from a male or female individual exhibit drastically different cytokine signatures and a different evolution of those signatures with age. The male organoids demonstrated an overall reduction in cytokine secretion after an initial amplified immune response, while female organoids showed a persistent heightened immune response. There was reduced synapse density in the male organoids, whereas larger deposition of amyloid and tissue atrophy occurred in the female organoids. Crucially, these differential effects of dysregulated immune signaling occurred without the accumulation of pathological proteins and may represent early events in disease. Cumulatively, these studies achieved a quantitative characterization of the overall

immune milieu, made up of a diverse of collection of activation patterns and immune responses, that is sufficient to negatively impact neuronal health and identified cell-specific contribution of microglia.

## TABLE OF CONTENTS

<b>LIST OF FIGURES</b> .....	<b>vii</b>
<b>LIST OF TABLES</b> .....	<b>viii</b>
<b>ACKNOWLEDGEMENTS</b> .....	<b>ix</b>
<b>Chapter 1 Microglial Drivers of Alzheimer’s Disease Pathology: An Evolution of Diverse Participating States</b> .....	<b>1</b>
Abstract .....	1
Introduction .....	2
<i>Acknowledging the complexities of studying microglia in AD mouse models</i> .....	4
<i>Microglial signaling cascades interacting with pathological proteins</i> .....	6
<i>Both overactive and under-responsive microglia ineffectively respond to and clear proteinopathy</i> .....	9
<i>Unable to compensate, dysfunctional microglia worsen hallmark pathology</i> .....	14
<i>Depletion of microglia inconsistently ameliorates AD proteinopathies</i> .....	17
<i>Human cellular disease models are needed to recapitulate microglial states</i> .....	19
Conclusion .....	23
<b>Introduction to Chapter 2 From Cell-Specific to Tissue-Level Importance of Inflammatory States</b> .....	<b>25</b>
<b>Chapter 2 Amyloid-<math>\beta</math> Pathology-Specific Cytokine Secretion Suppresses Neuronal Mitochondrial Metabolism</b> .....	<b>27</b>
Abstract .....	27
Introduction .....	28
Methods.....	31
<i>Mice</i> .....	31
<i>Tissue collection and preparation</i> .....	31
<i>Quantification of total protein</i> .....	32
<i>Luminex multiplex assays</i> .....	32
<i>Cytokine profile data cleaning</i> .....	33
<i>Partial least squares modeling</i> .....	33
<i>Primary cell culture</i> .....	35
<i>Cytokine stimulation of primary culture</i> .....	36
<i>RNA isolation and NanoString nCounter analysis</i> .....	37
<i>Construction of protein-protein interaction networks</i> .....	38
<i>Seahorse Mito Stress Test</i> .....	38
Results .....	40
<i>The cytokine signature of progressive A<math>\beta</math> pathology is distinct from that of healthy aging</i> .....	40
<i>AD mice exhibit neuroimmune over-activation late in the disease timeline</i> ....	45
<i>Cytokine signature of progressive A<math>\beta</math> pathology induced widespread changes in neuron metabolic gene expression</i> .....	48
<i>A<math>\beta</math> pathology-specific cytokine signature impairs neuronal metabolism</i> .....	52
Discussion .....	54

Conclusion .....	57
<b>Introduction to Chapter 3 From Brain to Dish.....</b>	<b>59</b>
<b>Chapter 3 Alzheimer’s Disease Cerebral Organoids Exhibit Dynamic Neuroinflammatory Profiles .....</b>	<b>62</b>
Abstract .....	62
Introduction .....	63
Methods.....	65
<i>iPSC culture .....</i>	<i>65</i>
<i>Organoid differentiation and maintenance.....</i>	<i>66</i>
<i>PLX5622 treatment of organoids .....</i>	<i>67</i>
<i>Organoid preparation for immunostaining.....</i>	<i>68</i>
<i>Organoid imaging .....</i>	<i>69</i>
<i>Organoid lysate preparation.....</i>	<i>70</i>
<i>Luminex multiplex assays.....</i>	<i>71</i>
<i>Cytokine profile data cleaning.....</i>	<i>71</i>
<i>Partial least squares modeling.....</i>	<i>72</i>
<i>Statistical Analyses.....</i>	<i>73</i>
Results.....	74
<i>N141I and isogenic control iPSC-derived cerebral organoids innately develop microglia .....</i>	<i>74</i>
<i>Cytokine secretion is initially increased in AD organoids prior to an overall down-regulated cytokine profile compared to isogenic controls. ....</i>	<i>77</i>
<i>Down-regulation of cytokine secretion in AD 4-month-old organoids coincides with decreased synapse density.....</i>	<i>79</i>
<i>A<math>\beta</math> and pTau levels largely remain constant over time, but A<math>\beta</math> accumulates in larger deposits in AD organoids .....</i>	<i>81</i>
<i>A<math>\beta</math> levels are unchanged following microglia reduction in AD organoids, while pTau is affected from 2 to 3-months but not 2-4 or 3-4 months.....</i>	<i>83</i>
<i>Aging female AD H141I organoids exhibit continued up-regulation of select cytokines, in stark contrast to the overall diminished cytokine secretion of male H141I organoids.....</i>	<i>86</i>
<i>Aging female N141I organoids exhibit a modest increase in pTau levels, but not A<math>\beta</math>, although robust amyloid deposition and tissue atrophy is observed at 3-months .....</i>	<i>88</i>
Discussion .....	90
Conclusion .....	95
<b>Chapter 4 Summary of Research, Implications, And Future Research Directions .....</b>	<b>97</b>
Summary of Research .....	97
Implications.....	98
Future Research Directions.....	99
Conclusions.....	100
<b>REFERENCES .....</b>	<b>102</b>
<b>APPENDIX.....</b>	<b>138</b>

## LIST OF FIGURES

Figure 1-1: The combined actions of an evolving population of diverse microglial activation states contribute to Alzheimer’s disease progression.....	13
Figure 2-1: Unique cytokine signatures predict aging in 5xFAD and wild-type hippocampi.....	44
Figure 2-2: Cytokines are up-regulated in aged 5xFAD hippocampus but dampened in comparison to wild-type prior to protein deposition.....	47
Figure 2-3: Cytokine signature of AD progression generates widespread gene expression changes in healthy neurons. ....	51
Figure 2-4: Wild-type primary hippocampal neurons treated with cytokine signature of AD progression exhibit decreased mitochondrial respiration.....	53
Supplementary Figure 2-1: Heat-map of Z-scored hippocampal cytokine concentrations.....	58
Figure 3-1: Microglia and astrocytes develop in AD and isogenic organoids.....	76
Figure 3-2: Cytokine signature predictive of genotype in male N141I organoids reverses over experimental timeline. ....	78
Figure 3-3: Synapse density decreases over time in AD organoids along with slight increase in microglia population .....	80
Figure 3-4: A $\beta$ and pTau levels are the same between AD and isogenic organoids, despite more concentrated A $\beta$ deposition in AD organoids.....	82
Figure 3-5: Microglia depletion prevents synapse loss, and early but not later affects tau pathology in AD organoids.....	85
Figure 3-6: Cytokine secretion decreases in organoids derived from the male N141I iPSC line over time and increases in those of the female <sup>N141I</sup> iPSC line.....	87
Figure 3-7: AD organoids from a female N141I iPSC line demonstrate proteinopathy around tissue atrophy.....	89
Supplementary Figure 3-1: Female PSEN2 N141I organoids exhibit robust tissue atrophy after 5-months in culture.....	96

**LIST OF TABLES**

Table 2-1: Calculations of Seahorse Mito Stress Test Assay Measurements.....	40
<i>Supplementary Table 2-1: Significantly differentially expressed genes of cytokine-treated neurons compared to vehicle-treated neurons.....</i>	<i>138</i>
<i>Supplementary Table 2-2: Significantly differentially expressed genes of cytokine-treated astrocytes compared to vehicle-treated astrocytes.....</i>	<i>139</i>

## ACKNOWLEDGEMENTS

Earning a PhD is nothing short of a journey, and thankfully I have had an incredible support system to not only make it through but come out a more confident scientist with many memories and friendships to carry me into my next chapter. I would like to first thank the members of the Proctor lab, past and present, Lynne Beidler, Mandy Snyder, Rebecca Fleeman, Dennis Chan, Rhea Sullivan, Nathan Morris, Rachel Kang, and Chaemin Kim for being my day-to day support and always encouraging me through challenging experiments and lending a helping hand. Becca, especially, was there through most of the journey. We navigated being the first students in a lab, starting everything from the ground up, and we always leaned on each other for support. Lynne was there with me in the very beginning when we spent our early days unboxing lab supplies and growing the mouse colony. She continues to be an always appreciated ear through my successes and hardships and will always be the first person I call with anything hockey related. Mandy is my lab rock. She is a master of all things experiments and takes the time to help me work through any challenge. But I will always appreciate the check-ins and silly photos even more. I would like to thank my classmate and friend, Brianna, who is always willing to talk me through experiments and help me troubleshoot the most frustrating failures. Our laughter and (often sleep-deprived) silliness and constant stream of memes helped me get through the longest of lab days. I am so thankful to my lab family throughout my PhD work, and I can't wait to have them along with me for my next journey.

I would also like to thank my mentor, Dr. Elizabeth Proctor, for allowing me to establish stem cell culture in the lab and devise a project completely of my own design. She always supported me through its many reworkings and failures, and encouraged me to become a thoughtful, independent scientific thinker. Thank you for your unwavering support of all your students in and out of lab, encouraging us to have fun, practice self-care, and take the time we needed when life got to be too much.

Thank you to my committee, Dr. Justin Pritchard, Dr. Irina Elcheva, Dr. James Connor, Dr. Bruce Gluckman, and Dr. Lance Lian for being the multidisciplinary team I needed to integrate all the components

of a complex and completely new project. I wholly appreciate your support and guidance from the level of experimental design to my development as a scientist.

I would like to thank my family for their unconditional love and support through this journey. They were often subject to the aftermath of long days of stressful experiments but were always there for me. My parents have been my biggest academic supporters since day one, but this never came at the expense of my happiness, and I will always be able to count on their support through it all. Geena and Poppy will always be my loudest cheerleaders. Katie, who probably received the longest phone calls through it all, was always there when I needed support or distraction. Finally, I would like to thank my favorite four-legged friends, Felix, Kalli, Scout, and Bailey, who can get me through anything with a hug and a kiss on their little nose.

### **Funding**

This work was supported by a grant from the H.G. Barsumian, MD Memorial Fund, the National Institute on Aging grant R21AG068532, the NIH T32 training grant 5T32NS115667-02, the NIH grant R01AG072513, and start-up funds from Penn State College of Medicine Departments of Neurosurgery and Pharmacology.

### **Disclaimer**

Findings and conclusions do not necessarily reflect the view of the above funding agencies.

## Chapter 1

### **Microglial Drivers of Alzheimer's Disease Pathology: An Evolution of Diverse Participating States**

#### **Abstract**

Microglia, the resident immune-competent cells of the brain, become dysfunctional in Alzheimer's disease (AD), and their aberrant immune responses contribute to the accumulation of pathological proteins and neuronal injury. Genetic studies implicate microglia in the development of AD, prompting interest in developing immunomodulatory therapies to prevent or ameliorate disease. However, microglia take on diverse functional states in disease, playing both protective and detrimental roles in AD, which largely overlap and may shift over the disease course, complicating the identification of effective therapeutic targets. Widely-used mouse models pose added complexity in untangling microglial involvement. Models overexpressing familial Alzheimer's disease mutations exhibit incomplete pathophysiology, and mouse microglia are transcriptionally and functionally distinct from human microglia, especially in aging and neurodegeneration. Extensive evidence gathered using these models supports an active role of microglia in pathology progression, though results vary and can be contradictory between different types of models and the degree of pathology at the time of study. Here, we review microglial immune signaling and responses that contribute to the accumulation and spread of pathological proteins or directly affect neuronal health. We additionally explore the use of induced pluripotent stem cell (iPSC)-derived models to study living human microglia and how they have contributed to our knowledge of AD and may begin to fill in the gaps left by mouse models. Ultimately, mouse and iPSC-derived models have their own limitations, and a comprehensive understanding of microglial dysfunction in AD will likely only be established by an integrated view across models and an appreciation for their complementary viewpoints and limitations.

## Introduction

Alzheimer's disease (AD) is a progressive neurodegenerative disorder that was first histologically characterized by neuron and synapse loss, reactive gliosis, and misfolded aggregated proteins, including extracellular amyloid beta (A $\beta$ ) plaques and intracellular neurofibrillary tangles composed of primarily hyperphosphorylated tau.<sup>1</sup> AD is estimated to affect 6.5 million Americans aged 65-years and older and is projected to affect 12.7 million by 2050 as the aged population grows.<sup>2</sup> There are currently no proven methods to prevent, slow, or cure the disease, which in part is due to an incomplete understanding of the disease's complex etiology. Neuroinflammation, once thought to be a noncontributing consequence of AD pathology, is now recognized as an active driver of disease and may be capable of initiating neurodegeneration.<sup>3,4</sup> Evidence of early immune involvement prior to the development of clinical AD<sup>5,6</sup> and numerous immune-dependent mechanisms contributing to disease pathology and neuronal injury makes regulating neuroinflammation an attractive therapeutic target.<sup>7</sup> In mouse models of aging and neurodegeneration, modulating immune function can prolong life and improve cognition.<sup>8,9</sup> However, the shift between beneficial immune responses and detrimental neuroinflammation is difficult to distinguish, complicating the identification of successful immunomodulatory strategies.<sup>7,10</sup> Neuroinflammation is largely driven by microglia, the resident immune-competent cells of the brain.<sup>3</sup> In AD, microglia closely associate with amyloid plaques and neurofibrillary tangles,<sup>11,12</sup> and the majority of identified genetic risk factors are highly, and often exclusively, expressed by microglia, suggesting a role in disease development.<sup>4,13</sup>

In the presence of an insult, such as an extracellular misfolded protein, microglia become activated and undergo a variety of morphological and functional changes to initiate an immune response to restore brain homeostasis. The diverse responses of activated microglia depend on the identity and context of the insult and can evolve over time. Previously, microglia were thought to adopt either a pro-inflammatory M1

state or a neuroprotective, reparative M2 state, but new appreciation for the heterogeneity of microglial activation states has led this to be questioned and calls for better classification methods,<sup>14-16</sup> specifically characterizations informed by gene expression and proteomic studies but, importantly, reflect microglial function and their dynamic nature.<sup>17</sup> The diversity and dynamics of microglial responses complicate the search for specific therapeutic targets that would robustly reduce or prevent disease pathology without also disrupting beneficial activities or creating deleterious, overactive responses. Microglial function is neuroprotective by nature, acting to restore homeostasis. Dampened microglial responses, which are observed in age and after prolonged insult,<sup>16,18,19</sup> may be advantageous to restore in early disease to promote beneficial function, such as phagocytosis of A $\beta$ . However, in advanced disease, the persistent pro-inflammatory state may promote further pathology and neuronal injury.<sup>18,20</sup> Importantly, the single-cell transcriptome profiling of microglia in AD mice demonstrates substantial heterogeneity in microglial gene expression states with worsening neurodegeneration, including the division of unique reactive phenotypes in late-stage disease.<sup>21</sup>

Whether microglial activation-driven pathology is an initiator of human AD is unknown. However, A $\beta$  plaques and neurofibrillary tangles can exist in the brains of healthy individuals,<sup>18,22,23</sup> suggesting they are insufficient to cause cognitive loss and AD. In the case of familial AD cases, although the disease presents later in life, abnormal A $\beta$  production is present since birth. Clinical manifestation may be held at bay by a homeostatic system able to compensate for accumulating pathology until mid-life. Some have suggested neuroinflammation and microglial dysfunction, predisposed by aging, may be the determining factor in the transition from outwardly undetectable presences of pathological aggregates in the brain to cognitive loss and clinical AD.<sup>24-26</sup> This idea is supported by the existence of microglial AD risk genes and clearance mechanisms that go awry in age and with prolonged insult.<sup>19,27</sup> Correspondingly, A $\beta$  accumulates in the brain with age,<sup>28</sup> after traumatic brain injury<sup>29</sup>, and infection,<sup>24</sup> which are all risk factors of sporadic AD. PET imaging of AD patients and healthy individuals of various ages and stages of disease reveals a

synergistic association of co-occurring A $\beta$ , tau, and activated microglia with cognitive impairment, and its predictive ability was unmatched by co-occurring A $\beta$  and tau, suggesting the intersection of aberrant microglial activation and proteinopathy may be necessary for the evolution to clinical manifestations.<sup>30</sup>

As will be explored in the following sections, microglia drive pathology in a variety of ways, such as in the sequestering of plaques, the hyper-phosphorylation of tau and its spread throughout the brain, and neuronal injury by aberrant synapse engulfment and inflammatory signaling.<sup>7,31</sup> Importantly, microglia-mediated neurotoxicity may be the predominant driving force behind neuron injury and death than that caused by proteinopathy.<sup>32</sup> Thus, targeting microglial function may ameliorate disease by both reducing proteinopathy and neuron death. In order to successfully target microglial dysfunction in disease, however, a comprehensive understanding of their immune signaling pathways and subsequent dysregulated responses is needed. There are numerous obstacles in the way of elucidating precise targetable contributions to AD, including the largely inaccessible nature of living human microglia and the fundamental differences between human and mouse microglia, which are a more readily accessible and manipulatable option to study in widely used mouse models.

### **Acknowledging the complexities of studying microglia in AD mouse models**

Mice do not naturally develop Alzheimer's disease, and in order to study AD pathology in mice, transgenic overexpression models of human AD mutations are often used.<sup>33,34</sup> Mutations in the genes amyloid precursor protein (APP), presenilin 1 (PSEN1), and presenilin 2 (PSEN2) result in the heritable, familial form of the disease, primarily causing the altered processing or accumulation of A $\beta$ . Some transgenic models overexpress multiple familial mutations in the same or different genes, resulting in rapid pathology development in the animals.<sup>35,36</sup> While familial AD is likely initiated by the abnormal accumulation of A $\beta$ , as the activity of the genetic mutations would suggest,<sup>3</sup> downstream processes also

result in the accumulation of tau pathology. The co-occurrence of A $\beta$  and tau pathology is also observed in the sporadic form of the disease, although there is still debate over whether A $\beta$ -dependent mechanisms initiate sporadic cases. It is without question, however, that both characteristic proteinopathies are necessary for the current characterization of the disease, which stresses an issue with the most basic familial AD mouse models: mouse models, whether they express a singular mutation or overexpress multiple familial mutations, do not develop subsequent tau pathology.<sup>34,37</sup> It is an egregious flaw that a model used to study disease pathophysiology does not give rise to a major disease component, and even more so that many models of this neurodegenerative disease do not experience neuron loss.<sup>33,35,38–40</sup> Some studies have introduced tau pathology by other means, such as the expression of tauopathy-relevant mutations or injecting tau oligomers and aggregates into the brain. While artificial introduction of tau deposition by these methods may offer insight into downstream interactions caused by the co-occurrence of A $\beta$  and tau pathology, the natural timeline of progression and underlying mechanisms by which that pathology would arise are lost. Overexpression in itself can have extraneous effects causing disease irrelevant phenotypes.<sup>34</sup> Notably, familial AD is also only a small fraction of cases, estimated to account for less than 5% of all cases,<sup>41</sup> and unknown mechanistic differences between familial and sporadic cases cannot be identified in current mouse models. The differential functions of AD risk genes have been studied in mice to gain insight into how specific alleles may increase one's risk to develop sporadic AD; however, the etiological events cannot be studied in a model that does not develop the disease. That being said, mouse models allow for the studying of cellular functions and interactions in a whole-body system over the animal's lifetime and can be precisely genetic modified, but there needs to be exceptional understanding for their limitations to decipher disease relevance.

Using a variety of mouse models, microglia have been shown to contribute to proteinopathy and neuronal injury. However, in addition to the concerns of engendered pathology in AD mouse models, the translatability of these results is further complicated by the inherent differences between mouse and

human microglia. Histologically, these differences were appreciated early on. Distinct plaque-associated microglial activation patterns and an overall dampened immune response were observed in a familial AD mouse model compared to those of the AD brain.<sup>37</sup> More recently, transcriptomic studies have revealed an absence of numerous genes involved in the human microglial immune response in mouse microglia,<sup>42,43</sup> and, notably, there was limited overlap in changes in gene expression over the course of aging and neurodegeneration between human and mouse microglia.<sup>42,44</sup> In aging, in particular, of the limited number of genes to be differentially expressed in both human and mouse microglia, roughly half of these genes were regulated in opposite directions.<sup>42</sup> In addition to gene expression, the protein sequences of some microglial genes implicated as sporadic AD risk genes, including as TREM2 and CD33, are only 50% identical.<sup>45,46</sup> These differences, particularly observed in aging and neurodegeneration, are troubling for the identification of human relevant molecular targets capable of modulating the course of AD. Successful strategies in mice, including those targeting the immune response such as non-steroidal anti-inflammatory drugs, have not shown the same promise in humans.<sup>47</sup>

### **Microglial signaling cascades interacting with pathological proteins**

TREM2, triggering receptor expressed on myeloid cells 2, is a transmembrane innate immune receptor found on myeloid cells. Microglia are the primary TREM2 producing cell-type in the central nervous system.<sup>48</sup> TREM2 signaling modifies the activity of reactive microglia by enhancing phagocytic activity and suppressing the production and secretion of pro-inflammatory cytokines.<sup>49-51</sup> TREM2 activity is often regarded as protective, as it promotes “good” debris removal activity and suppresses “bad” pro-inflammatory functions that, although necessary for brain homeostasis, can be harmful to neurons in excess.<sup>52</sup> Variants of TREM2 are linked to the development of AD, and TREM2 expression is increased in the brain and CSF of AD patients and correlates with disease severity.<sup>53,54</sup> It was initially thought that TREM2 activity exacerbates AD pathology.<sup>55</sup> However, it is now thought that increased expression of

TREM2 is a compensatory mechanism in AD, where increased TREM2 signaling is a product of overcoming insufficient clearance of pathological proteins.<sup>56</sup>

In APP23, 5xFAD, and APPPS1 models with robust amyloid pathology, TREM2 expression levels are increased in microglia and other myeloid cells surrounding amyloid plaques.<sup>55,57-59</sup> *In vitro* TREM2 signaling promotes microglial clearance of A $\beta$ ,<sup>56,57</sup> and TREM2 knockout impairs the ability of microglia to surround amyloid plaques.<sup>55,60,61</sup> TREM2 signaling has also been investigated in the context of tauopathy. TREM2 is up-regulated in the brains of P301S mice,<sup>62</sup> a mouse model of primary tauopathy with neurofibrillary tangles and neuron loss present in multiple brain regions.<sup>63</sup> Silencing TREM2 expression in this model exacerbated tau pathology and worsened spatial learning deficits, hypothesized to be the result of increased activation of tau-phosphorylating kinases by pro-inflammatory factors normally suppressed by TREM2 signaling.<sup>64-67</sup> In line with the observation that TREM2 signaling modifies the microglia response to clear A $\beta$  and reduce neuroinflammation in amyloid models, the reduction of pro-inflammatory factors may slow the progression of tau hyperphosphorylation by preventing the hyperactivation of tau-phosphorylating kinases. As such, the up-regulation of TREM2 in the AD brain may have a two-fold benefit reducing tau and amyloid beta pathology. However, further investigation is needed to determine human-relevant TREM2 signaling and whether the observations of TREM2 signaling are consistent in the full landscape of the disease over time. This is highlighted by inconsistent effects of TREM2 knockout over time in mouse models. TREM2 deficiency has produced both neurotoxic effects and exacerbated tau pathology in a primary tauopathy model<sup>68,69</sup> as well as neuroprotection with the prevention of brain atrophy without affecting phosphorylated tau levels.<sup>70</sup> This could be attributed to the timeline of TREM2 knockout in the model either months before neuron loss is first observed or when substantial neuron loss is already present and suggests shifting roles of TREM2 involvement and efficacy of its modulation.<sup>71</sup> The protective effect of TREM2 knockout in late disease is consistent with TREM2's amplification of microglial

phagocytic ability and microglia's observed engulfment of damaged neurons,<sup>72</sup> and it suggests a detrimental effect of TREM2 in later stages of disease not appreciated in earlier mouse studies.

CX3CR1 is a microglial chemokine receptor that modulates the immune response. CX3CR1 activation regulates microglia migration and surveillance of the brain parenchyma as well as the pruning or removal of synapses and neurons during development and disease.<sup>73,74</sup> In amyloid mouse models, knockdown of CX3CR1 has beneficial effects on amyloid deposition, likely as a result of increased microglial phagocytosis of A $\beta$ .<sup>75-78</sup> Subsequent *in vitro* results suggested that the reduced amyloid pathology resulted from an altered microglia activation, whereby CX3CR1 deficiency increases the phagocytic ability of microglia and modifies its cytokine secretion profile.<sup>75</sup> However, knockdown of CX3CR1 in mice expressing human tau resulted in increased tau hyperphosphorylation, tau aggregation, and microglial activation.<sup>79</sup> These results suggest that knockout of CX3CR1 has opposite effects on amyloid and tau pathology.

The classical complement cascade, part of the innate immune response, is activated in response to pathogens and apoptotic cells and recruits phagocytic cells for their clearance. In the brain, the classical complement cascade is involved in microglia's pruning of synapses— a process that is dysregulated neurodegenerative disease.<sup>80,81</sup> Complement proteins are up-regulated in neurodegenerative disease and are both expressed and detected by microglia. Histological studies have demonstrated complement activation in the AD brain, particularly in association with amyloid plaques.<sup>82</sup> A $\beta$  is able to interact with the complement protein C1q to initiate the classical complement cascade.<sup>83</sup> Increased C1q expression and synaptic localization was observed in two AD mouse models prior to the appearance of amyloid plaques and correlated to soluble A $\beta$  levels.<sup>84</sup> Inhibition of C1q, C3, or the microglial complement receptor CR3 reduced synapse loss, implicating microglial phagocytosis of synapses by the complement cascade. Additionally, microglia in wild-type mice injected with A $\beta$  oligomers demonstrated increased engulfing of

synapses, recapitulating the phenotype observed in the amyloid mouse models. Knockout of C1q rescued this phenotype, suggesting a necessary role of complement for the A $\beta$ -mediated synapse loss.<sup>84</sup> In amyloid mouse models, although complement activation consistently exacerbates synapse loss, complement inhibition has been observed to worsen, lessen, and have no effect on amyloid pathology.<sup>85-90</sup> Downstream complement protein level differences and expression of their regulatory inhibitors between mice and humans in AD pathology and age have been attributed to this discrepancy.<sup>89,91</sup> In mouse models of tauopathy, complement activation is primarily linked to the exacerbation tau pathology.<sup>88,92</sup>

### **Both overactive and under-responsive microglia ineffectively respond to and clear proteinopathy**

Microglia become inefficient in the phagocytotic clearance of misfolded proteins with age due to a gradually increasing and persistent pro-inflammatory state, commonly known as “inflammaging.”<sup>16,18,93</sup> In this state, microglia become “primed” in a chronic inflammatory environment, initiating exaggerated immune responses to secondary stimuli. In neurodegeneration, primed microglia more rapidly contribute to A $\beta$  and tau pathology progression and negatively affect neuronal health and synapse plasticity<sup>94</sup> while simultaneously being less responsive to anti-inflammatory cues.<sup>95</sup> Microglial priming and subsequent reduced clearance ability is evident in amyloidopathy models. In the APP/PS1 model, the expression of A $\beta$ -binding scavenger receptors and A $\beta$ -degrading enzymes in microglia of 14-month-old transgenic mice were observed to be 2- to 5-fold lower than those of non-transgenic littermates.<sup>96</sup> Decreased expression of A $\beta$ -binding scavenger receptors and A $\beta$ -degrading enzymes was not observed in young transgenic animals.<sup>96</sup> The reduction of A $\beta$ -binding scavenger receptors and subsequent A $\beta$  uptake *in vitro* were linked to an increase in pro-inflammatory cytokines production.<sup>96</sup> Impaired A $\beta$  clearance by primed microglia is likely influenced by both age and chronic pathological insult. In the co-culture of 20-month-old APP/PS1 slices, the inability of aged microglia to clear A $\beta$  could be reversed by the presence of young microglia from either neonatal wild-type or neonatal APP/PS1 slices but not from aged wild-type slices.<sup>97</sup> Exogenous

human A $\beta$ <sub>42</sub> applied to microglia-depleted wild-type hippocampal slices was rapidly cleared by reintroduction of young (5 weeks) or adult (6 months) wild-type microglia, as well as young 5xFAD microglia. Microglia isolated from aged 5xFAD cerebellum, but not forebrain, could also deplete A $\beta$  deposits.<sup>98</sup> As the cerebellum in 5xFAD mice does not contain amyloid pathology,<sup>99,100</sup> the retained clearance capacity of both cerebellar microglia from aged 5xFAD mice and microglia from aged wild-type mice would indicate that prior exposure to pathology reduced microglial phagocytic capacity to clear A $\beta$  deposits, rather age or overall disease status.<sup>98</sup> These results would suggest that impaired microglial clearance in the presence of amyloid pathology is primarily a factor of chronic A $\beta$ -exposure and that naïve aged microglia can still readily engulf A $\beta$ .

In contrast to priming, microglia can become less responsive under chronic pathological insult. In this state, microglia similarly have an impaired ability to phagocytose A $\beta$ , linked to dysfunctional metabolic reprogramming. Exposure to A $\beta$  induces a shift from oxidative phosphorylation to glycolysis in microglia that is necessary for an immune response.<sup>19</sup> Prolonged A $\beta$  insult, however, gives rise to metabolic defects and diminished immune responses characterized by reduced cytokine secretion and phagocytosis by microglia with new immune stimuli. The microglia's "chronic tolerant phase" can be reversed by interferon- $\gamma$  stimulus to boost defective glycolytic metabolism and recover former levels of cytokine secretion and phagocytic ability.<sup>101</sup> Importantly, interferon- $\gamma$  treatment in 4.5-month-old 5xFAD mice over 3 months resulted in increased levels of phagocytosed A $\beta$  and reduced plaque burden and neuron death.<sup>19</sup> Restoring metabolic deficits in dysfunctional microglia prevents cognitive decline in multiple amyloidopathy models.<sup>9,19</sup> Contrastingly, interferon- $\gamma$  signaling has been associated with worsening tau pathology and neurodegeneration through microglial-mediated mechanisms.<sup>102</sup>

Chronic tau exposure can similarly prevent effective microglial responses by inducing microglial senescence, which is observed in both tauopathy mouse models and human patients.<sup>103–107</sup> Microglia

surrounding amyloid plaques, in contrast, are not associated with cellular senescence.<sup>105</sup> Cellular senescence is the permanent arrest of the cell cycle, and senescent microglia exhibit a unique secretory profile that promotes neuroinflammation. Senescent microglia exhibit impaired phagocytic abilities and motility,<sup>108</sup> and have commonly been observed in age, stimulated by phenomena such as DNA damage and oxidative stress.<sup>109</sup> Tau exposure induces senescence in primary wild-type murine microglia, which in turn leads to impaired tau clearance.<sup>103</sup> Removal of senescent microglia and astrocytes reduces hyperphosphorylation of tau and subsequent neurofibrillary tangle deposition and neuron death in mouse models of primary tauopathy.<sup>104,105</sup> Importantly, senescent glia were removed rather than replaced, indicating that senescent glia undergo a pathological gain of function that specifically contributes to pathology progression, potentially through their senescence-associated secretory phenotype.

The functional identifiers outlined above (primed, tolerant, senescent) describe opposing responses to chronic insults of the AD brain. In the presence of A $\beta$ , microglia can enter a heightened pro-inflammatory state (primed), while others may become less sensitive to stimuli and exhibit reduced cytokine secretion (tolerant). With tau exposure, microglia become senescent, ineffectively clearing pathological proteins while exhibiting a proinflammatory secretome, further contributing to pathology progression. Whether these states can co-occur within brain micro-environments or what governs the transition to (or between) each identity has not been determined. But beyond overarching identifiers like homeostatic, senescent, or primed, transcriptomic studies reveal extensive complexity in microglial states in the healthy and AD brain, both temporally and spatially.<sup>110,111</sup> Single-cell transcriptomics of microglia from an AD mouse model demonstrate a diverse evolution of microglial states in advancing neurodegeneration, and distinct phenotypes in late-stage disease.<sup>112</sup> In humans, single-cell profiling of *post mortem* cortical tissue revealed multiple unique microglial subpopulations in both end-stage AD patients and healthy aged individuals.<sup>113</sup> Importantly, changes in gene expression consistent with the widely recognized disease-associated microglial (DAM) phenotype<sup>114,115</sup> are identified in both AD and healthy samples.<sup>17</sup> The DAM phenotype,

recognized in numerous neurodegenerative disease mouse models, is characterized by a down-regulation of homeostatic genes and an increase in genes involved in lysosomal, phagocytic, and other immune response pathways and is mediated by TREM2 signaling.<sup>71</sup> Other states distinct from the DAM phenotype, such as those closely related to interferon signaling, have been identified in transcriptomic studies, although how these translate to microglial function is unknown.<sup>44,112</sup> Intermediate activation states, such as between a homeostatic phenotype and a DAM expression profile, have been observed<sup>114</sup> and trajectories of an underlying spectrum of shifting transcriptional profiles of microglia can be modeled,<sup>112</sup> suggesting that microglial states are dynamic and regulatory elements can be leveraged to modulate their function. Individual activation states result in unique downstream functions, but, as transcriptomic studies demonstrate, the tissue-level population of microglial states is heterogeneous and evolves with age and disease. The composition of the microglial population collectively drives disease, and the identification of successful therapeutic targets requires the characterization of the dominant states, their respective dysfunctions, and the synergistic/antagonist activity between them. (Figure 1-1)

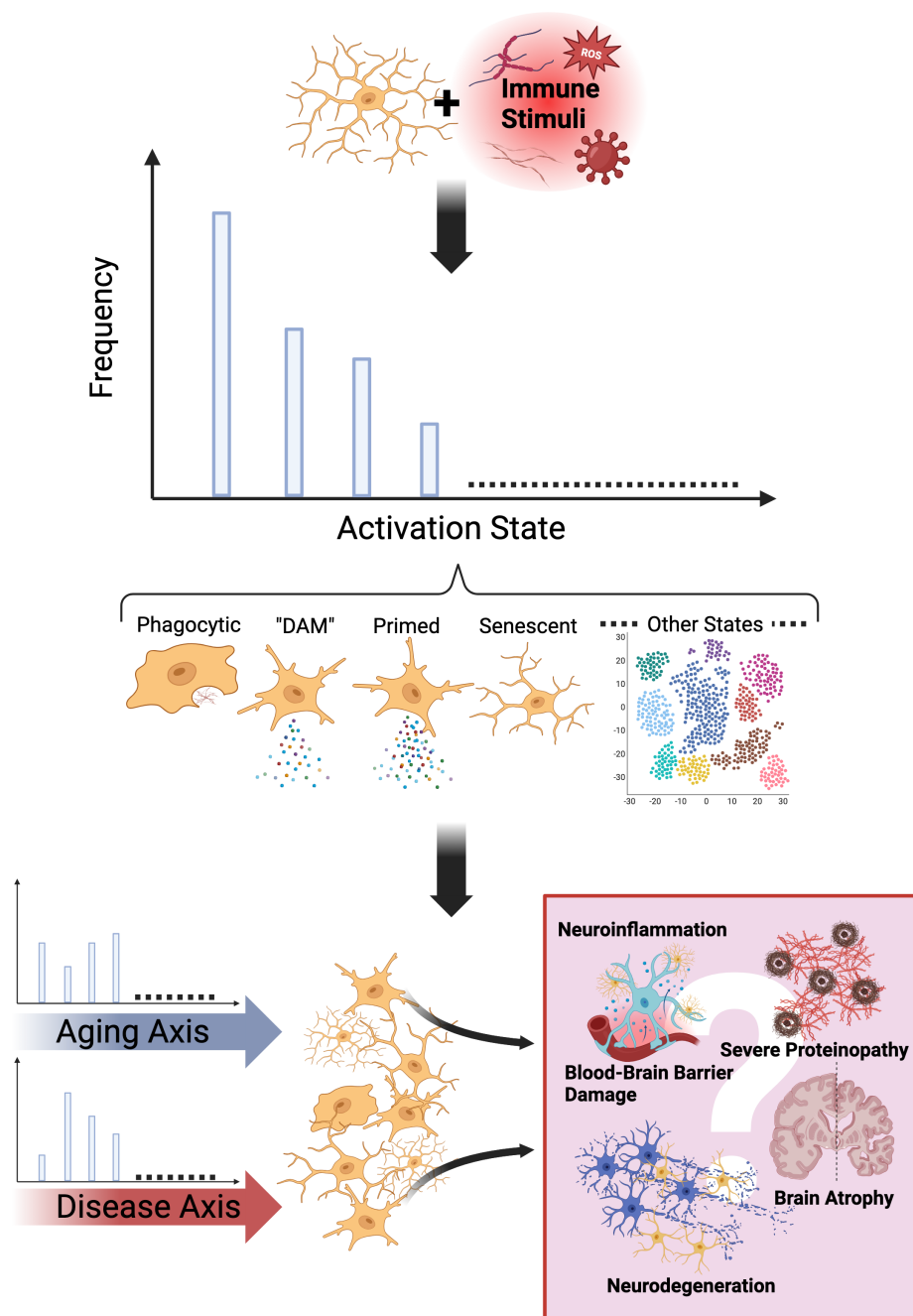


**Figure 1-1. The combined actions of an evolving population of diverse microglial activation states contribute to Alzheimer's disease progression.** Following an immune stimulus, microglia become activated in an effort to restore brain homeostasis. Commonly observed activation states in aging and neurodegenerative disease include primed, disease-associated, phagocytic, and senescent microglia. Transcriptomic studies have identified a vast diversity of activation states of unknown function, and a comprehensive classification of microglial states has not been defined. Each individual state can independently contribute beneficially and/or detrimentally to AD pathology, such as the clearance or spread of misfolded proteins by phagocytic microglia or the amplified secretion of pro-inflammatory cytokines by primed and disease-associated microglia contributing to neuronal injury and the hyperphosphorylation of tau. The composite population of microglia, however, and its combinatorial effect of individual states drive disease. The distribution of microglial activation states and subsequent dominant downstream activities and effect on AD pathology evolves over the course of disease. Functional characterization of microglial states and their relative frequency in progressing AD is needed for the identification of successful therapeutic targets to restore beneficial microglial function or reduce detrimental dysfunction within optimal treatment windows. Created with BioRender.com

### **Unable to compensate, dysfunctional microglia worsen hallmark pathology**

Microglia have long been known to phagocytose and clear both soluble and fibrillar A $\beta$ .<sup>116-118</sup> However, with age and chronic insult microglia lose their ability to effectively phagocytose and clear A $\beta$ ,<sup>96</sup> and can initiate amyloid aggregation.<sup>63,119</sup> It has been hypothesized that microglia may compensate for ineffective clearance by sequestering A $\beta$  in the form of plaques to prevent neuronal damage.<sup>120,121</sup> In line with this, amyloid plaque levels plateau in the brain at the onset of clinical symptoms and do not correlate with neuron death,<sup>122,123</sup> and extensive plaque burden can be found in the brain of cognitively healthy people.<sup>22,124</sup> Aggregation of A $\beta$  is initiated by low pH<sup>125</sup> and high (micromolar) concentration of A $\beta$  monomers.<sup>126</sup> Low pH and high concentration of monomeric A $\beta$  are not found in the extracellular space; thus, A $\beta$  aggregation has been hypothesized to occur elsewhere.<sup>127</sup> Microglia from a combination amyloid and tau mouse model of AD (3xTg<sup>128</sup>) were found to have A $\beta$  aggregates in their lysosomes.<sup>127</sup> Notably, while some of these microglia were associated with existing extracellular amyloid plaques, others had no existing plaques in their vicinity but contained A $\beta$  aggregates in size comparable to small plaques. In the latter case, the lack of any nearby amyloid plaques would suggest that the lysosomal plaques did not result from internalization of existing aggregates. Non-plaque-associated microglia of human postmortem brains have also been found to contain A $\beta$  aggregates, regardless of the individual's dementia- or disease-status.<sup>127</sup> Accordingly, dense-core plaque formation was prevented in APP/PS1 mice by eliminating receptor tyrosine kinases necessary for phagocytosis. In turn, levels of diffuse A $\beta$  increased and amyloid deposition was observed in blood vessels, corresponding to worsened memory deficits and suggesting that plaque formation in microglial lysosomes may be protective.<sup>120</sup> Similarly, impaired microglial phagocytosis by TREM2 deficiency in 5xFAD mice resulted in more diffuse plaques without the presence of surrounding microglia.<sup>61</sup> The diffuse plaques were closely associated with increased neurite damage, which was hypothesized to be the result of exposed protofibrillar A $\beta$  that would otherwise be contained in microglia-sequestered dense-core plaques.<sup>129</sup> These results suggest a potential role of microglia in the initial

aggregation and subsequent deposition of amyloid plaques in the Alzheimer's disease brain as a protective effort. While plaques are not regarded as overtly toxic and may shield neurons from A $\beta$  oligomers that contribute to synapse disruption and cognitive deficits,<sup>130,131</sup> as a consequence of their interaction with A $\beta$  and A $\beta$  plaques, microglia display impaired surveillance activity and dampened homeostatic functions<sup>132</sup> and promote the spread of A $\beta$  in the brain.<sup>133</sup> Further, chronically activated microglia can detrimentally affect neuron health in the secretion of proinflammatory factors that spur on the production of reactive oxygen species, directly injure neurons and synapses, and contribute to the accumulation of tau pathology.<sup>31</sup> Thus, protective efforts by microglia in the sequestering of A $\beta$  is not a completely benign response in disease.

Ineffective microglial clearance also gives rise to hallmark tau pathology. Microglia phagocytose soluble and insoluble forms of tau *in vivo*.<sup>134–136</sup> However, microglia cannot effectively break down tau and will release it,<sup>106,134</sup> promoting its spread in brain and likely contributing to the accumulation of tau in regions not connected by synapses.<sup>137,138</sup> Human PET imaging demonstrates parallel propagation of microglial activation and tau pathology, following Braak-like stages.<sup>30</sup> Microglia-mediated tau spread has been demonstrated by the reduction of tau pathology in brain regions effected in advancing disease by the elimination of microglia in primary tauopathy models.<sup>135</sup> It was determined that the microglia-mediated spread of tau was driven by the secretion of exosomes containing tau seeds (pathological tau that has the capacity to induce tau aggregation), and tau spread was similarly prevented by the inhibition of exosome synthesis.<sup>135</sup> Importantly, microglia from wild-type and tauopathy mice do not express tau mRNA and, thus, do not natively contain tau; however, they contain tau seeds that are released into the culture medium *in vitro*.<sup>134</sup> Similarly, microglia cultured in medium containing tau seeds reduce but do not clear all of the tau, suggesting that microglia can uptake extracellular pathological tau but are unable to effectively break it down.<sup>134</sup> Microglia isolated from *post mortem* brains of AD and primary tauopathy patients also contain

and release tau seeds capable of initiating aggregation,<sup>134</sup> and microglia and various tau species co-localize in *post mortem* brain tissue of Alzheimer's disease patients and healthy individuals.<sup>136</sup>

Microglia not only deposit tau seeds in pathology-naïve regions but promote hyperphosphorylation of tau protein. Activated microglia directly lead to tau hyperphosphorylation through the secretion of cytokines and downstream activation of kinases.<sup>64-67</sup> Microglia isolated from a combined mouse model of human tau and knockout CX3CR1, previously shown to have exacerbated tau pathology with increased microglia activation,<sup>79</sup> are capable of inducing tau hyperphosphorylation when transferred to non-transgenic mice.<sup>67</sup> Similarly, tau protein from primary wild-type mouse neurons transfected with human tau exhibit no aggregation, but when the neurons are co-cultured with activated microglia, aggregated tau accumulates in neurites.<sup>65</sup>

In concert with microglial spread of tau and ineffective A $\beta$  clearance, microglial dysfunction results in a vicious circle of progressing pathology, whereby activated microglia foster a pro-inflammatory environment, which damages neurons, hyper-phosphorylates tau, and induces the production reactive oxygen species; in turn, these downstream events chronically activate the microglia and lead to undesirable, ineffective response states that further promote neuroinflammation and pathology progression. It is important to note that numerous microglial-independent mechanisms drive disease, such as A $\beta$ -dependent tau phosphorylation<sup>139,140</sup>, prion-like seeding, and synaptic tau spread.<sup>141-143</sup> Thus, restoration of beneficial microglial function may be insufficient to completely disrupt disease processes. Subsequently, effort has been made to determine the magnitude and nature of microglial contribution in the initiation and progression of disease.

### **Depletion of microglia inconsistently ameliorates AD proteinopathies**

The depletion of microglia from the brain is a recent strategy applied to isolate the role and contribution of microglia in disease. Use of this strategy is made possible by the discovery that reduction or complete removal of microglia in mice does not cause abnormalities in cognition or behavior.<sup>144,145</sup> Widely-used methods to reduce the microglia populations are Cre recombinase strategies to ablate cells expressing microglia-specific markers or application of inhibitors of colony-stimulating factor receptor 1 (CSFR1) such as PLX3397 and PLX5622. CSFR1 signaling is required for microglia differentiation from yolk sac-derived progenitors during development and mature microglia homeostasis and survival.<sup>145</sup> PLX5622, the more selective inhibitor, demonstrates greater than 20-fold selectivity over homologous receptors and exhibits improved blood-brain barrier (BBB) penetrance.<sup>127,144</sup> PLX5622 administration results in more rapid elimination of microglia and, unlike PLX3397, does not affect the viability of oligodendrocyte progenitor cells with prolonged treatment.<sup>146</sup> Both molecules have been used *via* cerebral injection or PLX-treated chow to deplete or near-eliminate microglia in the mouse brain.

The effects of microglial depletion have been studied in the context of amyloidopathy and tauopathy in mice. With existing evidence of the dual contribution of hyperphosphorylation and spread of tau by microglia, it is reasonable to expect reduced tau pathology after microglia depletion. In fact, near-complete elimination of microglia prevents neurodegeneration and reduces the level of hyperphosphorylated tau and its spread in aged primary tauopathy mice whether treatment is initiated prior to or after the onset of tau deposition in the models.<sup>32,102,135</sup> However, without near-complete microglial elimination, neurodegeneration still occurs, as even a small population of activated microglia can lead to neurodegeneration.<sup>32</sup> A moderate 30% reduction in the microglial population in aged tauopathy or 3xTg mice exhibits no effect on tau pathology, though substantial tau aggregation and neuron loss was already present at the time of treatment.<sup>144,147</sup> It is not immediately clear from these studies if microglia contribute

to tau pathology accumulation or neuron loss consistently over time— a crucial element of identifying therapeutic target sufficient in preventing neurodegeneration and its effective window.

In amyloidopathy models, microglial depletion largely reduces plaque burden; however, this does not always result in favorable disease outcomes. For example, while plaques are reduced in the brain tissue, deposition of A $\beta$  in the brain vasculature is observed.<sup>127</sup> Interestingly, microglial depletion in amyloidopathy commonly produces cognitive improvements, which are not dependent on amyloid changes. Specifically, microglial depletion in 5xFAD mice, prior to the onset of extra-neuronal A $\beta$  plaque deposition, prevents considerable plaque deposition (~90%), decreases intraneuronal amyloid levels, and improves fear-associated memory.<sup>148</sup> Similar reduction is found after the start of amyloid deposition.<sup>127,149</sup> However, microglial depletion in later stages of the disease does not ameliorate or prevent further plaque deposition,<sup>150</sup> although depletion prevented neuron loss, reduced overall neuroinflammation, and improved contextual memory.<sup>150</sup> In the 3xTg model, late-stage depletion similarly improved cognition without modulation of amyloid or tau levels.<sup>144</sup> As such, microglia may contribute to neuron loss and memory impairment independently of pathology progression.

Part of the discrepancy in effect seen in microglial depletion studies is likely a result of the study's goal and experimental design; that is, some sought incomplete microglia reduction<sup>144,147</sup> to determine if there was a therapeutic benefit of this approach that could be used on humans, while others completely ablated microglia to parse out their contribution to disease.<sup>32,102</sup> A comprehensive view of the evolving timeline of microglial contribution to disease onset and progression cannot be deduced from the summation of these studies, and is particularly muddled by the distinct timeline of pathology spread in different mouse models.<sup>147</sup> It is worth noting that even with plaque reduction, microglia elimination did not always result in reduced levels of soluble or insoluble A $\beta$ -38, A $\beta$ -40, or A $\beta$ -42.<sup>127</sup> This result is surprising because microglia are known to phagocytose A $\beta$ .<sup>116-118</sup> Because microglia's phagocytic ability and enzymatic

degradation of A $\beta$  is impaired with age and continued inflammatory insult,<sup>96</sup> it is feasible that the removal of already-impaired microglia does not affect existing A $\beta$  levels, but does impact their deposition in plaques. These seemingly contradictory results highlight the potential for specific treatment windows for modulating microglial function to therapeutic benefit, but these windows would completely rely on the distribution of microglial states present (i.e., homeostatic, phagocytic, primed, senescent, etc.) (Figure 1-1).

### **Human cellular disease models are needed to recapitulate microglial states**

The differences between murine and human microglia and the imperfections of AD mouse models stress the need for human cell models to understand the role of microglia in a disease-relevant landscape. Especially in the case of AD where many cell types contribute to its development and progression through complex, inter-dependent mechanisms,<sup>38</sup> the understanding of cellular interactions in their true microenvironment is of utmost importance and is arguably the largest advantage of mouse models. However, there is a critical need for the identification and verification of human-relevant cellular mechanisms, which in the case of microglia may largely be limited in mouse models. Advances in multi-cell type human induced pluripotent stem cell (iPSC) models, highly reminiscent of the human brain in cell-cell interactions and cellular function, is making this need more achievable.<sup>46</sup>

To bridge the gap between various mouse models and end-point *post mortem* human tissue, which does not allow for the manipulation of living cells or reveal changes within individuals over time, iPSC-derived models allow for the study of living human cells that cannot be isolated and cultured from mature tissues. Since their invention, numerous protocols have been developed for derivation of diverse brain cell types using two-dimensional and three-dimensional cell culture methods. Unlike mouse models overexpressing familial AD mutations, iPSC-derived neuronal cells from familial patients develop both A $\beta$

and tau pathology. Importantly, cells derived from individuals with sporadic cases of AD also develop varying degrees of pathology, creating new opportunities for studying genetic risk factors and unique mechanisms of sporadic disease.<sup>151</sup> iPSC-derived models exhibit continued accumulation of A $\beta$  and tau aggregates over months of culture,<sup>152,153</sup> promoting the investigation of longitudinal changes contributing to advancing disease states without the over-expression of AD-relevant or -irrelevant genes.

Numerous protocols for differentiating microglia have been developed<sup>154-157</sup> and iPSC-derived microglia from Alzheimer's patients and those carrying risk factor alleles have been studied in isolation or in co-culture with other neuronal cell types. In a comprehensive study, microglia were differentiated from iPSC lines derived from AD patients of a variety of genetic backgrounds, and isogenic controls were created to investigate how disease-associated mutations and alleles alter microglia function and contribute to disease.<sup>158</sup> The study demonstrated that APOE4, the strongest and most common genetic risk factor for AD, resulted in impaired microglial phagocytic ability and mitochondrial respiration and increased cytokine secretion, while mutations in APP and PSEN1 did not result in robust functional changes. These results point toward a functional deficit of APOE4 microglia in response to pathological insults in AD, whereas familial mutations in APP and PSEN1 likely do not directly contribute to microglial dysfunction in disease. These findings highlight the potential of distinct microglial roles in sporadic and familial AD, and that heterogeneity in microglial dysfunction can be more readily identified using human iPSC-derived models than in current animal models. Others have similarly demonstrated APOE4-mediated phagocytic deficits and increased pro-inflammatory phenotypes of sporadic AD patient-derived microglia. Interestingly, the conversion of APOE4 to the more common APOE3 isoform ameliorated multiple disease-relevant phenotypes, including the impaired microglial uptake of A $\beta$ .<sup>159</sup> In addition to APOE, other microglia-expressed AD-relevant genes have been investigated in iPSC-derived microglia, including TREM2. TREM2 missense mutations in iPSC-derived microglia-like cells resulted in decreased expression levels of TREM2 and subsequent impairment of migration and phagocytosis.<sup>160</sup> Similarly, TREM2 loss-of-function

mutations impair the ability of microglia to shift to a glycolytic metabolism to mount an immune response and, subsequently, prevents the phagocytosis of A $\beta$ .<sup>161</sup>

Although iPSC-derived cells are relatively immature as revealed by low expression of microglia-specific genes,<sup>158,162</sup> studies of human iPSC-derived microglia, complete with rigorous isogenic control strategies, will be crucial in identifying disease-relevant pathways among complex genetic interactions. Improved iPSC-derived microglial maturation, with gene expression and function more representative of microglia isolated human adults, has been achieved through culture with other brain cell types.<sup>156,162-164</sup> Not only do improved differentiation methods continue to overcome the shortcomings of iPSC-derived cells for the study of adult-onset disease, but models of increasing complexity are being developed to better reflect the cell-cell interaction and brain microenvironment, such as a iPSC-derived tri-culture system of neurons, astrocytes, and microglia to investigate cell-type specific interactions in neuroinflammation.<sup>163</sup> Upon inflammatory stimulus, cultures containing microglia showed an increase in the complement protein C3, a common marker of neuroinflammation. C3 levels were dramatically increased in the tri-cultures of microglia, neurons, and astrocytes as compared to those of microglia-neuron co-cultures. It was determined that increased C3 in the tri-culture system was induced by a microglia-astrocyte feedback loop, whereby microglial secreted factors amplify production of C3 in astrocytes which, in turn, directly stimulated production in the microglia. The same study also examined the astrocyte-microglia cross-talk in tri-cultures of control microglia and astrocytes with human embryonic stem cell-derived neurons carrying a familial AD mutation or those derived from its isogenic control. C3 levels of the tri-cultures were significantly increased in those containing familial AD neurons compared to control neurons, suggesting a neuronal and/or pathology influence in the exacerbation of astrocyte-microglia signaling in a disease context.<sup>163</sup>

Three-dimensional iPSC-derived cerebral organoids comprising various neuronal cell types allow for increased model complexity that more accurately represents native physiology with mature connectivity

and cell-cell interactions. These cerebral organoids have demonstrated more advanced AD pathology compared to 2D culture methods,<sup>165-167</sup> and will be advantageous for identifying human-specific microglia-neuron interactions and initial screening of drugs.<sup>166,168</sup> A caveat to organoid differentiation, however, is that often the inhibition of mesoderm and endoderm development is used to drive the differentiation of neuronal cells, inhibiting the development of microglia and other mesoderm-originating cell types.<sup>162</sup> Recently, the development of a protocol that does not use inhibition strategies, developing self-patterning organoids with complex cortical-like layers and confined markers of distinct brain regions,<sup>169,170</sup> was found to innately give rise to microglia.<sup>162</sup> The organoids' microglial population, however, vary between specimens and are typically proportionally smaller than the population in the human brain. Other *in vitro* strategies have overcome this limitation by introducing iPSC-derived microglia to organoids in defined quantities,<sup>159,171</sup> which also allow for the investigation of region-specific microglial functional differences using modified organoid protocols that induce ventral or cortical identities.<sup>171</sup> This type of regional specificity is advantageous in the context of AD, where regional differences in microglial gene expression and function have been previously observed *in vivo*<sup>111,172</sup> and may contribute to AD-specific spread of pathology in the brain.<sup>173</sup> It is important to note that strategies incorporating microglia into already developed organoids prevent microglia from participating in early neurogenesis and network formation -- key microglial roles in brain development.<sup>174</sup> As such, others have overcome this limitation by forming organoids with the combination of neural and macrophage progenitors whose resulting microglia contributed to synaptic pruning during neuronal network maturation.<sup>175</sup>

These techniques can be used to identify human-relevant cell signaling pathways, though *in vitro* models are not a part of a whole-body system. Others have integrated human iPSC-derived cells and organoids into the brains of mice to investigate them in the context of a whole organism, and in the case of organoids, introduce *in vivo* vascularization for improved functionalization.<sup>176,177</sup> Human iPSC-derived microglia transplanted into the brains of mice revealed that human microglia express human-specific

signatures comparable to those of the adult human brain, and that transcriptomic changes from neurological insult are species-specific.<sup>176</sup> Integrating human cells in mouse models allows for the longitudinal study of human-specific cell activity in the context of a whole-body system. However, like mouse models, iPSC models (monoculture, co-culture, organoids, etc.) have their own limitations.<sup>178</sup> While improved techniques continue to emerge, early AD organoid studies have revealed characteristic functional changes and late-stage pathology hallmarks.<sup>153,179–181</sup> Organoid models have also been used to study non-genetic factors of sporadic AD such as the potential role of pathogens in pathology development and blood-brain barrier leakage simulated by serum exposure.<sup>182,183</sup> To date, however, organoid culture has not been used to investigate how innate microglia contribute to AD pathology.

## **Conclusion**

Microglia actively contribute to Alzheimer's disease in a complex, multi-faceted manner, and are likely an early driving force in disease capable of contributing to both A $\beta$  and tau pathology accumulation and neuronal injury through diverse mechanisms. The detrimental activities of microglia are not executed by one activated population of cells, and are, instead, carried out by heterogenous populations comprising different microglial states of largely unknown origin, though influenced by the pathological, aged brain milieu. Chronic A $\beta$  exposure can induce a primed phenotype, whereby microglia are over-reactive to stimuli, mounting an exaggerated pro-inflammatory response with impaired phagocytotic ability and reduced response to anti-inflammatory stimuli. A $\beta$  activation of microglia, and their subsequent release of inflammatory factors, activate kinases that hyper-phosphorylate tau, initiate the production of reactive oxygen species, and activate complement signaling that contributes to synapse loss. Contrastingly, in chronic tau exposure, microglia can become senescent, exhibiting impaired homeostatic function while secreting a unique profile of immune factors that intensify the proinflammatory environment. Transcriptomic studies reveal diverse sub-groups of microglia that transition with advancing disease,

although the functional changes of each activation states have not been characterized. How the distribution of microglial activation states evolve over time and their combined effect on pathology progression and neuronal injury remains unknown. Recovery of beneficial microglial function and/or the reduction of detrimental actions contributing to pathology accumulation and neuron injury would likely offer substantial therapeutic benefit. However, the presence of an evolving distribution of diverse states may mean that the modulation of one state can exacerbate the effects of another, particularly if therapies are applied at the tissue level, where microenvironments of varying levels of insults and microglial states would exist. Importantly, an understanding for whether these states are (i) static and predictable given a known microenvironment or whether (ii) microglia are able to transition between states and can be influenced to do so will inform modulation strategies. At the moment, there is a nascent understanding of the heterogeneity of microglial populations and their respective contributions to disease. There is a critical need for the in-depth characterization of microglial dynamics over the course of the disease, not readily achievable in current AD models. The difficulty in identifying human-relevant targets among a very complex, interwoven network of immune cues and signaling cascades is likely in part due to incomplete etiology of disease and animal-specific differences in AD mouse models. In light of contrasting, distinct microglial dysfunctions in amyloid and tau models, future therapies should be informed by and tested in models containing both pathologies, such as human iPSC-derived organoids which also leverage human protein-protein interactions and species-specific signaling. However, a comprehensive understanding of microglial heterogeneity in AD will only be achieved by holistic integration of results from many types of models, with a deep understanding for their limitations.

## Introduction to Chapter 2

### From Cell-Specific to Tissue-Level Importance of Inflammatory States

Chapter 1 sets the stage for an investigation into human microglia and the many hats that they wear, perhaps interchangeably, in neurodegeneration. The AD field is just beginning to appreciate the complexity of reactive microglial phenotypes, often characterizing them through single-cell transcriptomic studies with added layers of spatial and temporal information. What I believe is still needed, however, is the functional information that comes as the consequence of those states. There is a disconnect between an enormous amount of literature describing single microglial genetic manipulations and treatments that confer some change in Alzheimer's disease pathology and the purely genetic and transcriptomic studies that outline impressive heterogeneity in the innerworkings of microglia without indication of how that translates to functional phenotypes. There is still uncharted, but largely simple, territory that needs to be hashed out. That is, there is focus on exact transcriptomic states without the knowledge of what the overall immune profile in the brain is and how that affects resident cells. Transcripts are differentially regulated, and individual genes are known to have specific effects, but when they're all together, what happens? Cytokines can be questioned in a similar manner. They can regulate the expression of other cytokines and act synergistically or antagonistically, but they do not work in isolation. There needs to be a better understanding for the overall immune milieu of the progressing diseased brain and its contribution as an entire system, or broken down regionally, so we can better dissect and appreciate the diverse players that converge on a larger neuroinflammatory brain state. In the next chapter, I describe a study that began in the first handful of months in the newly founded Proctor laboratory as the regional profiling of cytokine secretion over time in the AD mouse brain. The study has since transformed into a complementary view of the organoid work with its tissue-level characterization of the AD immune milieu and its collective effect on neurons, which are ultimately at the mercy of the diverse microglial states and, relatedly or unrelatedly, degenerate in AD.

While microglia are not front and center in the next chapter, they are the main contributors of neuroinflammation, and it is not unreasonable to suspect the cytokines of the AD brain's inflammatory profile would have originated largely from microglia. And, importantly, little is known about the multivariate network of immune cues in progressing disease. This initial study offers a broad survey of dysregulated immune function that can offer insight into how to approach its dissection and what questions should be asked. In the following chapter, we gain an appreciation for collective immune states that converge on neurons within an aged whole-body system, which we can later put into the framework of dissecting specific cellular dysfunction in a simpler model of human cells. Both vantage points are necessary for the understanding of disease-driving immune responses in AD.

*This chapter has been published previously: M. K. Kuhn, R. M. Fleeman, L. M. Beidler, A. M. Snyder, D. C. Chan, E. A. Proctor. "Amyloid- $\beta$  pathology-specific cytokine secretion suppresses neuronal mitochondrial metabolism," *Cellular and Molecular Bioengineering*, in press. doi:10.1107/s12195-023-00782-y (2023).*

## Chapter 2

### **Amyloid- $\beta$ Pathology-Specific Cytokine Secretion Suppresses Neuronal Mitochondrial Metabolism**

#### **Abstract**

Neuroinflammation and metabolic dysfunction are early alterations in Alzheimer's disease brain that are thought to contribute to disease onset and progression. Glial activation due to protein deposition results in cytokine secretion and shifts in brain metabolism, which have been observed in Alzheimer's disease patients. However, the mechanism by which this immunometabolic feedback loop can injure neurons and cause neurodegeneration remains unclear. We used Luminex XMAP technology to quantify hippocampal cytokine concentrations in the 5xFAD mouse model of Alzheimer's disease at milestone timepoints in disease development. We used partial least squares regression to build cytokine signatures predictive of disease progression, as compared to healthy aging in wild-type littermates. We applied the disease-defining cytokine signature to wild-type primary neuron cultures and measured downstream changes in gene expression using the NanoString nCounter system and mitochondrial function using the Seahorse Extracellular Flux live-cell analyzer. We identified a pattern of up-regulated IFN $\gamma$ , IP-10, and IL-9 as predictive of advanced disease. When healthy neurons were exposed to these cytokines in proportions found in diseased brain, gene expression of mitochondrial electron transport chain complexes, including ATP synthase, was suppressed. In live cells, basal and maximal mitochondrial respiration were impaired following cytokine stimulation. We identify a pattern of cytokine secretion predictive of progressing amyloid- $\beta$  pathology in the 5xFAD mouse model of AD that reduces expression of mitochondrial electron transport complexes and impairs mitochondrial respiration in healthy neurons. We establish a mechanistic link between disease-specific immune cues and impaired neuronal metabolism, potentially causing neuronal vulnerability and susceptibility to degeneration in AD.

## Introduction

Alzheimer's disease (AD) is a progressive neurodegenerative disorder resulting in cognitive decline and memory loss. AD is estimated to affect more than 6.5 million people in the United State and 55 million worldwide, with prevalence predicted to increase with the world's growing aged population.<sup>184</sup> There are no proven therapies to prevent or cure the disease, which is in part due to an incomplete understanding of the disease's complex etiology. AD is histologically characterized by neuron and synapse loss, reactive gliosis, and misfolded aggregated proteins of extracellular amyloid beta (A $\beta$ ) plaques and intracellular neurofibrillary tangles.<sup>1</sup> Neuroinflammation is an early event in AD,<sup>3,185</sup> appearing before the development of clinical symptoms<sup>5,6</sup> and often prior to the detection of proteinopathy in AD mouse models.<sup>63,186,187</sup> Neuroinflammation is an active driver of disease and is sufficient to initiate neurodegeneration.<sup>3</sup> Importantly, the majority of known AD risk genes participate in immune response.<sup>4,13</sup> Immunomodulatory therapies are gaining interest for their potential to interfere with disease progression or even disrupt disease initiation. However, the entangled nature of the immune response complicates the identification of robust, effective targets that will not detrimentally affect immune signals necessary for brain health.<sup>3</sup> In this study, we examine the evolution of cytokine expression over aging and disease progression in a transgenic mouse model of AD (5xFAD)<sup>100</sup> and wild-type littermates to generate a systems-level profile of dysregulated immune signaling in the hippocampus, a primary brain region involved in AD onset and progression.<sup>188</sup> This systems biology approach allows us to identify key AD-implicated cytokine cues and their downstream detrimental effect on neuron health.

Neuronal support cells in the brain, called glia, provide immune regulation that is necessary to maintain brain homeostasis. However, their prolonged activation can cause damaging and even neurotoxic inflammation.<sup>20,189</sup> Microglia, the resident immune-competent cells of the brain, play essential roles in development and disease and are thought to be the primary contributor to neuroinflammation in AD.<sup>3,14,174</sup> Another glial cell type, astrocytes, offer a variety of support functions to neurons including metabolic

support and neurotransmitter regulation. Additionally, astrocytes play a role in the immune response, helping to clear debris and amplify microglial signaling cascades.<sup>10,163</sup> In neurodegenerative disease, beneficial immune responses, such microglial activation for the clearance of debris,<sup>14</sup> can become detrimental: prolonged microglial activation is accompanied by an overproduction of pro-inflammatory factors, aberrant synapse engulfment, and the release of nitric oxide.<sup>20,71</sup> Concurrently, dampened immune responses result in ineffective neuroprotection.<sup>16,18</sup> The shift between detrimental and beneficial roles of immune activation, in combination with the substantial overlap in these roles, complicates the identification of therapeutic targets to ameliorate harmful neuroinflammation.<sup>10,71</sup> Consequently, these therapies may also have a limited therapeutic window.<sup>71</sup> Immunosuppressant drugs have not thus far been found to consistently reduce one's risk for AD or have protective effects in its progression.<sup>186</sup> However, the potential remains that if upstream, broad neuroinflammatory pathways cannot be modulated with enough specificity to benefit disease state, targeting of downstream pathways contributing to neuronal injury may prove to be more advantageous.

Metabolism deficits in AD are similarly characteristic of early disease and are closely intertwined with the immune response, contributing to pathology progression and neurodegeneration through an immunometabolic feedback loop.<sup>190</sup> Evidence suggests that metabolic dysregulation precedes proteinopathy and participates in the initiation of AD.<sup>191,192</sup> The complimentary and synergistic action of neuroinflammation and metabolic impairment in early disease creates a unique opportunity to maximize therapeutic effect by disrupting this immunometabolic feedback interaction – a potentially more efficacious target than immune signaling or metabolic function alone. However, the mechanism by which immunometabolic feedback injures neurons and promotes neurodegeneration remains unclear. Here, we investigate downstream dysregulation of neuronal metabolic pathways as a result of a disease-relevant signature of immune cues to identify specific and actionable neuronal vulnerabilities created by immunometabolic feedback in the hippocampus.

Cytokines, immune signaling molecules, both initiate and are a direct consequence of a variety of immune responses and cell-to-cell immune signaling<sup>193,194</sup> and are often dysregulated in the AD brain.<sup>16</sup> Cytokine signaling is highly interdependent, forming a complex web of communications between multiple cell types, and often results in a signaling cascade that prompts the secretion of additional cytokine cues.<sup>193</sup> These characteristics complicate the untangling of shifting beneficial and detrimental roles of immune responses in neurodegeneration, but highlight the necessity of a holistic view of cytokine signaling to describe the overall immune state of the brain. To identify key pathways implicated in disease, we profiled a broad panel of cytokines and used a multivariate mathematical modeling tool, partial least squares (PLS), to construct a signature of cytokine cues associated with AD progression. The actions and downstream effects of individual cytokines are often measured and investigated independently, leading to an incomplete and potentially incorrect understanding of their actions in concert. We applied our signature of AD-upregulated cytokines to healthy neuron and astrocyte cultures and analyzed the resulting differential gene expression and subsequent activation of pathways affecting neuronal viability and cellular metabolism. We determined that the AD cytokine signature suppressed gene expression of numerous mitochondrial electron transport chain (ETC) complex subunits and impaired the mitochondrial function of living neurons. Exposure to the cytokine signature representing the milieu of the AD brain thus predisposes neurons to injury from inadequate energy metabolism and reactive oxygen species (ROS) damage, which would in turn exacerbate neuroinflammation. Our established mechanistic link between the disease-specific cytokine signaling and impaired neuronal metabolism identifies opportunities to target specific detrimental downstream metabolic pathways to disrupt the complex, cooperative actions of neuroinflammation and dysregulated metabolism in disease

## Methods

### *Mice*

All animal procedures were approved by the Penn State College of Medicine Institutional Animal Care and Use Committee (PROTO201800449). 5xFAD (B6SJL, Jackson Laboratory) breeding pairs were purchased for the generation of animals used in the longitudinal study of cytokine profiles over Alzheimer's disease pathology progression. The 5xFAD strain is hemizygous for 5 familial Alzheimer's disease mutations under the Thy1 promoter for expression in the brain: the Swedish (K670N, M671L), Florida (I716V), and London (V717I) mutations in human amyloid beta precursor protein (APP) and the M146L and L286V mutations in human presenilin 1 (PSEN1).<sup>100</sup> Transgenic and noncarrier littermates were housed together and genotyped according to Jackson Laboratory's standard PCR assay protocol 31769 using DNA isolated from tail clippings. Even numbers of male and female mice (n=5 per sex, per group) were sacrificed for the timepoints of this study. CD1 breeder pairs and untimed pregnant females were purchased from Charles River for the generation of primary cell cultures. All animals were provided with food and water *ad libitum* and maintained under a 12-hour light/12-hour dark cycle.

### *Tissue collection and preparation*

We aged the mice to 30, 60, 120, and 180 days to profile cytokine concentrations prior to the deposition of intraneuronal A $\beta$  at 1.5 months, at the development of extracellular amyloid and gliosis at 2 months, at the first appearance of synaptic loss and cognitive deficits at 4 months, and with neuronal loss at 6 months in the 5xFAD model.<sup>100</sup> At each timepoint, 5xFAD mice and noncarrier littermates were sacrificed by unanesthetized decapitation using a mouse guillotine (Braintree Scientific). The brain was isolated and placed into cold HEPES-buffered Hanks' Balanced Salt solution (pH 7.8). The hippocampus

of the right hemisphere was dissected, meninges removed, flash-frozen in liquid nitrogen, and stored at -80°C. After all study samples were collected, hippocampi were thawed on ice and mechanically digested by trituration in 200 µL of RIPA buffer (Boston BioProducts P8340) with protease inhibitor cocktail (Thermo A32953, 1 Pierce mini Protease Inhibitor tablet/ 10 mL RIPA). Digested samples were vortexed vigorously for 1-2 minutes, rested for at least 20 minutes, and then centrifuged at 5000xg for 5 minutes. Supernatants were transferred to new sample tubes for analysis. An aliquot of each homogenate sample was set aside for total protein quantification, and the rest was flash frozen in liquid nitrogen and stored at -80°C for Luminex multiplex immunoassays.

### ***Quantification of total protein***

The total protein content of the hippocampal homogenate samples was quantified using the Pierce BCA Protein Assay Kit (Fisher 23225) according to the manufacturer's instructions. Samples were run in duplicate and absorbances read using a SpectraMax i3 minimax 300 imaging cytometer (Molecular Devices). Sample concentrations were quantified by linear regression using duplicate standard samples ran on each plate.

### ***Luminex multiplex assays***

Cytokine concentration levels of 5xFAD hippocampal homogenate samples were quantified using the Milliplex Map Mouse Cytokine/ Chemokine Magnetic Kit (Millipore MCYTMAG-70K-PX32), measuring a broad panel of secreted cytokines, on a the Luminex FLEXMAP3D platform. The assay was performed according to the manufacturer's protocol with minor modifications to accommodate the use of 384-well plates. The magnetic beads and antibody solutions were diluted 1:1 and used at half volume, and the streptavidin-phycoerythrin was used at half volume. Equal amounts of RIPA buffer and assay buffer

were used in the preparation of the standards and blanks. Homogenate samples were thawed and stored on ice. Samples were diluted to 0.3 mg/mL total protein using RIPA buffer, allowing 7.5 µg total protein per well, and assayed in technical triplicate.

### ***Cytokine profile data cleaning***

The Luminex Xponent software was used to interpolate sample cytokine concentrations from 5-point logistic standard curves. Concentrations below the detection limit ( $< 3.2\text{pg/mL}$ ) were assigned 0 pg/mL. The raw concentration data was processed using an automated in-house pipeline, available from GitHub at <https://github.com/elizabethproctor/Luminex-Data-Cleaning> (Version 1.02). Briefly, the pipeline removes readings generated from less than 20 beads (4 observations in the current dataset) and calculates the pairwise differences of the remaining technical triplicates. If the difference between one replicate is greater than twice the distance between the other two, that replicate is removed from the analysis. The average of the remaining technical replicates for each cytokine is then calculated for the final dataset for use in subsequent multivariate analyses. Following the automated data cleaning, we removed entire cytokines from the dataset if over half the readings were 0 pg/mL in a pattern that did not partition between experimental groups, such as disease or timepoint.

### ***Partial least squares modeling***

Cytokine signatures were constructed using the linear, supervised multivariate mathematical modeling tool partial least squares (PLS).<sup>195,196</sup> We chose PLS to account for the highly interdependent nature of cytokine expression and signaling. PLS allows for the identification of significant multivariate changes in correlative predictors (here, the cytokines) as they relate to a dependent response or group (e.g., timepoint). This aim is achieved by building linear combinations of the predictors (latent variables, LVs)

that maximize the covariation between the predictors and the response. This maximization of multivariate covariance in predictors with response allows us to identify subtle but meaningful patterns in cytokine expression that are undetectable using univariate analysis methods that are unsuitable for highly correlative variables.

Partial least squares regression (PLSR) was conducted for prediction of continuous numerical outcomes, such as timepoint, while partial least squares discriminant analysis (PLS-DA) was used in the discrimination of experimental groups, such as disease versus control. PLS models were built in R using the *ropls* package<sup>197</sup>. Cytokine data were mean-centered and unit-variance scaled prior to PLS modeling. To generate each model, the optimal number of latent variables was determined by repeated random subsampling cross-validation. Cross-validation test sets were randomly generated using 1/3 of the dataset if the number of samples used to build the model was >30 or 1/5 of the dataset if samples <30. Cross-validation was repeated 100 times. For every iteration, models were built using the training set (data excluded from test set) comprised of either 1, 2, 3, 4, or 5 LVs. The resulting models were used to predict the group identity or response value of each sample in the test set to estimate classification accuracy (in PLS-DA) or root mean squared error of cross validation (RMSECV) (in PLSR). RMSECV was calculated by:

$$RMSECV = \sqrt{\frac{\sum_{j=1}^n (P_j - A_j)^2}{n}}$$

Where n is the number of samples in the test set, P is the predicted value, and A is the actual value of the jth sample. The test/training set was randomly regenerated for the following iterations, and the average of the estimated classification accuracy or RMSECV following cross-validation was calculated for each of the 1, 2, 3, 4, or 5 LV PLS models. The model with the number of LVs resulting in the best accuracy/ lowest error was chosen for subsequent analysis and significance testing. A model's significance was calculated using a permutation test. For each iteration of the permutation test, the group identities or responses were randomly shuffled among samples, preserving the data landscape of the cytokine profiles while creating

randomized associations. Cross-validation was performed as described previously, preserving the number of latent variables comprising the “real” model, to estimate the true random accuracy. The p-value of the optimized experimental model was then calculated by comparison with the mean and standard deviation of the distribution of random models’ accuracy. For PLS models containing 1 latent variable, the second latent variable is shown in the scores plot for ease of visualization but was not included in the calculation of error, p-value, or Variable Importance in Projection (VIP) scores. Models presented in this study were orthogonalized for improved interpretability. Orthogonalization maximally projects covariation of the measured cytokines with the response to the first latent variable, prioritizing this covariation over variation in the measured cytokines between samples.<sup>198</sup> We identified key differential cytokines by their variable importance in projection (VIP) score, a measure of a variable’s normalized contribution to the predictive accuracy of the model across all latent variables.<sup>199</sup> Loadings on the first latent variable of cytokines with VIP score > 1, indicating greater than average contribution to the model, are designated as the cytokine signature of the given outcome (e.g. AD progression).

### ***Primary cell culture***

Primary hippocampal neuron and astrocyte cultures were generated from P0 CD1 neonates. Pups were sacrificed by decapitation using surgical scissors, and the brains were removed and placed in pre-chilled sterile dissection medium (HEPES buffered Hanks’ Balanced Salt solution, pH 7.8) on ice. Hippocampi were isolated and placed into a sterile Eppendorf tube containing cold dissection medium following the removal of meninges. For each cell culture experiment, hippocampi from 6-8 neonates were combined. The tube was centrifuged briefly, and the dissection medium was aspirated. Warm neuronal plating medium (Neurobasal Plus, 10% FBS, 1X GlutaMAX, 1X Penicillin-Streptomycin (Gibco): for neuron cultures) or glial medium (DMEM/F12, 20% FBS, 1X Penicillin-Streptomycin, 1mM Sodium

Pyruvate (Gibco), 10 ng/mL Epithelial Growth Factor: for astrocyte cultures) was added to the tube. The sample was manually triturated with a p1000 pipet followed by a p200 pipet.

For neuron cultures, the total cell concentration was measured using the Countess II automated cell counter (Invitrogen), and  $5.47 \times 10^5$  cells/cm<sup>2</sup> were plated in each well of a poly-D-lysine-coated Seahorse XFe24 V7 PS Cell Culture Microplate (Agilent) or a 24-well tissue culture plate. Following cell attachment 2-4 hours after neuron plating, plating medium was removed and neuronal culture medium was added (Neurobasal Plus, 1X B27 Plus supplement, 1X GlutaMAX, 1X Penicillin-Streptomycin (Gibco)). Half of the neuronal culture medium was changed after 5 days, and all the neuronal medium was changed on day 9-10 with the addition of experimental treatments. Neuron cultures were assayed or lysed on day 12-13.

For astrocyte cultures, the cell solution was transferred to a poly-D-lysine (Gibco)-coated tissue culture flask with additional glial medium. Glial medium in astrocyte culture flasks was replaced every 2-3 days until cells reached confluency. Flasks were then placed on an orbital shaker in a cell culture incubator for 2 hours at 180 rpm, and the cell culture medium containing non-adherent cells was removed. The remaining adherent astrocytes were washed with 1X PBS, detached using 0.05% trypsin-EDTA, quenched with fresh glial medium, and evenly distributed into the wells of a poly-D-lysine-coated 6-well tissue culture plate. Glial medium was switched every 2-3 days and treatments were applied at 50% confluency in the 6-well plates. All cell culture plates (neurons and astrocytes) were maintained at 37°C and 5% CO<sub>2</sub>.

### ***Cytokine stimulation of primary culture***

The up-regulated Alzheimer's disease-specific cytokine profile of IFN $\gamma$ , IP-10, and IL-9, as determined by the multivariate modeling, was applied to primary neuron and astrocyte cultures derived from CD1 P0 neonates. The combination cytokine treatment was applied 72 hours prior to experimentation in levels proportional to the concentrations we measured in 5xFAD 180-day hippocampus samples. Concentrations were centered in the nanomolar range previously used to study acute cytokine responses in

neuron cultures.<sup>200,201</sup> Recombinant murine cytokines were purchased from Peprotech, IFN- $\gamma$  (cat 315-05), IP-10 (cat 250-16), and IL-9 (cat 219-19), and reconstituted to 1 mg/mL in sterile water and diluted to 250  $\mu$ g/mL (IL-9) or 10  $\mu$ g/mL (IFN $\gamma$  and IP-10) in 0.1% cell-culture grade bovine serum albumin (Sigma A9418) in 1X PBS. 5nM IFN $\gamma$ , 12nM IP-10, and 500nM IL-9 or an equal amount of 0.1% bovine serum albumin vehicle were added to the appropriate neuronal or glial cell culture medium for treatment. Neuron cultures were treated 9 or 10 days after plating, and astrocytes were treated, following the removal of non-adherent cells, at 50% confluency. After a 72-hour stimulation, cells were assayed on the Seahorse XFe24 Extracellular Flux Analyzer or lysed for RNA isolation.

#### ***RNA isolation and NanoString nCounter analysis.***

Cytokine- or vehicle-stimulated primary CD1 astrocyte cultures in 6-well plates and neuron cultures in 24-well plates were lysed and their total RNA extracted using RNeasy Mini Kits (Qiagen 74104) according to the manufacturer's instructions. The lysis of 2 wells of astrocytes or 3 wells of neurons were combined for each biological replicate to minimize technical variation, resulting in N=3 biological replicates for each treatment/cell-type. The RNA content and quality of each sample was determined using the NanoDrop 2000 Spectrophotometer (Thermo). RNA samples had a 260/280 absorbance ratio of 1.9 or greater and a 260/230 ratio of 1.8 or greater, quality control guidelines outlined by NanoString to exclude samples containing protein or organic compound contamination. Targeted gene expression was quantified using NanoString nCounter technology and the Mouse Metabolic Pathways Panel, with the assay performed by the NanoString Proof of Principle Lab (Seattle, Washington) to measure expression of 768 metabolism-relevant genes and 20 common housekeeping genes. The raw expression data were processed using the NanoString nSolver Analysis software. All samples passed quality control (QC) with the default parameters. Data normalization was performed separately for neuron and astrocyte samples. For background thresholding, genes with a raw count less than 20 were reassigned a threshold count of 20, in

order to calculate fold changes to the same baseline reading. Data was normalized using a 2-step positive control and housekeeping gene normalization. For the selection of appropriate housekeeping genes for each cell type, housekeeping genes with counts under 100 were first removed. Then, the housekeeping genes with a coefficient of variation of 10% or less were kept for normalization (5 genes kept for neurons, 6 genes for astrocytes). Using the final normalized astrocyte and neuron expression data, the log<sub>2</sub> fold changes of cytokine versus vehicle treatment comparisons were calculated using the nSolver software. Genes with a significant log<sub>2</sub> fold change, as determined by a p-value of 0.05 or less, were kept for further analysis. Significantly differentially expressed genes were excluded if the average counts for both cytokine and vehicle treatments were both below 30, close to the assigned background threshold of 20.

### ***Construction of protein-protein interaction networks***

Significantly differentially expressed genes in cytokine-treated neurons and astrocytes were used to construct protein-protein interaction networks using the STRING database.<sup>202</sup> Pair-wise gene inputs were given a score based on known and predicted protein interactions from experimental, co-expression, and gene fusion evidence. The Cytoscape StringApp was used for network visualization<sup>203</sup> with the edge-weighted, spring-embedded layout. The nodes of the networks are individual significantly differentially expressed genes. The genes were characterized by their overall functional group.<sup>204</sup> Isolated sub-networks of 4 or fewer genes were removed.

### ***Seahorse Mito Stress Test***

Neuronal mitochondrial function following vehicle or cytokine treatment was characterized on the Seahorse XFe24 Extracellular Flux Analyzer platform (Agilent). The Seahorse Analyzer measures oxygen consumption rate (OCR) to quantify characteristics of mitochondrial function. During the Mito Stress test,

a series of compounds is injected into the cell culture medium to inhibit complexes of the mitochondrial electron transport chain (ETC) to isolate readings of basal respiration, maximal respiration, ATP production, and non-mitochondrial respiration. Following baseline oxygen consumption readings (basal respiration), oligomycin A, an inhibitor of ATP synthase, is added the cell culture medium and the subsequent drop in oxygen consumption corresponds to the mitochondrial ATP production by ATP synthase. The following addition of FCCP, an uncoupling agent that disrupts the mitochondrial membrane potential, allows for uninhibited electron flow, and the resulting increase in oxygen consumption demonstrates the maximal respiration of the mitochondria. Finally, rotenone and antimycin A (inhibitors of complex I and III, respectively, and together considered a mitochondrial poison) are added to disable the electron transport chain and, thus, residual consumption of oxygen is driven by non-mitochondrial processes.

Primary CD1 hippocampal neurons were stimulated with 5 nM IFN $\gamma$ , 12 nM IP-10, and 500 nM IL-9 for 72 hours prior to Seahorse assays. Neuron culture wells were washed with Seahorse assay medium and given fresh assay medium: DMEM (cat 103680-100), 10 mM glucose solution (cat 103577-100), 1 mM pyruvate solution (cat 103578-100), 2 mM glutamine solution (cat 103579-100) (Agilent). Neuron cultures were transferred to a non-CO<sub>2</sub> incubator for 1 hour prior to running the assay. All Seahorse compound stocks were diluted to 50 mM working stocks with assay medium and added to the appropriate Seahorse cartridge ports to give final well concentrations of 4  $\mu$ M oligomycin A, 4  $\mu$ M FCCP, and 1  $\mu$ M of both rotenone and antimycin A after each injection. Following the assay, the neuron culture wells were washed with 1X PBS, and the cells were lysed in 25  $\mu$ L lysis buffer (Millipore 43-040) by manual titration. The total protein content of each lysis sample was quantified using the Pierce BCA Protein Assay Kit (Fisher 23225) according to the manufacturer's instructions in technical triplicate with standards measured on each plate. Total protein content was used to normalize intra-plate variation using the Seahorse Wave software. Individual wells were excluded from subsequent analysis if the cells were not viable (i.e. near-zero OCR measurements) or did not appropriately respond to the compounds (e.g. FCCP did not increase oxygen

consumption). Each biological replicate was an independent Seahorse experiment of neurons derived from a unique group of neonates and was the average measurement (calculated according to Table 2-1) of the readings of 5-10 wells. Final OCR measurements of the biological replicates were normalized to non-mitochondrial respiration to account for batch effects.<sup>205</sup> Two-tailed Student's T Tests were conducted to determine significant differences in basal respiration, maximal respiration, ATP production, and proton leak in OCR measurements between cytokine and vehicle treatments. Statistical significance was determined by a significance level of less than 0.05.

Table 2-1: Calculations of Seahorse Mito Stress Test Assay Measurements

Measurement	Calculation
Non-mitochondrial respiration	Median OCR measurement following rotenone/antimycin A injection
Basal Respiration	Median OCR measurement, prior to the addition of oligomycin A – Non-mitochondrial respiration
ATP production	Basal respiration – minimum OCR measurement following oligomycin A injection
Maximal Respiration	Maximum OCR measurement following FCCP injection – non-mitochondrial respiration
Proton Leak	Minimum OCR measurement following oligomycin A injection – Non-mitochondrial respiration

## Results

### *The cytokine signature of progressive A $\beta$ pathology is distinct from that of healthy aging*

To define the evolution of the immune milieu of the hippocampus over the course of disease progression in the 5xFAD model, we first built a partial least squares regression (PLSR) model to regress timepoint against 5xFAD hippocampal cytokine concentrations (Fig. 2-1A). We chose to use a multivariate modeling method to identify patterns of cytokine expression rather than identify individual cytokines that correlate with age or genotype because a univariate analysis both cannot resolve differences in the evolution of the complex immune milieu (Supplementary Figure 2-1) and also is a mathematically incorrect choice

to model the underlying biology due to the highly interdependent nature of cytokine expression and signaling. We identified the above-average contributors to the predictive accuracy of our model (2 latent variables, RMSECV=58.4,  $p=10^{-5}$ ) using the variable importance in projection score (Methods). We found that IP-10, IL-9, and IFN- $\gamma$ , are up-regulated over the course of disease, and levels of IL-2 and IL-1 $\alpha$  decrease with disease progression. This signature describes a milieu that enacts a two-pronged increase in neuronal vulnerability: first, by increasing expression of canonically pro-inflammatory cytokines,<sup>206–212</sup> and second, by decreasing expression of cytokines with neuroprotective functions in the brain.<sup>213–215</sup> However, subtleties exist in these relationships, some cytokines having both pro- and anti-inflammatory actions, and others whose action is incompletely understood in the brain or in the context of AD.<sup>200,206,216–219</sup>

The cytokine signature of advancing A $\beta$  pathology, comprising increased IP-10/CXCL10, IL-9, and IFN- $\gamma$ , describes cytokines of a variety of neurotoxic and neuroprotective functions. IFN- $\gamma$ , largely regarded as a pro-inflammatory cytokine, activates immune cells and induces antiproliferative and proapoptotic functions in cancer and infection.<sup>220,221</sup> However, in the brain, IFN- $\gamma$  also displays a variety of protective functions.<sup>221</sup> IFN- $\gamma$  overexpression decreases A $\beta$  deposits through a promotion of phagocytosis by increased complement signaling and glial activation.<sup>222</sup> Similarly, IFN- $\gamma$  treatment restores the A $\beta$  phagocytic ability of microglia with dampened immune responses<sup>101</sup> and induces a neuroprotective microglial phenotype.<sup>223</sup> On the other hand, microglial activation by IFN- $\gamma$  can produce nitric oxide and contribute to neurodegeneration, as well as increase complement signaling associated with aberrant engulfment of synapses.<sup>221</sup> IFN- $\gamma$  directly affects neurons, reducing dendrite length and impairing synapse formation,<sup>224–226</sup> and can be neurotoxic.<sup>227</sup> IP-10/CXCL10 increases intracellular calcium levels and spontaneous activity in primary rodent neuron cultures.<sup>228–230</sup> Acute IP-10 treatments impair synaptic plasticity in mouse hippocampal slices<sup>231</sup> and induce apoptosis in human fetal neurons.<sup>232,233</sup> In contrast to IFN- $\gamma$  and IP-10, the function of IL-9 is not fully understood in brain. IL-9 has not previously been identified as relevant to AD, although variety of conflicting roles in development and other disease contexts have

been reported, the most well-documented of which is its antiapoptotic effect on numerous cell types,<sup>234</sup> including neurons.<sup>235</sup>

To distinguish the evolving milieu of immune cues in AD onset and progression from that of normal aging, which also exhibits an immune component (“inflammaging”),<sup>93,236,237</sup> we constructed a PLSR model regressing timepoint against cytokines profiles of wild-type samples (Fig. 2-1B). The key contributors to the predictive accuracy of the model (1 latent variable, RMSECV=51.9,  $p=10^{-5}$ ) are increased IFN- $\gamma$  and KC/CXCL1 and decreased MIP-1 $\alpha$  and IL-13 with advancing age. Notably, the up-regulated immune cues in healthy aging and AD are largely non-overlapping, indicating that AD onset and progression involves pathological changes in a distinct set of process from those that change in the normal course of aging. Emphasizing these distinct processes, MIG/CXCL9, while not a key contributor to our A $\beta$  progressive pathology signature, was identified as increasing with disease progression, but was absent in wild-type mice at all timepoints. In contrast, because the majority of cytokine species were down-regulated with aging in the wild-type model, all down-regulated species in the AD signature discussed above are also decreasing in healthy aging, suggesting a natural decrease in immune responsiveness or surveillance. However, we note that a key decreasing cytokine in healthy aging, MIP-1 $\alpha$ /CCL3, increases with disease, although not as a key contributor to the AD signature. We conclude that while similarities exist between the immune milieus of healthy aging and AD, which is fitting for a disease with the primary risk factor of age, they are minimally overlapping, supporting a fundamental shift in the brain rather than accelerated aging, as has been suggested by some.<sup>238</sup>

These models independently assess how cytokine levels change with the progression of aging or of AD. While there are distinct differences in the disease and wild-type models, particularly in the contributions of IP-10, IL-9, and MIP-1 $\alpha$ , there is also overlap, and any comparison of such separately-constructed models is necessarily qualitative. We observed cytokines implicated in AD, such as CXCL1

and IL-13,<sup>239–243</sup> to also be important for the prediction of age in wild-type samples. In order to directly and quantitatively compare the hippocampal immune milieu in AD or normal aging, we next constructed PLS models to differentiate the AD and wild-type groups at each. We note that we do not observe separation by sex on either latent variable in the PLSR models (Fig. 2-1A, B), indicating that any underlying sex differences in cytokine expression present in this mouse model are not driving the predictive normal aging or disease progression signatures.

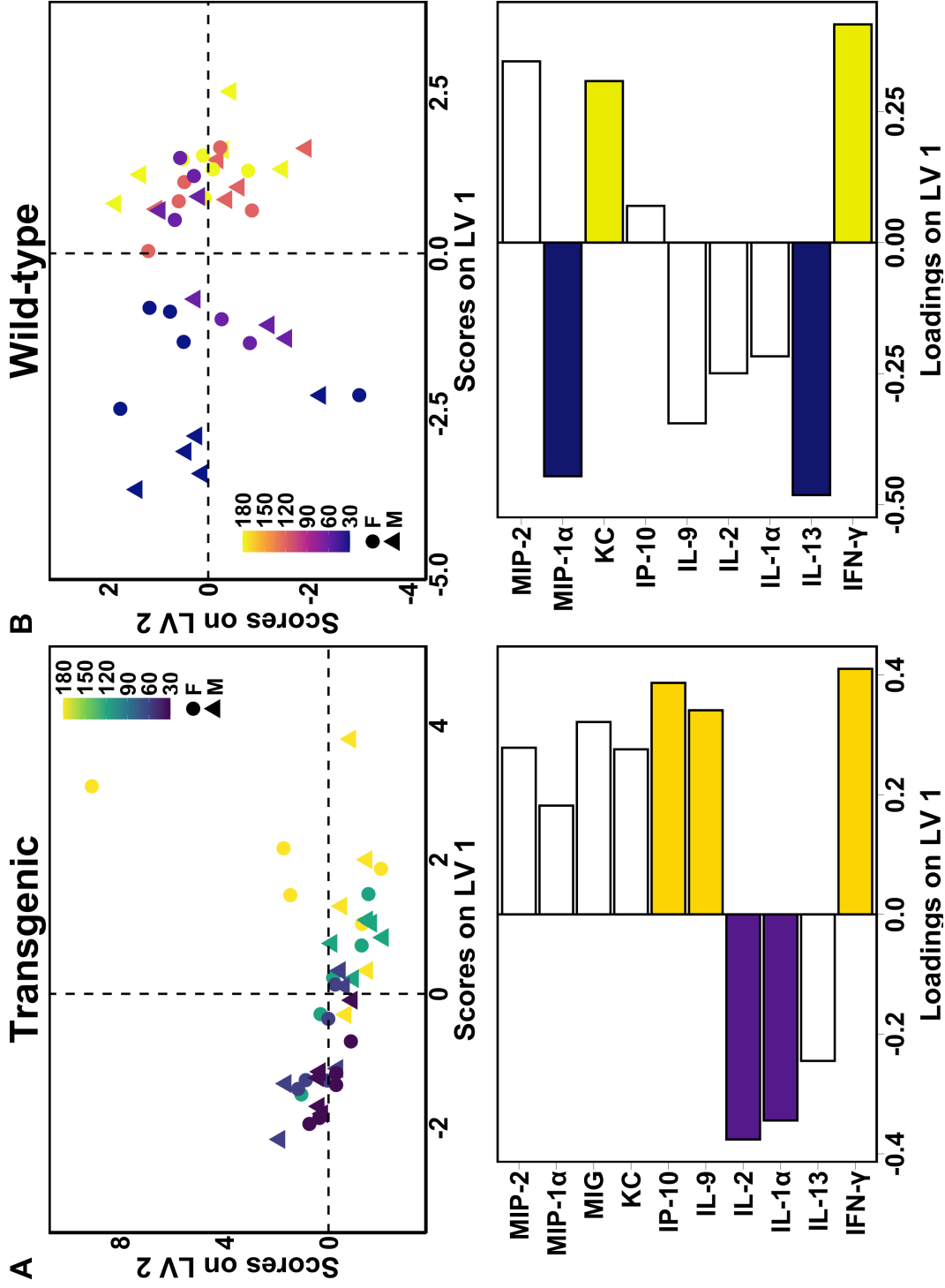


**Figure 2-1: Unique cytokine signatures predict aging in 5xFAD and wild-type hippocampi.** Scores plot (top) and LV1 loadings plot (bottom) of PLSR models regressing cytokine concentrations against timepoint in (A) 5xFAD hippocampus (2 LV, RMSECV: 58.4, p-value: <0.00001) and (B) wild-type hippocampus (1 LV, RMSECV: 51.9, p-value: 0.00001). Colored loadings signify cytokines with a VIP score > 1. Each point represents a single mouse with shape indicating the animal's sex and color indicating age at the time of tissue collection. PLS modeling is comparative and not absolute: older mice (positive scores on LV1) feature up-regulation of cytokines with positive loadings and down-regulation of cytokines with negative loadings, as compared to younger mice (negative scores on LV1)

### *AD mice exhibit neuroimmune over-activation late in the disease timeline*

To directly compare cytokine signatures of AD and wild-type control mice, we constructed partial least square discriminant analysis (PLS-DA) models to predict disease status at 30 or 180 days, representing prodromal and fully symptomatic AD, respectively. In 30-day-old hippocampus, prior to intracellular deposition of A $\beta$ , we discriminate AD from wild-type with 83% accuracy and high significance (p-value: <0.005, Fig. 2-2A). The strongest contributors to predictive accuracy, MIP-1 $\alpha$  and IL-9, are both down-regulated in AD before the development of pathology, in comparison to healthy controls. When we compare this result with the AD- and aging-specific progression signatures (Fig. 2-1), we find that both MIP-1 $\alpha$  and IL-9 decrease with healthy aging but increase with disease progression.

The 180-day PLS-DA model features a similarly high predictive accuracy (80%) and significance (p-value: <0.01, Fig. 2-2B) in discriminating cytokine expression in AD versus wild-type control hippocampus. The model describes an overall increase in cytokine levels in late-stage AD as compared to healthy controls. The strongest contributors to predictive accuracy were IL-9, IFN- $\gamma$ , and MIP-1 $\alpha$ , all up-regulated in AD. These results are in agreement with the AD- and aging-specific progression signatures, where IL-9 and MIP-1 $\alpha$  both increased with AD progression but decreased with healthy aging. While IFN- $\gamma$  increased in both AD progression and healthy aging, this direct comparison of AD with wild-type control at the 180-day time point demonstrates that the increase in disease is significantly more pronounced than that in healthy aging, a point that cannot be drawn from the comparison of the two separately-derived models in Figure 2-1. A similar point can be drawn for KC/CXCL1, which was also up-regulated in both AD progression and healthy aging but is significantly higher in disease samples at 180 days.

In total, these models reflect low immune activity at an early age in the AD brain, which may suggest prodromal compensatory regulatory mechanisms and increased vulnerability to disease. With the onset of disease pathology and fully symptomatic AD, the AD brain exhibits a significant increase in overall cytokine expression as compared to wild-type control, with a specific pro-inflammatory signature that

agrees with the time-evolution signature of A $\beta$  pathology progression when considered outside of comparison to healthy aging. As in our models of disease progression, we do not observe separation by sex on either latent variable in the PLSR models (Fig. 2A, B), indicating that any underlying sex differences in cytokine expression present in this mouse model are not driving the A $\beta$  pathology signatures at either time point.

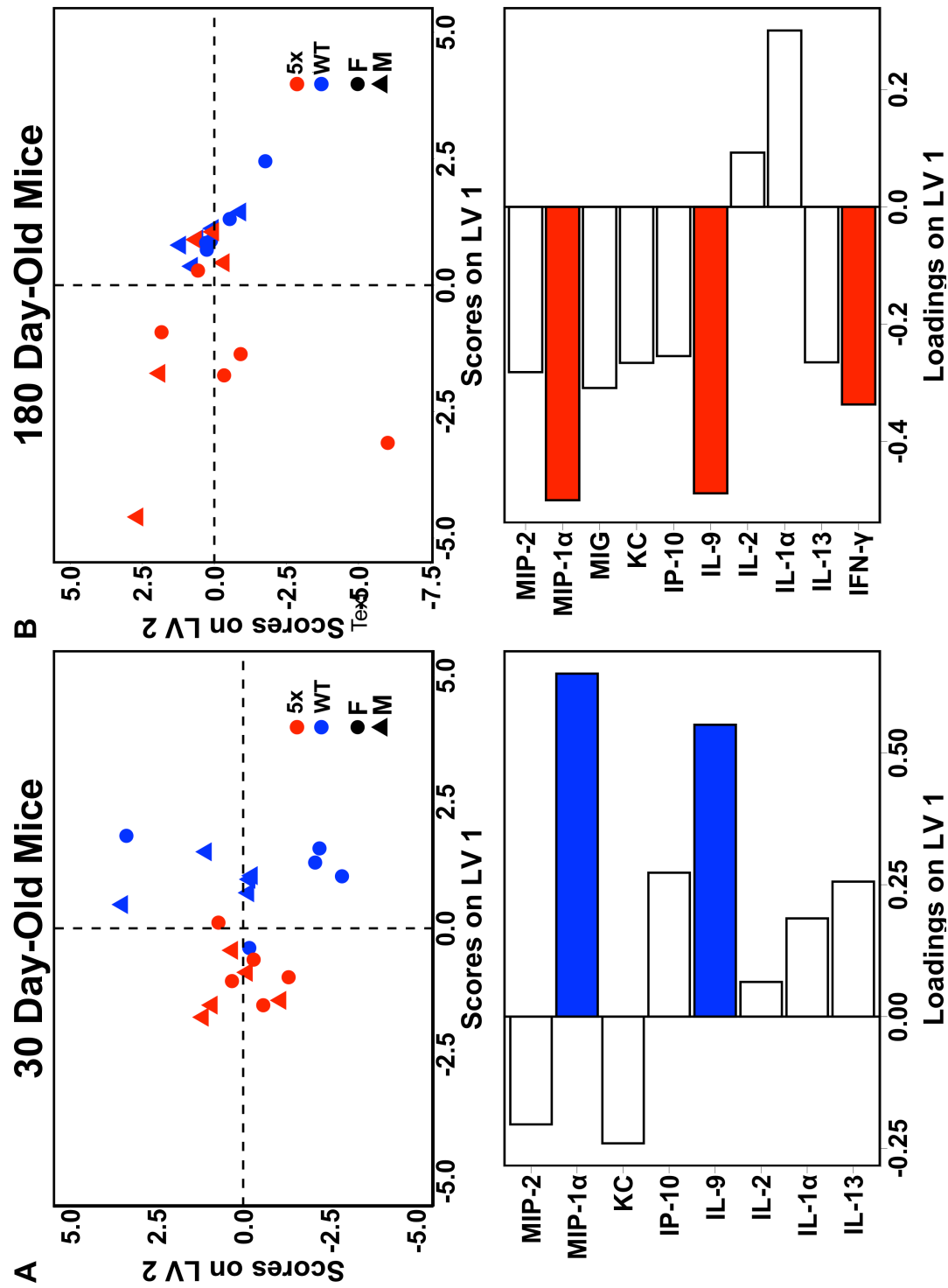


**Figure 2-2: Cytokines are up-regulated in aged 5xFAD hippocampus but dampened in comparison to wild-type prior to protein deposition.** PLS-DA scores plot (top) and LV1 loadings plot (bottom) of (A) 30-day 5xFAD vs wild-type hippocampus (2 LV, accuracy: 83%, p-value: <0.005) and (B) 180-day 5xFAD vs wild-type hippocampus (3 LV, accuracy: 80%, p-value: <0.01). Colored cytokine loadings signify cytokines with a VIP score > 1. Each point represents a single mouse with shape indicating the animal's sex and color indicating genotype. PLS modeling is comparative and not absolute: 5xFAD mice (negative scores) feature down-regulation of cytokines with positive loadings and up-regulation of cytokines with negative scores, as compared to wild-type mice (positive scores on LV1).

### ***Cytokine signature of progressive A $\beta$ pathology induced widespread changes in neuron metabolic gene expression***

The cytokine signature of A $\beta$  progression represents the evolving neuroimmune milieu in the AD brain. We next endeavored to characterize the effect of this evolving milieu on neuron health. We approached this question from two directions: the direct effect of the AD cytokine signature on neurons, and the indirect effect of loss of support to neurons *via* astrocyte dysfunction.<sup>244,245</sup> Astrocytes provide critical metabolic support to neurons, and disruption of this support would lead to increased neuronal vulnerability to insult. Importantly, we use the outbred, wild-type CD1 mouse to generate our cultures, in order to examine the effect of the cytokine signature of AD progression in the absence of AD pathology, aiming to isolate the independent effect of the immune cues and eliminate any confounding factors caused by the overexpression of amyloid-related proteins in the 5xFAD mouse model.<sup>34</sup>

We stimulated cultures with recombinant IFN- $\gamma$ , IP-10, and IL-9, in concentrations proportional to those measured in the 5xFAD hippocampus at 180 days of age and analyzed the expression of metabolism-associated genes (Methods). Metabolic and immune dysregulation are both early characteristics of the pre-clinical AD brain and are closely linked, contributing to an aggressive “immunometabolic” positive feedback loop that is capable of driving pathology progression.<sup>190</sup> Cellular metabolism also provides a critical readout of cellular health, allowing fine-tuned assessment of the large “grey area” between live, healthy cells and cell death. While gene transcript levels are not necessarily representative of the levels of their corresponding proteins, the acute response measured in these primary cell culture assays provides an understanding of the primary processes initiated with exposure to the immune environment associated with A $\beta$  progressive pathology.

As AD is a neurodegenerative disease that selectively affects neurons, we first investigated the direct effect of the cytokine signature of A $\beta$  pathology progression on healthy primary neurons. We identified significantly differentially expressed genes in neurons treated with the AD progression cytokine signature compared to vehicle-treated neurons (Supplementary Table 2-1) and analyzed their downstream

protein interactions using the STRING database (Methods). Out of the 155 significantly differentially expressed genes in neurons following cytokine treatment, 80 were included in the main neuron STRING interaction network. The resulting neuron interaction network (Fig. 2-3A) demonstrated a wide variety of affected genes. Unsurprisingly, the genes most substantially affected by cytokine stimulation were associated with immune response. Genes involved in immune response were closely linked to genes involved in stress response, autophagy, and protein degradation processes, all of which are key dysregulated systems in AD.<sup>38</sup> The network of affected neuronal transcripts also includes a down-regulated cluster of genes traditionally associated with the cell cycle. While neurons are post-mitotic cells, many of these genes have known functions in post-mitotic cells, including neurons: Plk1, cdc20, and kif2c are involved in the regulation of synapses, dendrites, and the cytoskeleton.<sup>246-248</sup> Cdk9 and npml are implicated in cell survival,<sup>249-252</sup> and ccna2 is associated with DNA repair in aging, rRNA homeostasis, and cellular senescence.<sup>253-255</sup> The downregulation of this cluster of genes with treatment suggests increased neuronal and synaptic vulnerability to injury. Strikingly, the neuron network includes a grouping of primarily down-regulated genes involved in mitochondrial respiration, including subunits of every complex involved in the electron transport chain. The significantly down-regulated genes include the subunits Ndufa1 (complex I), Sdhc (complex II), Uqcr11 (complex III), Ndufa4 (Complex IV), and Atp5d (ATP synthase or complex V).

The interaction network of differentially expressed genes (Supplementary Table 2-2) in cytokine-treated astrocytes compared to vehicle-treated astrocytes (Fig. 2-3B) demonstrated that fewer astrocyte genes were affected by the cytokine treatment than in neurons, and those that were affected are primarily involved in immune response. Out of the 54 significantly differentially expressed genes in astrocytes following cytokine treatment, 23 were included in the main STRING interaction network. However, hk3, involved in glycolysis, was up-regulated in the astrocytes, which may indicate activation of a response to increase neuronal metabolic support.<sup>256,257</sup> The astrocyte network also features a cluster of up-regulated proteasome related genes, many of which were also featured in the neuron network. Proteasomes are involved in the degradation of A $\beta$ , and their dysfunction has been linked to the abnormal accumulation of

pathological proteins in AD.<sup>258-260</sup> The differential gene regulation indicates that AD-associated cytokine cues may activate astrocytes to bolster neuronal support functions, but the response to the AD signature was less robust than in neurons.

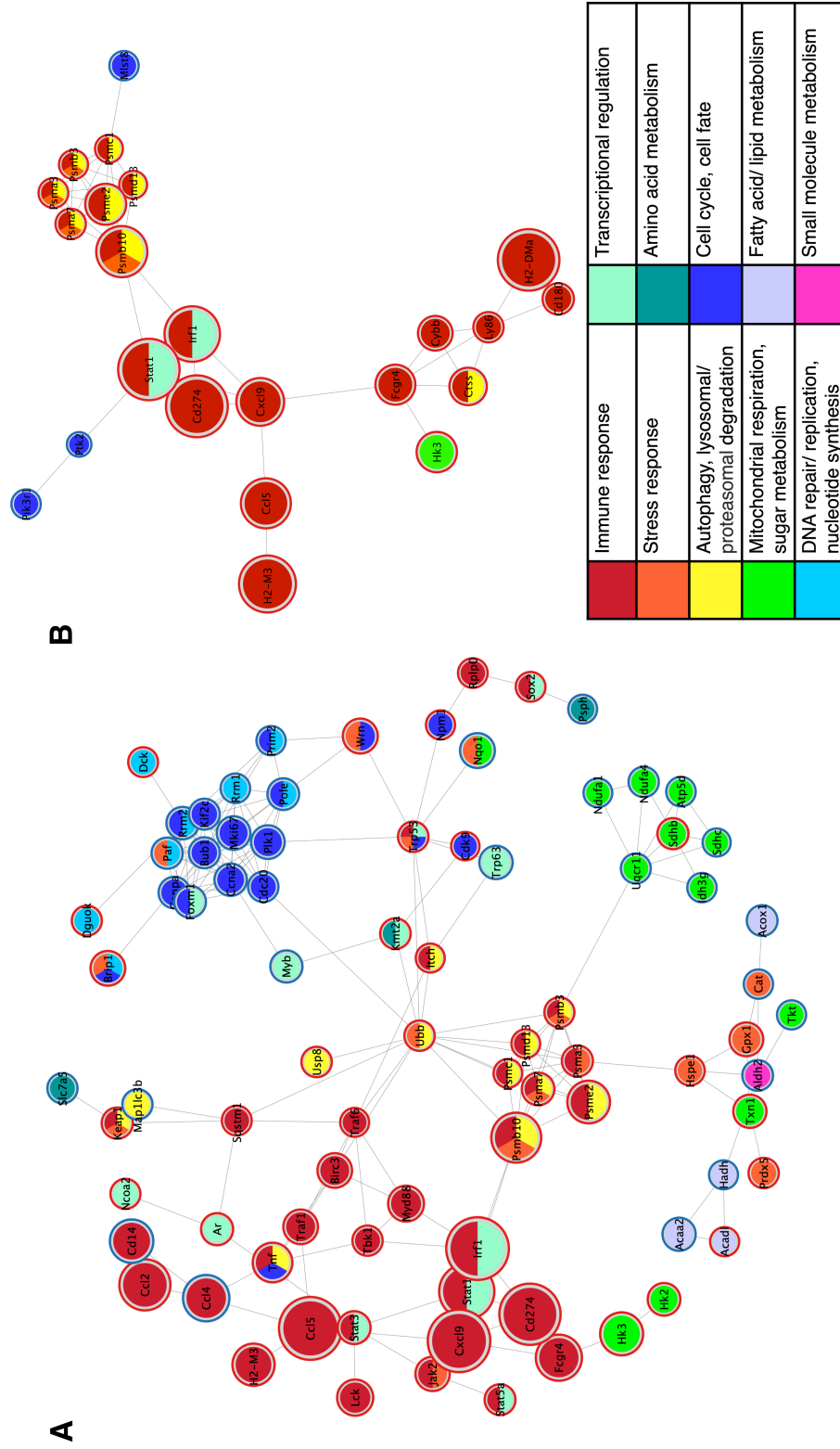


**Figure 2-3: Cytokine signature of AD progression generates widespread gene expression changes in healthy neurons.** STRING protein-protein interaction network of significantly differentially expressed genes in (A) neurons and (B) astrocytes in cytokine signature-treated primary cultures compared to vehicle controls. Individual genes, represented as nodes, are colored by their primary function(s) and sized according to the log<sub>2</sub> fold change between treatments. Nodes are outlined in red or blue to indicate up- or down-regulation, respectively, with treatment. Network edges denote the STRING interaction score, with a shorter edge length indicating a stronger interaction. Thus, nodes that are closer together are more strongly linked.

### *A $\beta$ pathology-specific cytokine signature impairs neuronal metabolism*

Treatment with the cytokine signature of AD progression resulted in marked down-regulation of sub-units in every electron transport chain complex. The resulting reduction of components responsible for mitochondrial respiration would result in significant impairment of neuronal oxidative phosphorylation. We stimulated primary neurons with the AD progression signature of IFN- $\gamma$ , IP-10, and IL-9 and quantified parameters of mitochondrial function through oxygen consumption measurements on the Seahorse Extracellular Flux Analyzer (Agilent) using the Mito Stress Test Assay (Methods).

We found an overall decrease in oxygen consumption as a result of cytokine treatment compared to the vehicle control (Fig. 2-4). Basal respiration was significantly decreased in cytokine treated neurons (Fig. 2-4B, p-value: 0.031). Maximal respiration, induced by the mitochondrial membrane uncoupling agent FCCP, was similarly decreased with cytokine treatment (Fig. 2-4C, p-value= 0.012). ATP production also decreased following cytokine treatment, although this finding was not statistically significant (Fig. 2-4D, p-value: 0.065). Finally, the proton leak, the mitochondrial oxygen consumption not due to the action of ATP synthase, was also significantly reduced with treatment (Fig. 2-4E, p-value= 0.00021). Overall, the observed functional decrease in neuron mitochondrial respiration is in agreement with the gene expression findings of down-regulated electron transport chain complexes. A variety of subunits from all 5 complexes were down-regulated in the neuron cultures with IFN- $\gamma$ , IP-10, and IL-9 treatment, and likely contributed the overall reduction in mitochondrial electron transport chain performance that negatively impacts neuronal health and resilience.

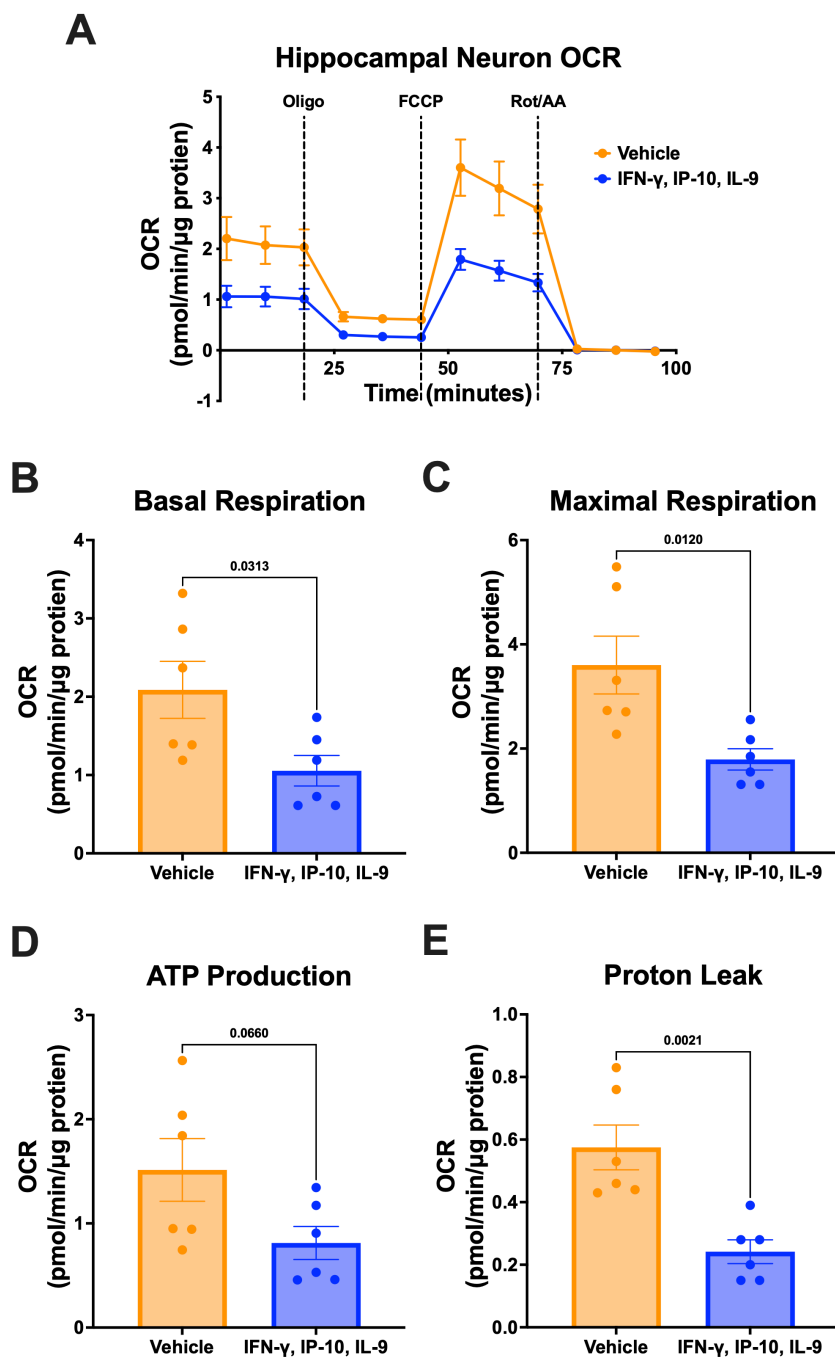


**Figure 2-4: Wild-type primary hippocampal neurons treated with cytokine signature of AD progression exhibit decreased mitochondrial respiration.** (A) Oxygen consumption during Seahorse Mito Stress Test following 72-hour vehicle (blue) or combination IFN- $\gamma$ , IP-10, IL-9 treatment (orange) and corresponding measurements of (B) basal respiration (p-value= 0.031), (C) maximal respiration (p-value= 0.012), (D) ATP production (p-value= 0.065), and (E) proton leak (p-value= 0.00021). P-values calculated by two-tailed student's t-tests. Results generated from the average of 6 independent biological experiments with 5-10 technical replicates for each of treatment and control. Seahorse oxygen consumption rate measurements are displayed as mean  $\pm$  standard error of the mean.

## Discussion

An incomplete understanding of AD etiology has prevented the development of successful strategies for prevention and treatment. Immune and metabolic dysfunction are among the earliest detectable pathologies in the disease, coinciding with or by some accounts preceding protein deposition.<sup>3,191</sup> A greater understanding of the mechanisms underlying immune and metabolic dysfunction in AD has the potential to facilitate early interference to ameliorate disease. However, the complex and all-encompassing nature of entangled beneficial and harmful immune responses with intercellular communication and neuronal support functions complicate the identification of robust and effective targets. Recent systems biology approaches address this issue by characterizing the molecular-, cellular-, and tissue-level processes disrupted in AD, but have rarely gone beyond descriptive findings of altered cellular pathways.<sup>38</sup> Here, we identified an AD-specific cytokine signature predictive of disease progression that defines the evolving immune state in the hippocampus, a primary site of neurodegeneration in AD and one of the earliest brain regions affected by the disease. Our signature was not exclusive to or built using a single cell type, instead representing the overall immunological milieu promoting AD progression. Notably, our signature does not include traditional pro-inflammatory cytokines associated with AD, such as TNF- $\alpha$ , IL-6, and IL-1 $\beta$ .<sup>3</sup> While these cytokines are likely present in the tissue, their levels were below our threshold for inclusion in the model. While the individual members of the strong up-regulated signature we identified, IFN- $\gamma$ , IP-10, and IL-9, have been linked to AD previously,<sup>242,261–264</sup> with the possible exception of IP-10 they have not been appreciated as playing a strong role in AD progression. Further, the pathological role of these cytokines in neuronal metabolic dysfunction has never before been identified. We attribute our identifications of these cytokines to the multivariate nature of our model: the synergistic action of these cytokine cues drove the predictive power of our model, emphasizing the importance of considering emergent manifestation of network activities when identifying potential critical drivers of disease with possible strategic value as therapeutic targets.

Astrocytes and neurons are metabolically coupled, and dysfunction in astrocytes could predispose neurons to injury and death. We studied the independent effects of our cytokine signature of AD progression on both cell types to identify potential pathways of neuronal injury and subsequent contribution to disease. Receptors for IFN- $\gamma$ , IP-10, and IL-9 are found on both neurons<sup>265–268</sup> and astrocytes,<sup>71,269–271</sup> supporting the study of their combined effect on each of these cell types. While A $\beta$  progressive pathology signature-stimulated changes in astrocyte gene expression were limited and primarily related to immune response, we identified numerous differentially expressed genes in neurons with known AD implications, such as regulation of synapse plasticity and dendrite projection and tryptophan and mitochondrial metabolism. We note that these assays were specifically performed in healthy, wild-type primary neuron cultures in the absence of any pre-existing AD pathology. Our objective was to determine the capacity of the AD progression cytokine signature to affect neuron health and viability, which is most cleanly demonstrated in the absence of any other AD-promoting factors. The fact that treatment with the cytokine signature altered expression of genes previously linked to Alzheimer's disease, in the direction that would promote disease and absent of any other AD-related factors present, demonstrates the power of our model to extract patterns of effectors with discernible value for mechanistic insight. These insights have broad potential toward predicting diverse types of outcomes in AD and AD risk; we have previously used the partial least squares method to identify brain cytokine signatures predictive of systemic metabolism<sup>272</sup> and to discover a previously unknown neurotoxic effect of VEGF in the presence of A $\beta$  aggregates.<sup>273</sup>

The suppression of neuronal mitochondrial metabolism by the cytokine signature of AD progression indicates that, at baseline under normal energy demands, neuronal metabolism in this immune environment does not function efficiently and would not be able to adequately respond to an increased energy demand when presented with a disease insult such as AD-related proteinopathy. The energy demands of the brain are great, far exceeding other organs of the body, and are primarily achieved through glucose metabolism.<sup>192</sup> Impaired metabolic capacity in neurons could predispose to neuronal injury and

neurodegeneration by an inability to sustain the energetic demand of synapse activity and other neuronal functions while under stress.<sup>192</sup>

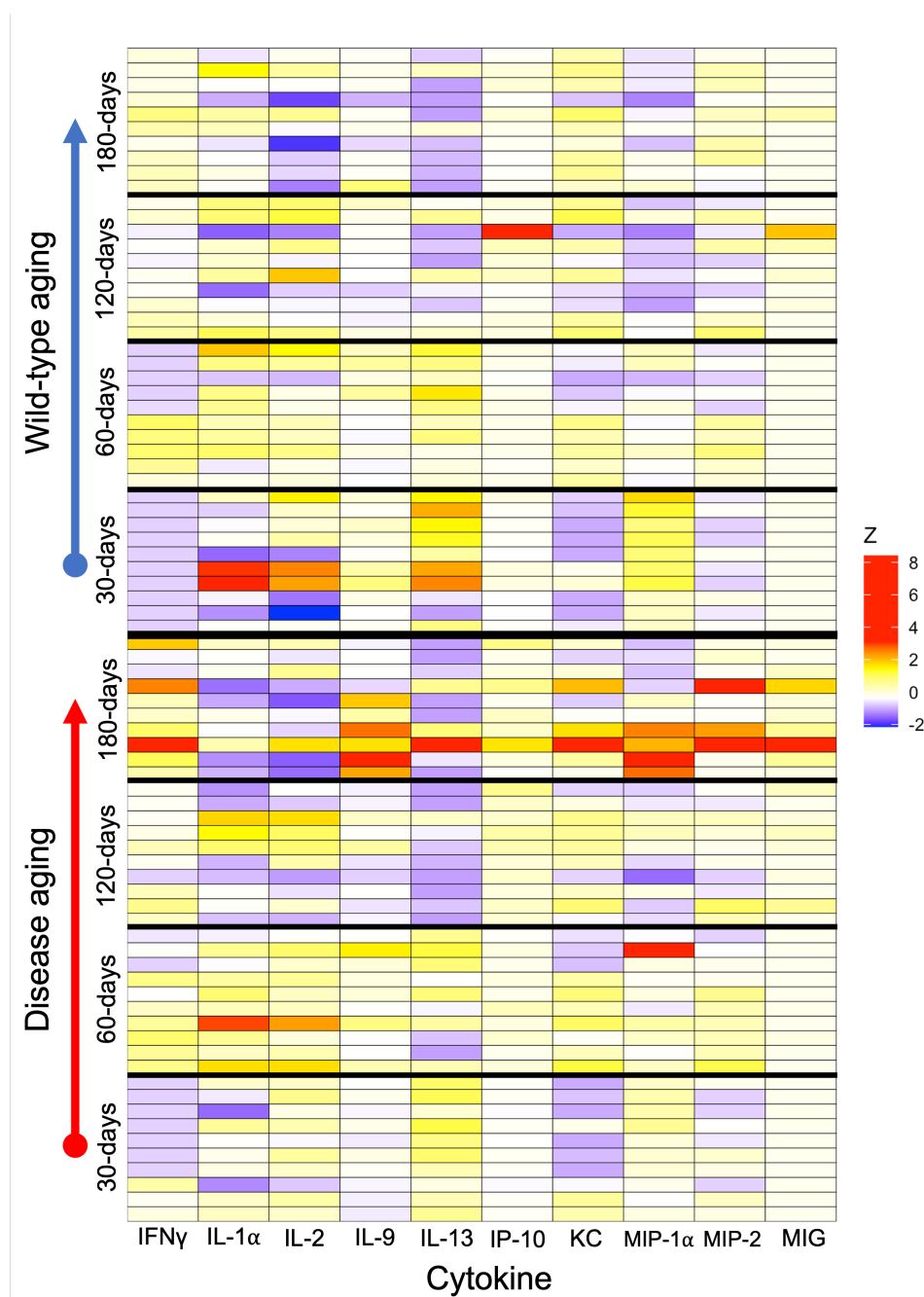
The cytokines comprising our signature of A $\beta$  pathology progression have not previously been connected to impaired metabolism. However, dysregulated immune signaling and metabolic impairment are both well-known features of AD etiology, and their synergistic connection has been established in other tissues and diseases such as cancer and type 2 diabetes.<sup>274,275</sup> In AD, glial activation and the accompanying cytokine release causes downstream metabolic stress,<sup>276</sup> which is largely characterized by an increase in reactive oxygen species (ROS) and decreased ETC activity.<sup>191,277–279</sup> While not directly connected to neuroinflammation or cytokine signaling, multiple subunits of mitochondrial ETC complexes are down-regulated in the AD brain,<sup>190</sup> including in the hippocampus,<sup>280</sup> temporal cortex,<sup>281</sup> and frontal cortex.<sup>282,283</sup> Outside of the brain, cytokines have been implicated in the reduced expression of ETC complex genes and impaired mitochondrial respiration in cultures of other cell-types, such as HepG2 cells (a cell line originating from a hepatocellular carcinoma),<sup>284,285</sup> cardiomyocytes,<sup>286</sup> and hepatocytes<sup>287,288</sup>.

Additionally, all three cytokines in our signature of A $\beta$ , IFN- $\gamma$ , IP-10, and IL-9, pathology progression are known to signal through the JAK/STAT pathway, which further regulates immune response by inducing gene expression of additional pro-inflammatory cytokines.<sup>289</sup> While this shared downstream signaling of the signature cytokines may be part of the mechanism of the functional phenotype we observe, the initial binding events to their distinct respective receptors, and the varying actions of those receptors, introduces a high level of complexity that obscures the specific additive and/or synergistic mechanisms by which the A $\beta$  progressive pathology signature cytokines in concert affect mitochondrial function. While the association between cytokine signaling and regulation of mitochondrial bioenergetics has not yet been explored in the brain, in other tissues pro-inflammatory cytokine signaling has been linked with decreased levels of peroxisome proliferator-activated receptor- $\gamma$  coactivator 1- $\alpha$  (PGC-1 $\alpha$ ).<sup>290</sup> PGC-1 $\alpha$  initiates signaling pathways regulating the expression of subunits from all 5 ETC complexes, which we found to be decreased in our gene expression measurements.<sup>291,292</sup> Since PGC-1 $\alpha$  signaling is present in neurons and

PGC-1 $\alpha$  levels are reduced in the AD brain, where its protein levels are negatively correlated with amyloid pathology,<sup>293,294</sup> suggesting a possible new avenue for exploring pathological dysregulation of the immunometabolic connection in AD.

## **Conclusion**

Here, we identified a hippocampal cytokine signature of A $\beta$  pathology progression that is predictive of advancing disease in the 5xFAD mouse model of AD. Exposure to this signature of AD progression was sufficient to initiate mitochondrial dysfunction in primary neuron cultures that was similar to that previously observed in AD, but in the complete absence of AD pathology. The resulting decrease in mitochondrial respiration predisposes neurons to injury and in the presence of a stressor such as proteinopathy could lead to energetic insufficiency and, ultimately, cell death. The cytokines comprising our signature of AD progression have not previously been connected to mitochondrial dysfunction, highlighting the power of a systems biology approach that considers the inter-relatedness of immune signaling. Overall, our findings support the existence of an immunometabolic feedback loop driving neuronal vulnerability in AD. Further investigation is needed to evaluate the relevance of the signature in human AD rather than the mouse model used here, particularly in the presence of tau pathology, which is absent in the 5xFAD model. However, the interdependency and redundancy of cytokine signaling, as well as the differences between mice and humans, make it likely that there is a corresponding human signature capable of driving mitochondrial dysfunction.



**Supplementary Figure 2-1: Heat-map of Z-scored hippocampal cytokine concentrations.** Normalized cytokine concentrations in individual animals from each genotype-age grouping. No individual cytokines emerge as unilaterally up- or down-regulated over the course of disease progression vs. normal aging.

## Introduction to Chapter 3

### From Brain to Dish

In Chapter 3, we are exiting a whole-body system with functional brain vasculature to enter a much more simplified model – the cerebral organoid, generated from pluripotent stem cells: a mini-brain taking up residence in a dish – for the study of human cells and their interactions. In Alzheimer’s disease, where variables such as age, systemic inflammation, lifestyle, and other external-to-brain factors play significant roles in disease onset and progression, whole-organism disease models serve to reproduce many of these variables as well as provide information on emergent outcomes such as cognition. It seems particularly counterintuitive to choose to move from these models to one that excludes key brain cell-types, is limited by diffusion, and only recently took on a whole new cellular identity from immature stemness. But all that considered, these pluripotent stem cells are nothing but remarkable. The human brain is largely a locked boxed, but iPSC-derived cerebral cells allow for their study over months in culture as well as precise genetic manipulation. Three-dimensional cerebral organoid cultures improve cell maturation with increased cell-cell signaling than monolayer culture and exhibit AD pathology reminiscent of the human brain. Over a few short years, many improvements have been made in the application of iPSCs in AD,<sup>295</sup> and studies have included a variety of cell types,<sup>296</sup> including those contained in organoids.<sup>297</sup>

Perhaps the most important advantage of human iPSC-derived models in AD research is the ability to study sporadic disease. This is not limited to the observation of differential function of risk genes in the human cell-context; cerebral organoids derived from sporadic AD patient cells develop A $\beta$  and tau pathology in just a few short weeks or months in the absence of disease-causing mutations. Meanwhile, an aggressive transgenic mouse model overexpressing numerous familial AD-causing mutations develops amyloid plaques in the same time period but never exhibits the abnormal accumulation of hyper-phosphorylated tau into neurofibrillary tangles and, in some models, never even exhibits neuron death. This

is the power of human iPSC-derived organoid models. They will likely never be able to exist in research without the complementary viewpoint of whole-organism animal models, but there is necessary information in a model of human cells expressing human proteins, albeit quite simplified. The human context is especially needed in the case of microglia, where the functional and gene-regulation differences between human and mouse microglia are stark. The first iPSC microglia differentiation protocol was only recently published, in 2016.<sup>298</sup> There have been other protocols developed since then,<sup>155–157</sup> and the field is just starting to work toward incorporating iPSC-derived microglia into organoid models, whether encouraging their development within the organoid<sup>299</sup> or the introduction of separately derived iPSC-microglia into mature organoids.<sup>159,171,300</sup>

The first protocol for deriving microglia-containing organoids was developed in 2018.<sup>299</sup> In the following year, I proposed to generate these organoids myself in an F31 fellowship submission, and perhaps unsurprisingly I received feedback expressing the lack of confidence in my ability to do so, not only from a lack of experience with stem cell and organoid culture, but from the fact that no one at the time had published independent verification of the ability to natively grow microglia in organoids. Importantly, in the brief period of time before resubmission, I grew organoids, validated the presence of microglia with immunostaining and RT-qPCR, and went through the nearly 200 papers that had cited the original publication. Of those papers, 11 were newly published papers independently verifying the existence of the organoid-derived microglia, and I made sure to cite them all. Of course, at that point the concern was no longer the microglia and was instead the organoids' use in the study of AD, as it wasn't yet known how AD pathology would develop over the experimental timeline because at the time no AD organoid studies had been performed. In fact, there still only exist a handful.<sup>165–167,301–305</sup>

When I entered graduate school one of my goals was to work with iPSCs, and having had knowledge of the shortcomings of AD mouse models from my undergraduate years, everything took shape

from there. I recognized that the handful of AD research groups branching out into iPSC work at the time were huge names, but there were so many incredible advantages to them. I wanted to help bring iPSCs to smaller labs, and as a graduate student who largely taught herself iPSC culture and organoid differentiation at the height of the pandemic, I hope I've achieved just that. Interest in organoids and microglia in AD have boomed primarily over the past year, and I am proud of my fledgling graduate student self for pouring over the literature and identifying gaps in the field that may be best explored in organoids. Nonetheless, the project, which has been scaled down a handful of times from its initial creation by an overzealous young researcher, may be the first demonstration of microglia-containing organoids in the AD field.

In the previous chapter, we profiled a broad overview of inflammatory signaling in the AD mouse brain. We identified a cytokine signature that was highly predictive of disease that suppressed mitochondrial respiration in neurons. The effect was observed in the absence of AD pathology in wild-type cells and supports the existence of pathology-independent neuroinflammatory roles in disease progression. It's well appreciated that Alzheimer's disease implacably marches along, driven by a feedback loop of accumulating proteinopathy capable of driving neuroinflammation and the direct accumulation of more pathology (prion-like spread, A $\beta$ -activated kinases, etc.). The subsequent aggravated immune activation worsens pathology and injures neurons, and injured neurons further contribute to immune activation and pathology spread (i.e. the release of pathological tau). These activities continue, exacerbating one another, in a circle. Disrupting the path of disease before pathology can take hold would be a game-changer, but to achieve this goal we need to have a better appreciation for early disease events like our neuron-sensitive cytokine profile. The identification of early cell-to-cell signaling that may confer AD risk offers unique opportunities to disrupt disease. In Chapter 3, we use a human cerebral organoid model of AD to advance our understanding of cell-type specific immune cues that negatively affect neurons.

## Chapter 3

### Alzheimer's Disease Cerebral Organoids Exhibit Dynamic Neuroinflammatory Profiles

#### Abstract

Neuroinflammation and the underlying dysregulated immune responses of microglia actively contribute to the progression and, likely, the initiation of Alzheimer's disease (AD). Fine-tuned therapeutic modulation of immune dysfunction to ameliorate disease cannot be achieved without the characterization of diverse microglial states that initiate unique, and sometimes contradictory, immune responses that evolve over time in chronic inflammatory environments. Because of the functional differences between human and murine microglia, untangling distinct, disease-relevant reactive states and their corresponding effects on pathology or neuronal health may not be possible without the use of human cells. In order to profile shifting microglial states in early AD and identify microglia-specific drivers of disease, we differentiated human induced pluripotent stem cells (iPSCs) carrying a familial AD PSEN2 mutation into cerebral organoids and quantified the changes in cytokine concentrations over time with Luminex XMAP technology. We used partial least squares (PLS) modeling to build cytokine signatures predictive of disease and age to identify key differential patterns of cytokine expression that inform the overall brain immune milieu and quantified the corresponding changes in protein pathology. AD organoids derived from a male and female iPSC line carrying the N141I PSEN2 mutation exhibit opposing cytokine signatures and a different evolution of those signatures with age, with the male organoids demonstrating an overall reduction in cytokine secretion after an initial amplified immune response, while female organoids show a persistent heightened immune response. There was reduced synapse density in the male organoids, which could be rescued upon microglial depletion, whereas larger deposition of amyloid and tissue atrophy occurred in the female organoids. Crucially, these differential effects of dysregulated immune signaling occurred without the accumulation of pathological proteins. In this study, we used microglia-containing AD organoids to

quantitatively characterize an evolving immune milieu, made up of a diverse collection of activation patterns and immune responses, to identify how a dynamic, overall neuroinflammatory state negatively impacts neuronal health and the cell-specific contribution of microglia.

## Introduction

The multifaceted disease-driving mechanisms that underlie Alzheimer's disease (AD) have complicated the development of successful therapeutic interventions. Whether the disease is familial (inherited through disease-causing genetic mutations) or sporadic (initiated by a combination of genetic, lifestyle, and environment risk factors) in origin, it is characterized by the largely predictable accumulation and spread of amyloid beta (A $\beta$ ) plaques and neurofibrillary tangles of primarily hyperphosphorylated tau (pTau) in the brain. However, the pathological events in the initiation of both types of AD are not fully understood. Neuroinflammation is an early attribute of the AD brain and can actively worsen disease through numerous aberrant immune responses including the secretion of cytokines that directly injury neurons, hyper-phosphorylate tau, or cause the production of reactive oxygen species.<sup>7,31</sup> Microglia, the resident immune-competent cells of the brain, are the primary cells driving neuroinflammation,<sup>306</sup> and likely play a critical role in early disease, as revealed by the numerous genetic risk factors that are uniquely expressed by microglia,<sup>4,13</sup> the ability of reactive microglia to initiate neurodegeneration,<sup>307</sup> and microglia-dependent mechanisms driving proteinopathy.<sup>306,308</sup> Although correcting their dysfunction may throw disease off its course, characterizing diverse microglial states has proven challenging, as unique immune stimuli and situational- or temporal-dependent cues may produce drastically different, and sometimes contradictory, responses.<sup>306,309</sup> These activation states cannot be easily teased apart, but transcriptomic studies have demonstrated their large diversity and dynamic nature, identifying a predictable evolution of states.<sup>310-312</sup> How transcriptomic signatures translate to microglial dysfunction, however, is difficult to

characterize and is made more challenging because of the differences between human and mouse microglia and AD models.

Mice and human microglia have critical differences that obscure physiological relevance, such as opposing gene regulation,<sup>42,44</sup> human-specific activation patterns, and decreased neuroinflammation in AD mouse models compared to the human brain.<sup>37</sup> Additionally, mice do not naturally develop AD and the overexpression of familial AD mutations is often used to produce AD pathology in the mouse brain. However, pathology is often incomplete<sup>34,37</sup> and accompanied by confounding effects of gene overexpression and the interaction of humanized proteins with mouse proteins and microenvironment.<sup>34</sup> Importantly, these factors may completely misrepresent events that initiate disease. Human induced pluripotent stem cell (iPSC)-derived models are becoming more widely used in AD research and are appreciated for their ability to more accurately represent A $\beta$  and tau pathology in the context of the human genome, which can be derived from both familial and sporadic patients.<sup>313</sup> Cerebral organoid models further improve cell-cell complexity and the development of more AD-reminiscent features.<sup>314-316</sup> Recently, microglia have been introduced into organoid models, either by their separate introduction or fostering their innate development.<sup>159,171,299</sup> Despite the growing appreciation for the importance of microglia in AD and human-specific responses, microglia-containing cerebral organoids have not yet been investigated in the study of AD. In this study, we employ a previously developed cerebral organoid model<sup>317</sup> that was optimized to give rise to microglia<sup>299</sup> to investigate microglia-driven changes and characterize the corresponding overall neuroinflammatory state.

The hiPSCs used in the study for AD modelling carry the familial presenilin 2 (PSEN2) mutation N141I, that predominantly causes an overall heightened neuroinflammatory state with exaggerated glial immune responses in the presence of immune insult, such as A $\beta$ .<sup>318,319</sup> The exaggerated immune response accompanied by the N141I mutation is reminiscent of a “primed” microglial phenotype<sup>320</sup> that describes an over-reactive state with amplified cytokine secretion as a result of a chronic inflammatory environment

commonly observed with age and AD.<sup>94</sup> In order to characterize changing immune responses in the organoid model over time, we profiled cytokine secretion in organoids derived from a male hiPSC line carry the PSEN2 N141I mutation and its isogenic control and built cytokine signatures predictive of age and genotype using the multivariate modeling tool partial least square (PLS) to identify key cytokines and differential regulation that correlated with observed pathology changes in the organoids. We identified an initially amplified cytokine profile that gradually decreased over months in culture, which coincided with decreased synapse density with minimal changes in the levels of pathological AD proteins. Microglial depletion prevented synapse loss and supports previously identified pathology-independent microglia-driven neuronal injury. Finally, we demonstrate organoids derived from either a male or female hiPSC line carrying the PSEN2 N141I mutation exhibit distinct cytokine profiles and subsequent effect on pathology.

## **Methods**

### ***iPSC culture***

We purchased previously characterized human iPSC lines for the generation of cerebral organoids. The iPSC line JIPSC1052 (SNV/WT, Jackson Laboratory), carrying the familial AD PSEN2 mutation N141I, and its isogenic control JIPSC1054 (REV/WT, Jackson Laboratory) are CRISPR-edited cell lines of an original parent iPSC line derived from a white male of 55-59 years of age (KOLF2.1J).<sup>321</sup> The isogenic control is a CRISPR-edited reversion of the CRISPR-introduced PSEN2 mutated gene back to wild-type to serve as a more robust control, having also gone through the gene editing process. An additional cell line carrying the N141I PSEN2 mutation (Coriell Institute AG25370, white female, 81 years-old at sampling) was derived from a female familial AD patient. iPSCs were maintained in mTeSR1 medium (STEMCELL Technologies) on Matrigel-coated plates (Corning, 356234) in a 5% CO<sub>2</sub>, 37°C cell culture incubator with daily medium changes. iPSC cultures were passaged every 4-5 days when the colonies reached 80%

confluency using the dissociation reagent ReLeSR (STEMCELL Technologies) according to the manufacturer's protocol. iPSCs were passaged 5-6 times post thaw prior to starting organoid differentiation. iPSC cultures were monitored daily for appropriate morphology and mycoplasma detection was performed every two-weeks in culture (MycoAlert, Lonza LT07-318).

### ***Organoid differentiation and maintenance***

The male N141I PSEN2 AD iPSC line (JIPSC1052, Jackson Laboratory), its isogenic control (JIPSC1055, Jackson Laboratory), and the female familial AD N141I iPSC line (AG25370, Coriell Institute) were differentiated into cerebral organoids according to a previously published protocol<sup>317</sup> with minor modifications to support the differentiation of the specific iPSC lines and to optimize the organoids' development of microglia<sup>299</sup> and are denoted as mORG<sup>N141I</sup>, mORG<sup>iso</sup>, fORG<sup>N141I</sup>, respectively. When iPSC cultures reached 80% confluency, the cells were dissociated into a single-cell solution with Accutase (STEMCELL Technologies), and 9,000 live cells were seeded in each well of U-bottom Ultralow attachment 96-well plates (Corning, 7007) in mTeSR1 medium containing 10  $\mu$ M Y-27632 ROCK inhibitor (STEMCELL Technologies) for the formation of embryoid bodies. iPSCs used in the generation of cerebral organoids demonstrated above 95% viability (Countess Automated Cell Counter, Invitrogen). After seeding the iPSCs in U-bottom plates (Day 1), a half change of the mTeSR1 medium was performed (without ROCK inhibitor) on Day 3. On day 5, the embryoid bodies were transferred to individual wells of Ultralow attachment 24 well plates (Corning, 3473) using a cut p200 pipette tip. Embryoid bodies were cultured in the 24 well plates containing neural induction medium for 7 full days with medium changes on days 7 and 9. On day 12, the organoids were embedded in Matrigel and transferred to 60mm dishes containing cerebral organoid differentiation (COD) medium without vitamin A. Briefly, individual organoids were transferred to dimples in a Parafilm sheet with a cut p200 pipette tip (16 organoids/dish). Residual medium around each organoid was removed and 20-30 $\mu$ L of Matrigel was added drop-wise to each organoid dimple.

Organoids were positioned to the center of the droplet using a p10 pipette tip. Each sheet of Matrigel-embedded organoids was incubated for 20 to 30 minutes at 37°C. After Matrigel polymerization, COD medium was added to the dish overtop the organoids to dislodge them from the Parafilm sheet, which was then removed. On day 14, the COD medium without vitamin A was replaced. On day 17, the medium was replaced with COD medium with vitamin A, and the dishes were placed on an orbital shaker at 80 rpm (KS 260 Control, IKA). Dishes were placed on the orbital shakers in stacks of 4 with 2 empty dishes on the bottom of each stack to prevent condensation from accumulating on the underside of the lids. Medium was replaced every 3-4 days. After 1 month in culture, the organoids were split into new dishes with 8 organoids per dish to prevent organoids from fusing together.<sup>322</sup> Neural induction medium and COD medium was prepared according to the original protocol,<sup>317</sup> except for the inclusion of 0.1µg/mL heparin, as opposed to 1µg/mL, in the neural induction medium as detailed by Ormel *et al.*<sup>299</sup> Large fused organoids or those not exhibiting optimal morphology<sup>317,322</sup> were excluded from the study. All the organoids used in the study came from a single batch, denoted as the organoids produced from one single-cell solution preparation that underwent the same differentiation steps. Organoids were cultured for 2-, 3-, or 4-months prior to sample collection.

### ***PLX5622 treatment of organoids***

For microglia depletion studies, PLX5622 (in DMSO, MedChemExpress) was added to the COD medium for a final concentration of 5 µM with each medium change. The volume of DMSO in the cell culture medium was less than 1%. PLX5622 or equal amounts of vehicle control was applied from 2- to 3-months, 3- to 4-months, or 2- to 4-months in culture prior to sample collection.

### ***Organoid preparation for immunostaining***

For the fixation of organoids for immunostaining, groups of organoids were transferred to conical tubes and washed with 1X PBS. The PBS was replaced with 4% (wt/vol) PFA, and the organoids were incubated at room temperature for 15 minutes. The PFA was then aspirated, and the organoids were washed 3 times with 1X PBS, with a 10-minute gentle agitation on a rocker at room temperature for each wash. The final PBS wash was replaced with 30% (wt/vol) sucrose solution. Organoids in sucrose were incubated at 4°C on a rocker at very slow speed until all the organoids had sunk to the bottom of the tube (typically 48-72 hours). After the sucrose sink, organoids were transferred to embedding molds in OCT compound (Tissue-Tek). Embedding molds were filled halfway with OCT compound and frozen at -20°C. In each tube, half of the sucrose solution was removed and replaced with OCT compound. The organoids in sucrose/OCT were then incubated at room temperature for 30-60 minutes with gentle agitation. All of the sucrose/OCT solution was then replaced with OCT compound, and the tubes were incubated for another 30-60 minutes with gentle agitation at room temperature. After the equilibration with OCT, a thin layer of OCT was applied to the frozen OCT in the embedding mold. The organoids were then quickly transferred on top on the liquid OCT layer using a cut P1000 pipette tip (6 organoids per mold). Organoids were gently arranged as desired in the mold and more OCT was applied to cover them. The molds were quickly frozen on a metal block in liquid nitrogen. Frozen OCT-embedded organoids molds were stored at -80°C. Organoid blocks were cryosectioned using a cryostat (Leica) at 20µm at -20°C on Superfrost Plus Microscope Slides (Fisherbrand). Organoid slides dried completely at room temperature before being stored at -80°C.

For immunostaining, organoid slides were thawed and allowed to dry completely at room temperature before washing and blocking. Slides were washed in 1X PBS three times with gentle agitation for 5-10 minutes at room temperature. A hydrophobic barrier was drawn around each grouping of organoids (Super HT Pap Pen, Kiyota International) and blocking solution was added (90% PBS, 10% normal goat serum, and 1% of 10% Triton-X-100 Solution). Slides were incubated in the blocking solution at room

temperature for 1 hour. The blocking solution was then replaced with primary antibodies in blocking solution (anti-TUBB3 (Abcam ab78078, ab52623), -AT8 (Thermo MN1020), -IBA1 (Wako 019-19741, -Tmem119 (Invitrogen PA5-119902), -GFAP (Abcam ab207165), SYN1 (Abcam ab254349), and -A $\beta$ -40/42 (Millipore AB5076)). Slides were incubated at 4°C overnight in a humidity chamber. Slides were then washed with PBS 3 times and secondary antibodies (Alexa Fluor 555 goat anti-mouse (Invitrogen A21425) and Alexa Fluor 488 goat anti-rabbit (Invitrogen, A11070) in blocking solution were added to the slides for 1 hour at room temperature. Following the secondary antibody incubation, slides were washed in a weak serum solution (1% normal goat serum, 99% PBS) for ten minutes with gentle agitation at room temperature and subsequently washed an additional 2 times with PBS. Coverslips were mounted with Prolong Diamond Antifade Mountant with DAPI (Invitrogen) and placed flat in the dark for 24 hours at room temperature prior to storage at 4°C.

### ***Organoid imaging***

Organoid slides were viewed and imaged using a fluorescence microscope (Nikon Eclipse 80i, Nikon DS-Fi3 camera, NIS-Elements AR software). Some fluorescent signals were not uniform across the organoid sections, such as the isolated clusters of astrocyte GFAP staining. In these instances, when the magnification did not allow for the entire organoid section to be imaged, images were collected from the region(s) of each organoid that displayed the largest signal intensity in order to accurately assess differences in pathology staining/ cell populations. Images of sections from the middle of the organoid displaying necrosis were excluded from analyses. Images were processed and analyzed in ImageJ. Background correction of single-color channel images was performed by subtracting the mean intensity of the background from image. Histogram stretching was performed on images not used for quantitative analysis; however, a minimum maximum value of 200 was used to prevent one color signal from over-powering the others. For the measurement of mean intensity of the organoid sections, outlines were manually drawn around each

organoid and the mean intensity was measured. Large tears and ventricle-like pockets<sup>322</sup> within the organoids were excluded from the mean intensity measurement. If the signal was too weak to see the outline of the organoid (as was the case in the Tmem119 signal after microglia depletion), the brightness of the image was increased in order to draw the outline and was reset prior to taking the intensity measurement. Tmem119, rather than IBA1, was used for the PLX-treatment experiments to assess the depletion of microglia because it was more representative of the population within the whole organoid, as the expression was more widespread and consistent between sections of the same organoid. For Tmem119 signal intensity quantification, images were taken of whole organoids (4X magnification) to appreciate entire the population visible in a cross section, while A $\beta$  and pTau images were taken at 10X magnification of organoid region(s) demonstrating the largest fluorescence intensity to better visualize the morphology of A $\beta$  and pTau deposits.

### ***Organoid lysate preparation***

Organoid lysate samples were collected for the quantification of cytokine and pathological protein concentrations in the organoids. Groups of 3 to 5 organoids were transferred to Eppendorf tubes and washed with cold 1X PBS. Organoids were combined for individual samples to have adequate total protein concentration and volume for multiple multiplex assays. To remove the Matrigel surrounding the organoids, the PBS was replaced with Cell Recovery Solution (Corning), and the organoids were incubated at 4°C for 30 minutes. The organoids were then washed with cold PBS. The tubes were briefly spun down and the PBS was aspirated. Cold cell lysis buffer (Millipore 43-040) containing protease inhibitor cocktail (1:100, Sigma) was added to the organoids, and the organoids were mechanically digested with trituration using a p1000 and then a p200 pipette. Following the trituration, the tubes were vortexed for 1-2 minutes and kept on ice at least 20 minutes. The samples were then centrifuged at room temperature for 10 minutes at 10,000 x g. The supernatants were transferred to a new tube and aliquoted for separate assays and BCA total protein

quantification. The aliquots were flash frozen in liquid nitrogen and stored at  $-80^{\circ}\text{C}$ . The total protein content of the organoid lysate samples was quantified using the Pierce BCA Protein Assay Kit (Fisher 23225) according to the manufacturer's instructions. Each sample was run in triplicate and absorbances read using a SpectraMax i3 minimax 300 imaging cytometer (Molecular Devices). Sample concentrations were quantified by linear regression using triplicate standard samples ran on each plate.

### ***Luminex multiplex assays***

The cytokine concentrations of organoid lysate samples were quantified on the Luminex FLEXMAP3D platform using the Milliplex human cytokine and chemokine magnetic bead panel kit (Millipore HCYTOMAG-60K, mORG<sup>N1411</sup> and mORG<sup>iso</sup> samples) and the Milliplex human cytokine/chemokine/ growth factor panel A magnetic bead panel kit (HCYTA-60K, fORG<sup>N1411</sup>), measuring a broad panel of immune signaling proteins that allow for an unbiased survey of immune cues activating a diverse set of downstream intracellular pathways. A $\beta$  and pTau levels in the organoids were quantified with Milliplex human amyloid beta and tau kit (Millipore HNABTMAG-68K) on the Luminex (all samples). The assays were performed according to the manufacturer's protocols with minor modifications to accommodate the use of 384-well plates. The magnetic beads and antibody solutions were diluted 1:1 and used at half volume, and the streptavidin-phycoerythrin was used at half volume. Samples were diluted to 1.2 mg/mL total protein using assay buffer and added to the plate for 30  $\mu\text{g}$  total protein per well. Samples were assayed in technical triplicate.

### ***Cytokine profile data cleaning***

Cytokine concentrations for each sample were interpolated from 5-point logistic standard curves using the Luminex Xponent software. Concentrations below the detection limit ( $< 3.2\text{pg/mL}$ ) were assigned

0 pg/mL. The raw concentration data was processed using an automated in-house pipeline, available from GitHub at <https://github.com/elizabethproctor/Luminex-Data-Cleaning> (Version 1.02). The pipeline removes readings generated from less than 35 beads (custom input value) (0 observations in the datasets) and then calculates the pairwise differences of the remaining technical triplicates. If the difference between one replicate is greater than twice the distance between the other two, the replicate is removed from the dataset. The average of the remaining technical replicates for each cytokine is then calculated for the final dataset. We then manually removed entire cytokines from the datasets for subsequent analyses if over half the readings were 0 pg/mL but did not partition between experimental groups, such as genotype or timepoint. The proteins IL-17E/IL-25, IL-17F, IL-18, IL-22, IL-27, M-CSF, MIG/CXCL9, PDGF-AA, PDGF-AB/BB were removed from the fORG<sup>N1411</sup> dataset, so the male and female organoid cytokine datasets consisted of the same cytokines for multivariate analysis.

### ***Partial least squares modeling***

The linear, supervised multivariate mathematical modeling tool partial least squares (PLS)<sup>195,196</sup> was used to construct cytokine signatures predictive of a response of interest (ex: AD vs control). Cytokine expression and signaling is highly interdependent, and PLS allows for the identification of significant multivariate changes in correlative predictors (the cytokines) as they relate to a dependent response or group (such as, genotype or timepoint). This is achieved through PLS's construction of linear combinations of the predictors (latent variables, LVs) that maximize the covariation between the predictors and the response. This maximization of multivariate covariance in predictors with the response allows us to identify subtle but meaningful patterns in cytokine expression that are undetectable using univariate analysis methods, which are unsuitable for highly correlative variables. We generated PLS regression (PLSR) models for the prediction of continuous numerical outcomes and PLS discriminant analysis (PLS-DA) models for the prediction of experimental groups models<sup>323</sup> in R with the *ropls*

package.<sup>197</sup> For PLSR models, repeated random sub-sampling cross-validation repeated 100 times with 1/5<sup>th</sup> of the data left out for each test set (n=15) estimating the average root mean squared error of cross validation (RMSECV) was used to determine the optimal number of LVs for each model. For PLS-DA models, leave-one-out cross validation (n=10) to estimate the average classification error was used to determine the optimal number of LVs for each model. The cytokine data were mean-centered and unit-variance scaled prior to PLS modeling. The models were orthogonalized to maximally project covariation of the measured cytokines with the response to the first latent variable, which improves interpretability by prioritizing predictor/response covariation over variation in the measured cytokines between samples.<sup>198</sup> A model's significance was evaluated using a permutation test. In each iteration, the sample identities are randomly reassigned to unchanged cytokine signatures. The randomized data is used to generate models for cross validation to measure the performance of the random models compared to the "real" experimental model. The p-value of the optimized experimental model is then calculated by comparison of its accuracy/RMSECV with the mean and standard deviation of the distribution of random models' accuracy or RMSECV. Models containing 1 LV are visualized using 2 LVs, but only 1 LV was used in the calculation of the model's accuracy/RMSECV and significance. The VIP score, a measure of a variable's normalized contribution to the predictive accuracy of the model across all LVs,<sup>199</sup> was used to identify key cytokines in the models, where a VIP score > 1 indicates a greater than average contribution to the model.

### ***Statistical Analyses***

Statistical tests were performed using Graph Pad Prism Version 10.0.1. To evaluate the statistical significance of changes in protein level or fluorescence intensity between genotype and timepoints, two-way ANOVA with Tukey's multiple comparison test was used. A one-way ANOVA with Tukey's multiple comparison test was used for timepoint comparisons in the female N141I organoid samples and PLX5622 and vehicle treatment comparisons. Unpaired two-tailed Student's t-tests were used to determine

significance between two populations. A Grubbs' test was used to identify outliers in the datasets. All data are expressed as mean  $\pm$  standard deviation.

## Results

### *N141I and isogenic control iPSC-derived cerebral organoids innately develop microglia*

A chronic, aberrant neuroinflammatory state contributes to Alzheimer's disease proteinopathy accumulation and neuronal injury.<sup>324</sup> The familial AD N141I PSEN2 mutation is observed to heighten the immune response of microglia and astrocytes.<sup>320</sup> In order to dissect N141I-driven changes in glial function and the presentation of AD pathology, a male PSEN2 N141I hiPSC line and its isogenic control were used to generate cerebral organoids (denoted as mORG<sup>N141I</sup> and mORG<sup>iso</sup>, respectively), which were cultured for 2-, 3-, or 4-months. It has been previously demonstrated microglia are found throughout the organoid after 2 months in culture and their transcriptomes closely resemble those of adult human microglia.<sup>299</sup> The microglia continue to mature, increasing expression levels of microglia-specific genes, in the following months.<sup>299</sup> In a pilot study, organoids were cultured for up to 6-months, and widespread tissue atrophy was observed by 5-months (Supplementary Figure 3-1). We chose to end the experimental timeline at 4-months to eliminate confounding effects of robust cell death on the immune response and pathology changes in the organoids. We verified the existence of microglia and astrocytes in our organoids with the immunostaining of the cell-type specific markers GFAP (astrocytes) and Tmem119 and IBA1 (microglia)(Fig 3-1). Tmem119, a transmembrane protein expressed by microglia and not other brain cell-types or infiltrating macrophages,<sup>325</sup> is found throughout the organoids (Fig 3-1A). The Tmem119 signal is distinct from but closely associates with neuron projections (Fig 3-1B). The single cell preparation of the organoids demonstrates Tmem119-positive cells (Fig 3-1D). The organoids demonstrate clusters of astrocyte populations, which also closely associate with neurons. (Fig 3-1C,E). The microglia activation marker,

IBA1, is also expressed in the organoids, though much more sparsely (Fig 3-1E). Microglia and astrocyte populations overlap in the organoids (Fig 3-1E). It is worth recognizing that in the literature these cells derived directly from iPSCs or within organoids may not be fully mature microglia and are occasionally instead referred to as “microglia-like cells”.<sup>298,299,326–329</sup> With the presence of Tmem119 and IBA1 positive cells, proteins regarded as microglia-specific markers in the brain,<sup>299,325</sup> they will be referred to as microglia with the acknowledgement that their full likeness to endogenous human microglia is unknown.

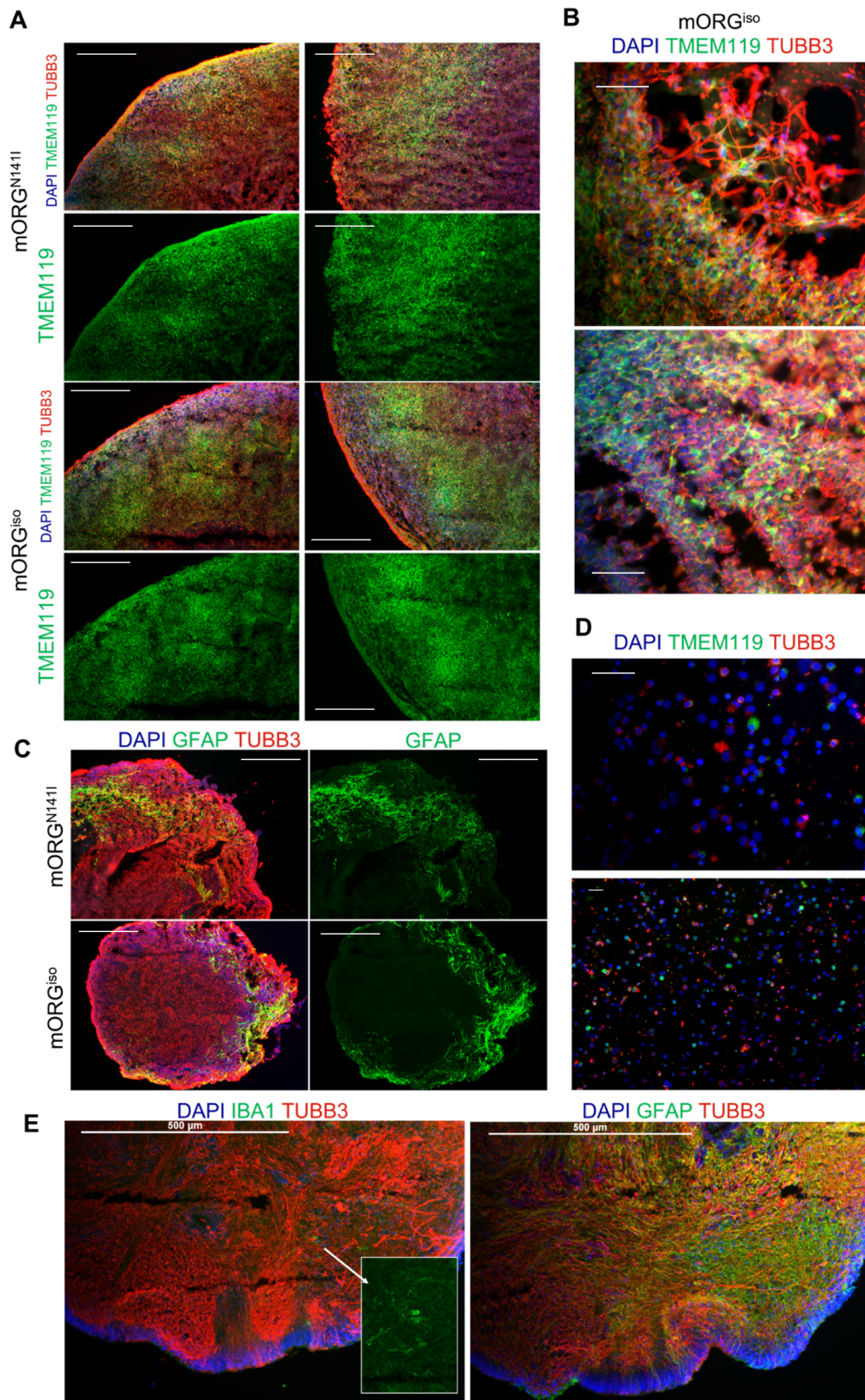


**Figure 3-1: Microglia and astrocytes develop in AD and isogenic organoids.** (A) Composite (red: TUBB3, green: Tmem119, blue: DAPI) and green channel (Tmem119) images of 3-month-old mORG<sup>N1411</sup> (top grouping) and mORG<sup>iso</sup> (bottom grouping), scale bars: 250 $\mu$ m. (B) Magnification of Tmem119 and TUBB3 signals emphasizes separate microglia and neuron projections, scale bars: 50 $\mu$ m. (C) Composite (red: TUBB3, green: GFAP, blue: DAPI) and green channel (GFAP) images of 3-month-old mORG<sup>N1411</sup> (top) and mORG<sup>iso</sup> (bottom), scale bars: 250 $\mu$ m. (D) Tmem119 (green), TUBB3 (red), and DAPI (blue) immunostaining of a single-cell preparation of an isogenic control organoid, scale bars: 50 $\mu$ m. (E) Sequential organoid sections demonstrating overlapping microglia (IBA1, left) and astrocyte (GFAP, right) populations, scale bars: 500 $\mu$ m.

***Cytokine secretion is initially increased in AD organoids prior to an overall down-regulated cytokine profile compared to isogenic controls.***

To characterize the effect of the PSEN2 N141I mutation on the organoids' inflammatory state, we profiled the immune milieu of mORG<sup>N141I</sup> and mORG<sup>iso</sup> by measuring cytokine concentrations over 2- to 4-months in culture. We used partial least squares discriminant analysis (PLS-DA) to construct cytokine signatures predictive of genotype (AD vs control) to identify changes in immune signaling in the organoids over time and distinguish mutation-dependent differences in the cytokine profiles (Fig 3-2). In 2-month-old organoids (Fig 3-2A. PLS-DA: 2 latent variables, accuracy: 90%, p-value: <0.005), unique cytokines are up-regulated in AD or control organoids. Key cytokines, determined by a VIP score greater than 1 (having a greater than average contribution to the model), up-regulated in the AD organoids are IL-4, IL-12p70, IFN $\alpha$ 2, GRO, Flt-3L, and FGF2, while increased IP-10 (CXCL10) and IL-1Ra expression are key cytokines in the prediction of isogenic organoids. In 3-month-old organoids (Fig 3-2B. PLS-DA: 2 latent variables, accuracy: 80%, p-value: <0.05) there is a shift in the cytokine profile from that of the 2-month-old organoids. In the AD organoids, there is diminished expression of key 2-month AD cytokines, such as IL-12p70, IFN $\alpha$ 2, GRO, and Flt-3L, and now undetectable levels of IL-4 (which was excluded from the model), while demonstrating an increase in VEGF, Fractalkine, and FGF-2. The cytokine signature of the AD 4-month-old organoids (Fig 3-2C. PLS-DA: 3 latent variables, accuracy: 80%, p-value: <0.05) demonstrates further reduction of all cytokines, excluding VEGF, showing a complete switch of the 3-month-old correlation of AD organoids with up-regulated Fractalkine and FGF-2. The comparison of cytokine signatures over the months in culture demonstrates an initial up-regulation of cytokines in AD organoids, which diminishes overtime and is completely reversed at 4-months where cytokines are up-regulated in the control organoids.

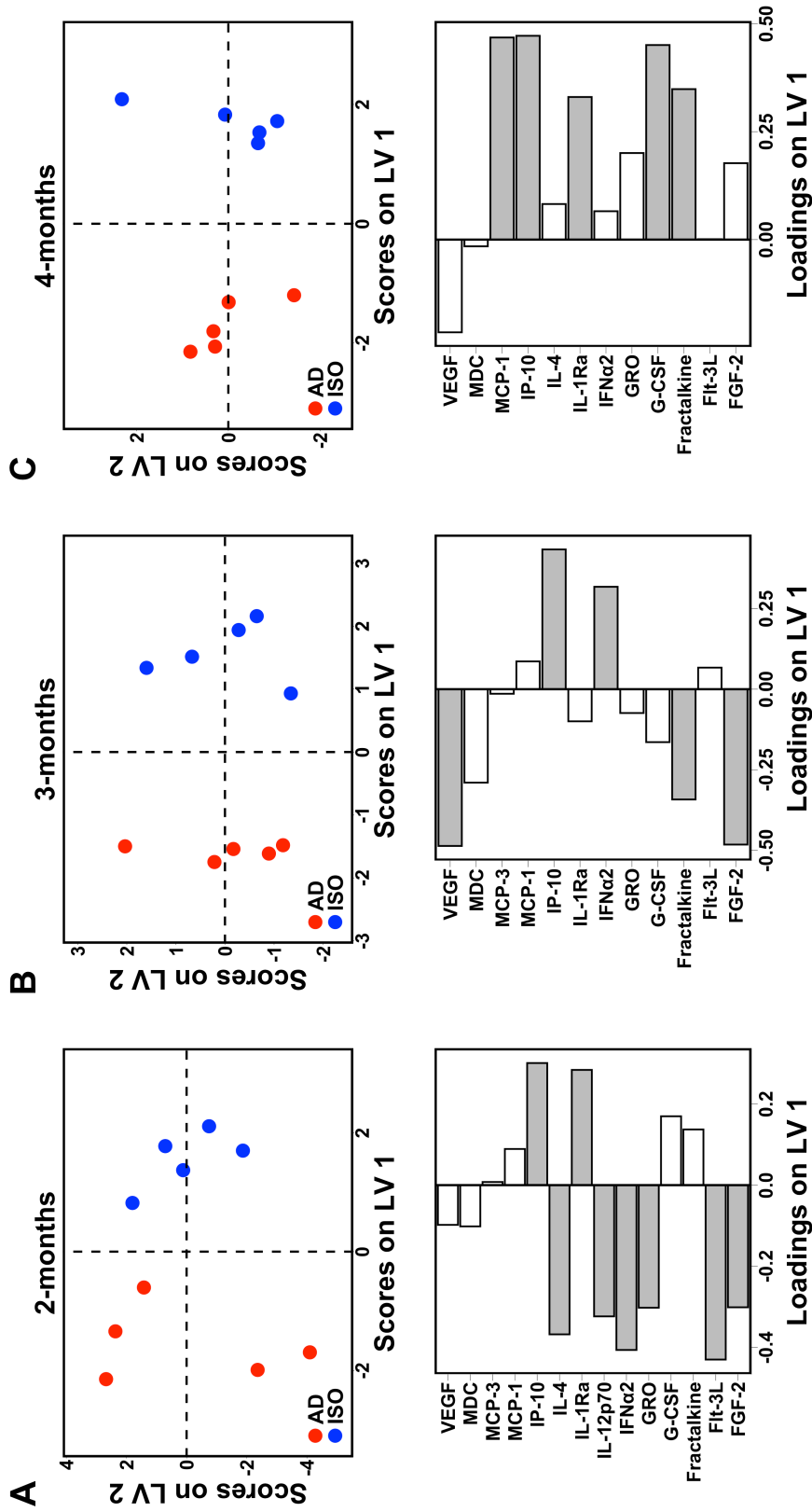


**Figure 3-2: Cytokine signature predictive of genotype in male N1411 organoids reverses over experimental timeline.** PLS-DA scores plot (top) and LV1 loadings plot (bottom) of (A) 2-month-old AD vs isogenic control organoids (2 LV, accuracy: 90%, p-value: <0.005), (B) 3-month-old AD vs isogenic control organoids (2 LV, accuracy: <0.05), (C) 4-month-old AD vs isogenic control organoids (3 LV, accuracy: 80%, p-value: <0.05). Shaded loadings indicate a VIP score > 1. Each point represents a single sample comprising 3-5 organoids derived from the male N1411 cell line and its isogenic control. Positive loadings indicate an up-regulation of cytokines with positive scoring samples, while negative loadings feature the down-regulation of cytokines with samples of positive scores.

***Down-regulation of cytokine secretion in AD 4-month-old organoids coincides with decreased synapse density***

We wanted to verify that the decrease in cytokine secretion of aging AD organoids represented a diminished reactive glial phenotype and was not a result of cell death within the organoids. The organoids did not display tissue atrophy over the culture period (Figure 3-3A). Subsequently, we investigated if there was a change in the microglia population, as microglia-specific loss could also mimic the phenotype. We did not observe a loss of Tmem119 signal over the culture period in either the AD or isogenic organoids and instead saw an overall increase in signal from 2- to 4-months (Figure 3-3C). Thus, the decreased cytokine profile of aging mORG<sup>N1411</sup> is not due to a loss of microglia over time and is likely a result of a dampened immune response. Notably, from 2- to 4-months, a reduction of SYN1, a presynaptic marker, coincided with the increase of the Tmem119 signal in the AD organoids (Fig 3-3B), indicating decreased synapse density. Initially at 2-months, there was increased SYN1 in AD organoids compared to controls (Fig 3-3B).

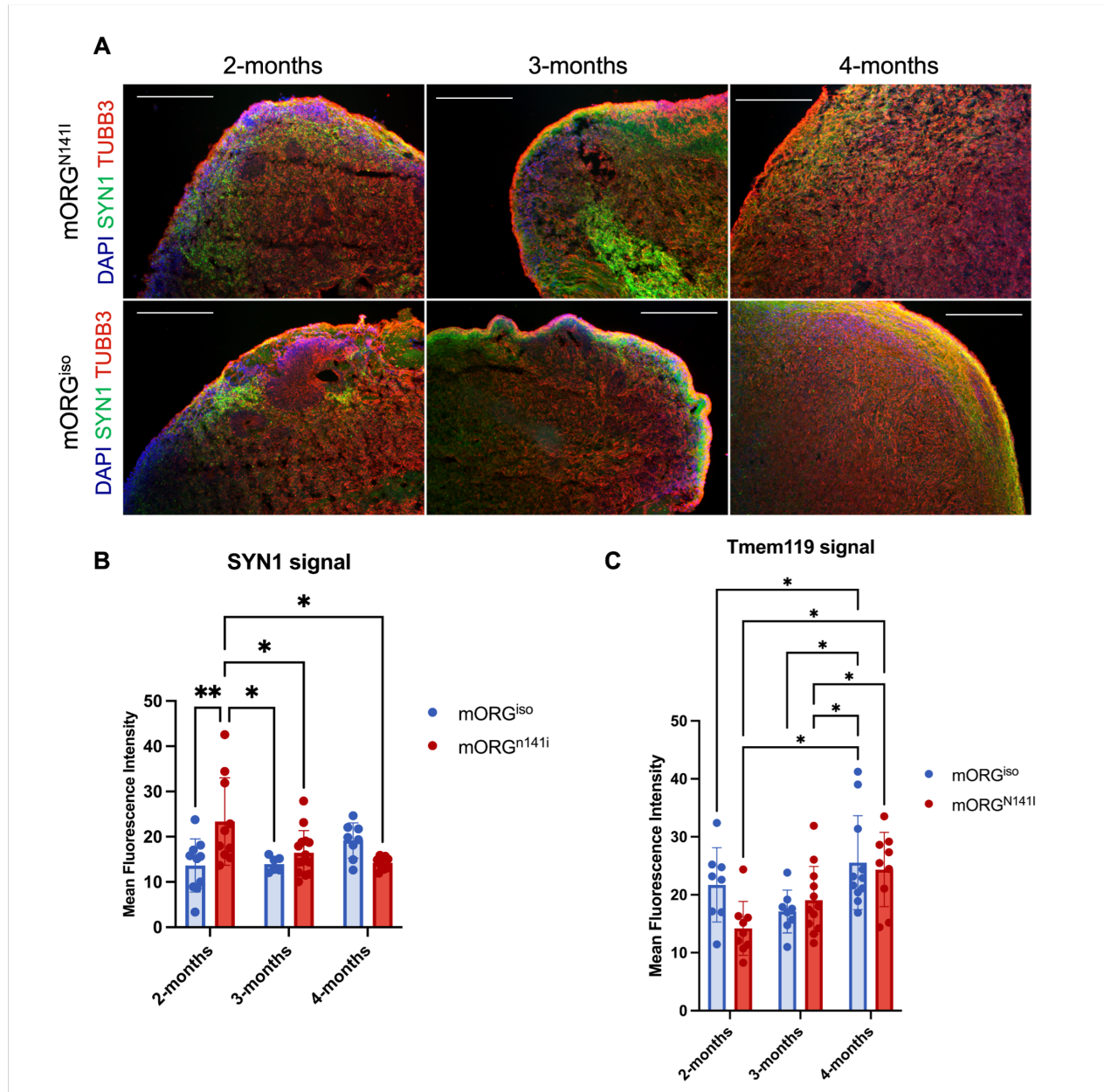


**Figure 3-3: Synapse density decreases over time in AD organoids along with slight increase in microglia population.**

(A) Composite images (red: TUBB3, green: SYN1, blue: DAPI) of 2-, 3-, and 4-month-old mORG<sup>N141I</sup> (top) and mORG<sup>iso</sup> (bottom), scale bars: 250 $\mu$ m. (B) Quantification of mean fluorescence intensity of SYN1 immunostaining in organoid sections from 2- to 4-months. Two-way ANOVA with Tukey's multiple comparison test. 2-month-old mORG<sup>iso</sup> vs 2-month-old mORG<sup>N141I</sup>, p-value < 0.005. 2-month-old mORG<sup>N141I</sup> vs 3-month-old mORG<sup>iso</sup>, p-value < 0.05. 2-month-old mORG<sup>N141I</sup> vs 3-month-old mORG<sup>N141I</sup>, p-value < 0.05. 2-month-old mORG<sup>N141I</sup> vs 4-month-old mORG<sup>N141I</sup>, p-value = 0.01. (C) Quantification of mean fluorescence intensity of Tmem119 immunostaining in organoid sections from 2- to 4-months. 2-month-old mORG<sup>iso</sup> vs 4-month-old mORG<sup>iso</sup>, p-value < 0.05. 2-month-old mORG<sup>N141I</sup> vs 4-month-old mORG<sup>iso</sup>, p-value < 0.05. 2-month-old mORG<sup>N141I</sup> vs 4-month-old mORG<sup>N141I</sup>, p-value < 0.05. 3-month-old mORG<sup>iso</sup> vs 4-month-old mORG<sup>iso</sup>, p-value < 0.05. 3-month-old mORG<sup>N141I</sup> vs 4-month-old mORG<sup>iso</sup>, p-value < 0.05. 3-month-old mORG<sup>N141I</sup> vs 4-month-old mORG<sup>N141I</sup>, p-value < 0.05. Data are mean  $\pm$  SD.

*A $\beta$  and pTau levels largely remain constant over time, but A $\beta$  accumulates in larger deposits in AD organoids*

Given the amplification of glial immune responses as a result of the N141I mutation, the dramatic down-regulation in cytokine secretion in older AD organoids rather than a persistent or worsening heightened immune response is surprising. It has been observed that under chronic A $\beta$  exposure microglia can enter a “chronic tolerant phase” exhibiting a diminished cytokine secretion profile and impaired phagocytic ability,<sup>101</sup> which can exacerbate the accumulation A $\beta$  pathology. Correspondingly, persistent immune activation and cytokine release, which may be present at 2-months, can directly increase A $\beta$  and tau pathology in AD. We then investigated changes in A $\beta$  and pTau levels in the organoids that could explain the observed immune phenotype in the aging organoids (increasing A $\beta$  overtime to dampen the immune response) and support the expected effects on pathology from the dysregulated immune signaling. Surprisingly, A $\beta$ 40, A $\beta$ 42, and pTau levels of AD and isogenic control organoids did not differ from 2- to 4-months in culture, and A $\beta$ 40 and A $\beta$ 42 levels did not increase in overtime in either the AD or control organoids (Fig 3-4A). There was a moderate increase in pTau levels in the 4-month organoids (Fig 3-4A, right). At 3-months, AD and control organoid immunostaining similarly did not reveal any differences in A $\beta$  or pTau signal (Fig 3-4B,D). However, 3-month-old AD organoids did demonstrate larger concentrated areas of A $\beta$  compared to controls (Fig 3-4C). The results indicate that the mORG<sup>N141I</sup> may have exhibit altered deposition rather than the accumulation of A $\beta$ .

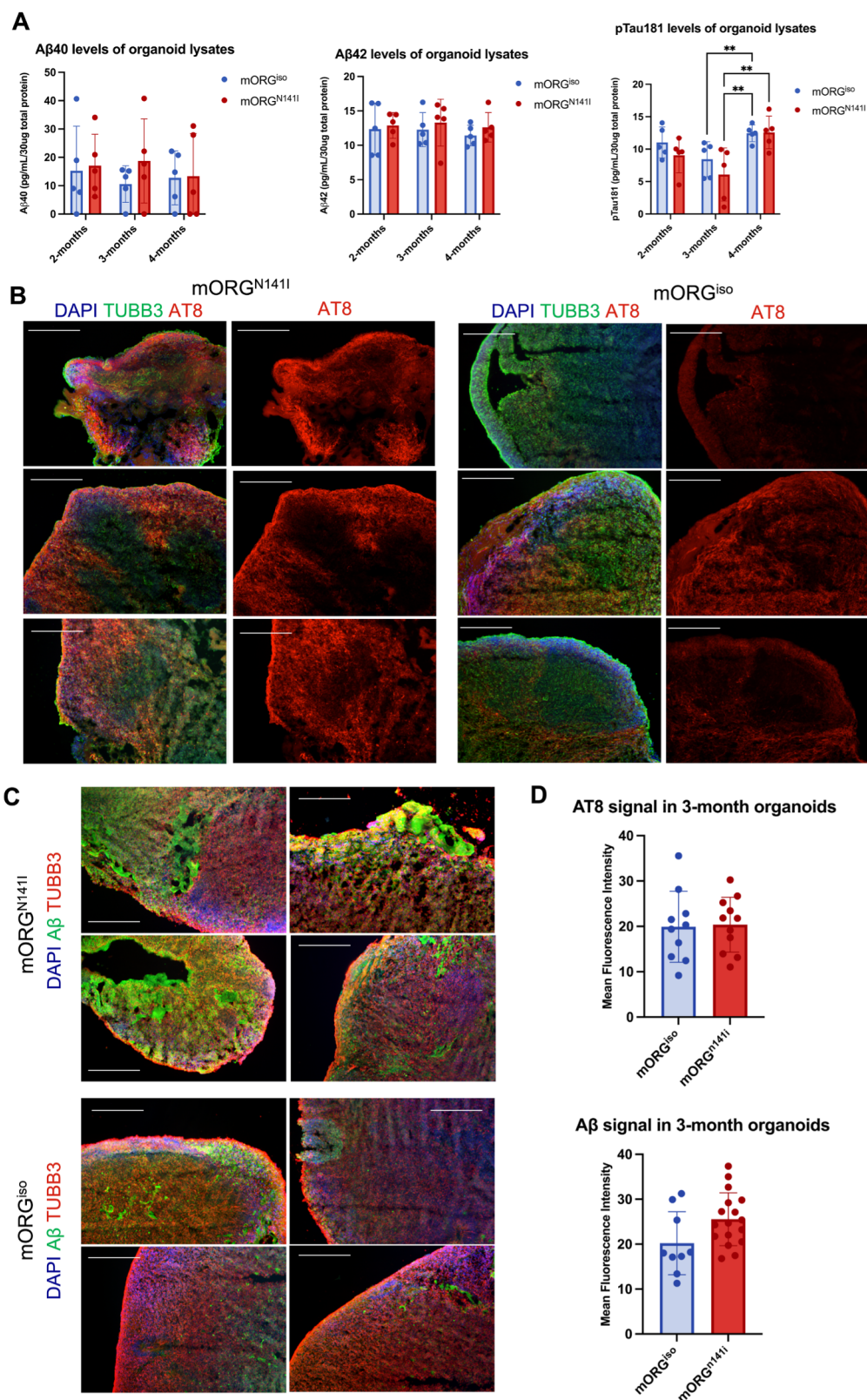


**Figure 3-4: A $\beta$  and pTau levels are the same between AD and isogenic organoids, despite more concentrated A $\beta$  deposition in AD organoids.** (A) A $\beta$ 40 (left), A $\beta$ 42 (middle), and pTau-181 (right) protein levels in mORG<sup>N1411</sup> and mORG<sup>iso</sup> lysates from 2- to 4-months. Each sample represents the lysate of a combined 3-5 organoids. Two-way ANOVA with Tukey's multiple comparison test. 3-month-old mORG<sup>iso</sup> vs 4-month-old mORG<sup>iso</sup>, p-value < 0.005. 3-month-old mORG<sup>N1411</sup> vs 4-month-old mORG<sup>iso</sup>, p-value < 0.005. 3-month-old mORG<sup>N1411</sup> vs 4-month-old mORG<sup>N1411</sup>, p-value < 0.005. (B) Composite (red: AT8, green: TUBB3, blue: DAPI) and red channel (AT8) images of 3-month-old mORG<sup>N1411</sup> (left grouping) and mORG<sup>iso</sup> (right grouping), scale bars: 250 $\mu$ m. (C) Composite images (red: Tubb3, green: A $\beta$ , blue: DAPI) of 3-month-old mORG<sup>N1411</sup> (top grouping) and mORG<sup>iso</sup> (bottom grouping), scale bars: 250 $\mu$ m. (D) Quantification of mean fluorescence intensity of pTau AT8 (top) and A $\beta$  (bottom) immunostaining in 3-month-old organoids. Each point is a unique organoid section. Unpaired Student's t-test. Data are mean  $\pm$  SD.

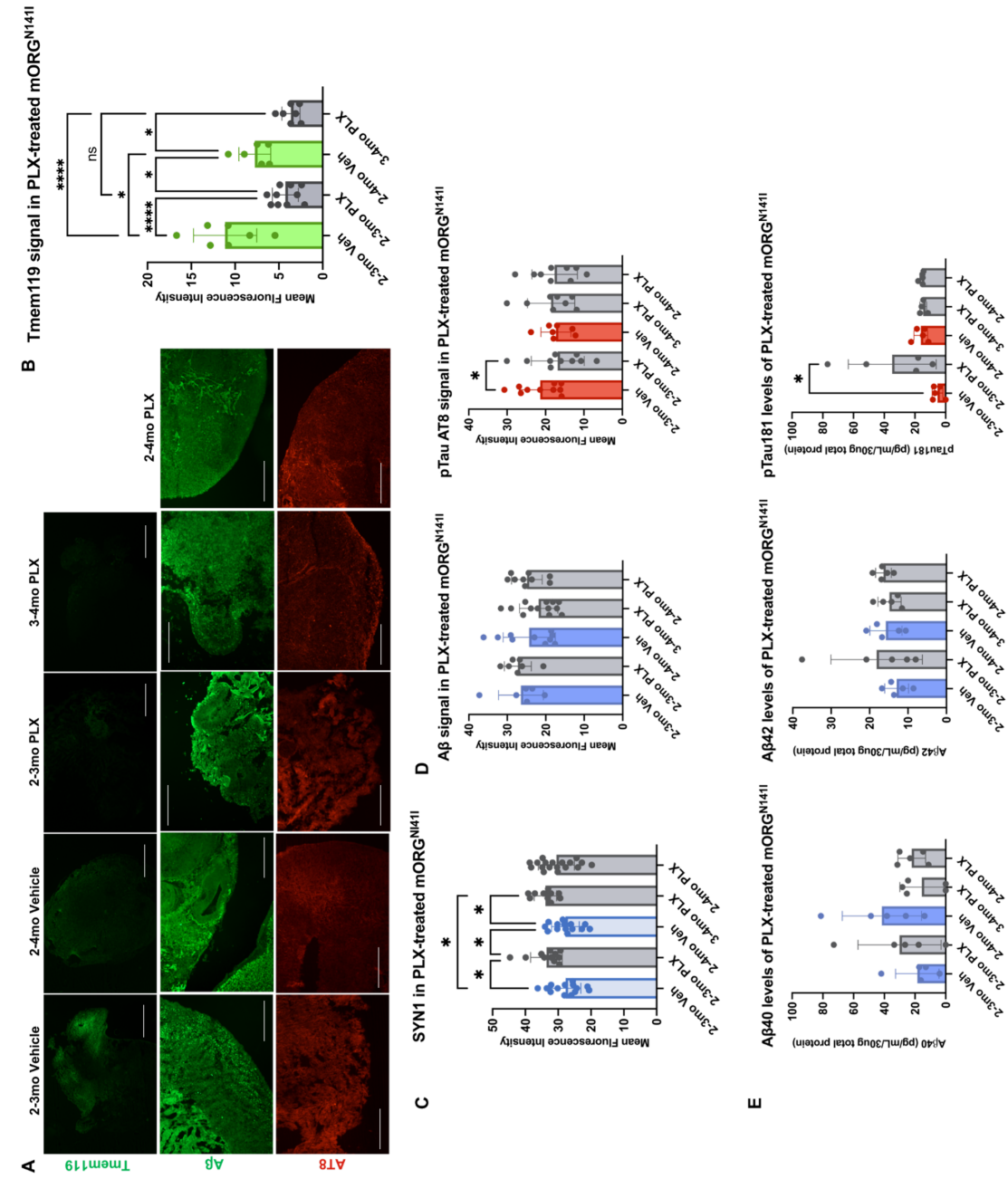
***A $\beta$  levels are unchanged following microglia reduction in AD organoids, while pTau is affected from 2 to 3-months but not 2-4 or 3-4 months***

To continue to tease apart a potential microglia-dependent effect on AD pathology in the N141I organoids, we investigated the depletion of microglia by colony stimulating factor 1 receptor (CSF1R) signaling inhibition with the application of the small molecule PLX5622. CSF1R signaling is required for microglia homeostasis and survival, and its inhibition results in the apoptosis of microglia.<sup>145</sup> PLX5622 has been used previously to eliminate >95% of microglia *in vivo* and in *ex vivo* brain slices.<sup>127,146</sup> Microglia depletion with PLX5622 has previously been studied in a variety of AD and tauopathy mouse models and often results in positive effects on tau pathology<sup>32,102,135</sup> but varying influence on A $\beta$ .<sup>127,149,330</sup> However, some studies demonstrate contradictory results, which may be attributed to the type of mouse model used, the presentation of pathology at the time of experimentation, and the degree of microglia depletion achieved. Microglia depletion in a human AD cerebral organoid model more reminiscent of human disease<sup>313</sup> may improve our understanding of how microglia can drive AD pathology. We added 5  $\mu$ M or equal amounts of vehicle control to the organoid culture medium with each medium change for the duration of the experimental timeline. PLX5622 treatment was applied to the organoids from either 2- to 3-months of age, 3- to 4-months of age, or 2- to 4-months of age to parse out the microglia-specific effects that correspond to shifting immune responses observed over time (Fig 3-2) and address the dynamic nature of reactive microglial states that differentially affect disease pathology in AD.<sup>309</sup> Following PLX5622 treatment, we observed >50% reduction in Tmem119 signal (Fig 3-5A,B). The reduced Tmem119 signal intensity was the same between 2- to 3-month PLX-treated AD organoids and 3- to 4-months PLX-treated AD organoids, suggesting the same level of microglial depletion was achieved from both starting points.

The fluorescence intensity of A $\beta$  and pTau staining did not change as a consequence of PLX-treatment with the exception of 2- to 3-month PLX-treatment which mildly decreased pTau AT8 (Fig 3-5A,D). Consistently, quantified levels of A $\beta$ 40 and A $\beta$ 42 in organoid lysates did not change with PLX-treatment (Fig 3-5E). A change in pTau-181 in AD organoid lysates was similarly only observed in the 2-

to 3-month PLX-treated organoids. However, during this treatment timeline, levels of pTau-181 increased. Tau has 85 different phosphorylation sites, which variably increase the aggregation propensity of tau or decrease its association with microtubules.<sup>331</sup> AT8 and pTau-181 correspond to unique phosphorylation sites on tau that are found to be increased in tauopathy. Importantly, different phosphorylation sites have been associated with specific pathology (i.e. around plaques) or location (i.e. colocalized with synapses).<sup>332</sup> Similarly, numerous kinases may differentially phosphorylate tau at various sites<sup>333</sup>. Depending on the microglial signals that were reduced upon microglial depletion, such as a decrease in cytokine secretion that activate tau-phosphorylating kinases, the difference in affect is not unreasonable. Additionally, the semi-quantification of signal intensity does not wholly reflect protein concentration. Importantly, the sole effect on pTau occurred as a result of microglial depletion from 2- to 3-months when cytokine secretion was up-regulated(Fig 3-2A).

These results highlights the potential of the shifting contribution of dysregulated immune responses to disease progression over the course of disease. Earlier in the AD organoid culture timeline when glia were exhibiting an overreactive phenotype, which can drive the accumulation of AD pathology,<sup>309,324</sup> the depletion of microglia would likely affect the accumulation of pathology with the subsequent loss of increased detrimental pro-inflammatory cytokine signaling (or beneficial signaling). In contrast, at later timepoints, when the immune response in the AD organoids is largely diminished compared to controls, microglia depletion may affect the organoids less. Most strikingly, however, was increased SYN1 levels after PLX5622 treatment (Fig 3-5C). The SYN1 signal was indistinguishable between 2- to 3-months and 3- to 4-months, suggesting the microglial depletion, whether initiated before or after the dampened cytokine secretion observed in the 3- and 4-month immune milieu could prevent synapse loss.



***Aging female AD H141I organoids exhibit continued up-regulation of select cytokines, in stark contrast to the overall diminished cytokine secretion of male H141I organoids***

The presentation of AD pathology in our mORG<sup>N141I</sup> is inconsistent with a previous study investigating the N141I mutation in iPSC-derived organoids. Familial AD patient-derived cerebral organoids carrying the N141I mutation have been previously demonstrated to exhibit increased level of A $\beta$ 42,<sup>302</sup> in contrast to our organoids. Importantly, these organoids were derived from a female patient and were differentiated using a kit that has not been found to give rise to microglia. In order to probe the consistency of the longitudinal cytokine signatures between cell lines, we generated organoids from an hiPSC line derived from a female familial AD patient carrying the PSEN2 N141I mutation and profiled cytokine secretion in fORG<sup>N141I</sup> cultured for 2-, 3-, and 4-months. We constructed cytokine signatures predictive of advancing age using partial least square regression (PLSR) in mORG<sup>N141I</sup> and fORG<sup>N141I</sup>. Consistent with the PLS-DA models (Fig 3-2), the mORG<sup>N141I</sup> PLSR model demonstrates a decrease in cytokine secretion over time, exhibiting a spectrum of aging 2- to 3- to 4-month organoid samples along LV 1 (a continuum from yellow to orange to red) (Fig 3-6A, PLSR: 1 LV, RMSECV: 0.745, p-value: 0.01). Importantly, a significant PLSR model could not be generated for mORG<sup>iso</sup> cytokine profiles, indicating there was no predictable signature of cytokines that differentiated increasing age in their isogenic counterparts. The mORG<sup>N141I</sup> PLSR model is in stark contrast to the fORG<sup>N141I</sup> PLSR model which demonstrates a distinct increase of select cytokines with age (VIPs: MIP-1 $\beta$ , MCP-1, IL-8, IL-4) and a down-regulation of others (VIPs: IL-9, Fractalkine, FGF-2, Eotaxin) (Fig 3-6B, PLSR: 1 LV, RMSECV: 0.766, p-value: 0.01). Additionally, the fORG<sup>N141I</sup> samples had more non-zero cytokine concentrations. IL-6, a cytokine often implicated in Alzheimer's disease particularly in its activation of a variety of kinases that hyper-phosphorylate tau<sup>64</sup> was detected in fORG<sup>N141I</sup> samples but not in mORG<sup>N141I</sup> samples. IL-4, which plays a role in regulating phagocytosis,<sup>334</sup> is uniquely up-regulated in aged fORG<sup>N141I</sup>.

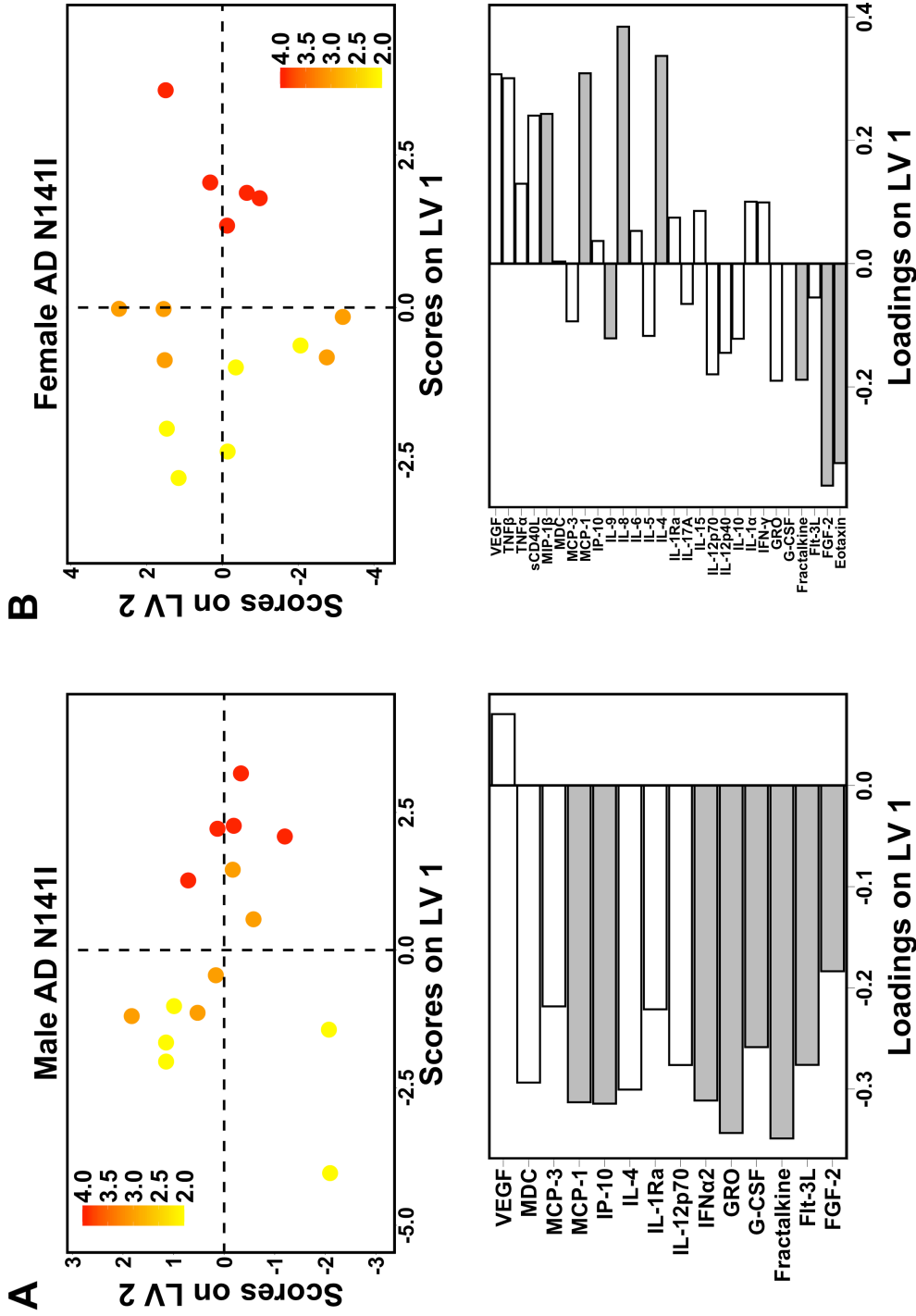


**Figure 3-6: Cytokine secretion decreases in organoids derived from the male N141I iPSC line over time and increases in those of the female N141I iPSC line.** PLSR scores plot (top) and LV1 loadings plot (bottom) of (A) mORG<sup>N141I</sup> from 2- to 4-months in culture (1 LV, RMSECV: 0.745, p-value: 0.01) and (B) fORG<sup>N141I</sup> from 2- to 4-months in culture (1 LV, RMSECV: 0.766, p-value: 0.01). Shaded loadings indicate a VIP score > 1. Each point represents a single sample comprising the lysates of 3-5 organoids. Samples with positive scores (aged mORG<sup>N141I</sup> or fORG<sup>N141I</sup>) correlate with increased levels of cytokines with positive loadings and the down-regulation of cytokines with negative loadings.

*Aging female N141I organoids exhibit a modest increase in pTau levels, but not A $\beta$ , although robust amyloid deposition and tissue atrophy is observed at 3-months*

We then evaluated the levels of A $\beta$  and pTau over the culture timeline, to determine if there were alterations in pathology as a consequence of the amplified cytokine profile in aged fORG<sup>N141I</sup> (Fig 3-7). Immunostaining of fORG<sup>N141I</sup> at 3-months demonstrates distinct amyloid deposition (Fig 3-7A) that encapsulates groupings of cell nuclei and lies along gaps in the tissue, completely devoid of neuronal projections. These atrophied areas are localized to one or two regions within each section, and the majority of area of each organoid shows moderate A $\beta$  deposition (Fig 3-7A, left-most image) comparable to that seen in mORG<sup>N141I</sup> and mORG<sup>iso</sup> images (Fig 3-4C). A $\beta$ 40 and A $\beta$ 42 levels of fORG<sup>N141I</sup> lysates (Fig 3-7C) did not change from 2- to 4-months in culture, however, pTau-181 levels went from being undetectable to detectable at 4-months of age (Fig 3-7C). Given the cytokine-driven accumulation of tau pathology in Alzheimer's disease, an increase in pTau levels is consistent with the persistent heightened immune response phenotype observed over time in the female organoids (Fig 3-6). In contrast to the organoids derived from the male N141I cell line, we did not observe a significant decrease in SYN1 levels (Fig 3-7D).

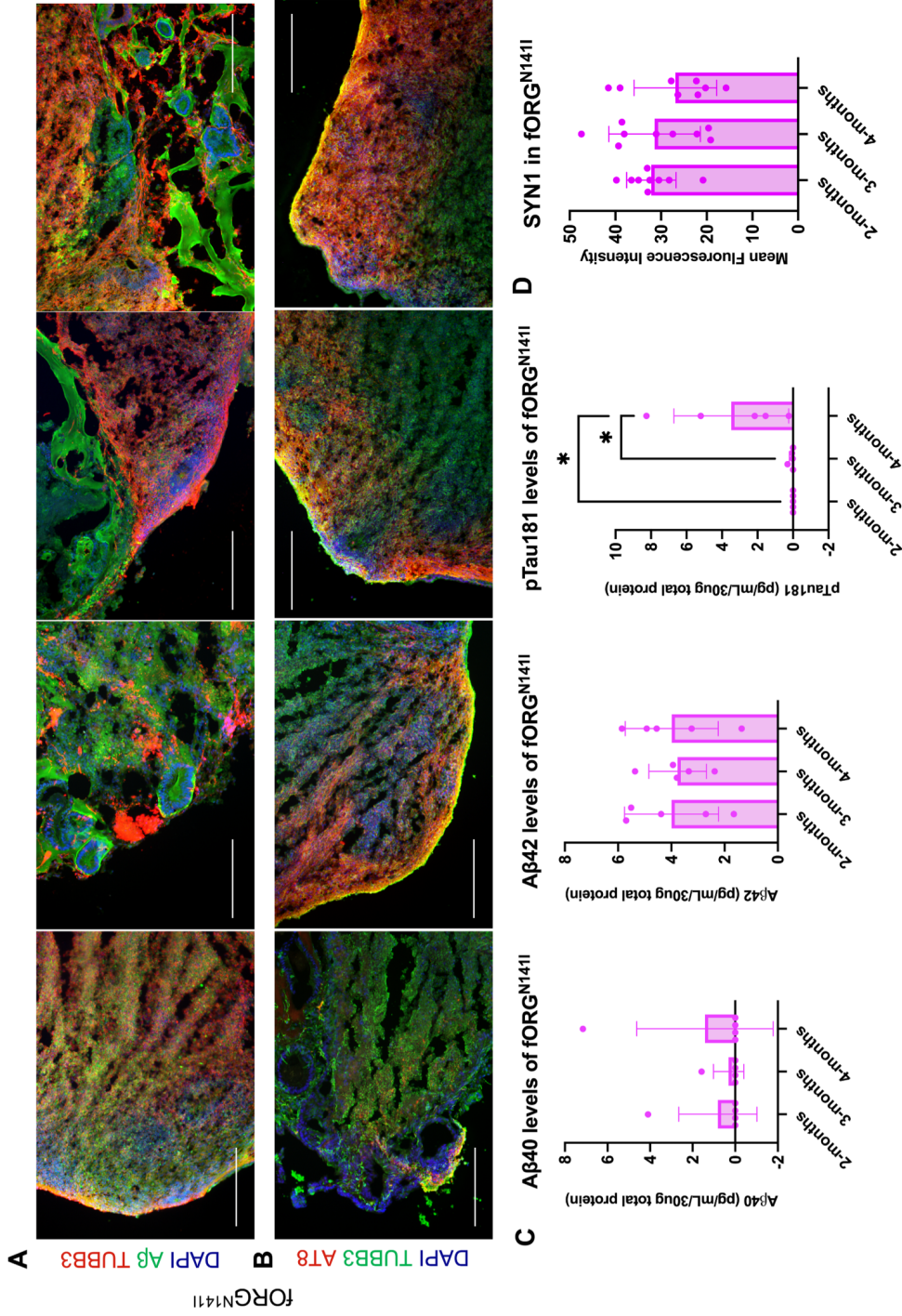


**Figure 3-7: AD organoids from a female N1411 iPSC line demonstrate proteinopathy around tissue atrophy.** (A) Composite images (red: TUBB3, green: A $\beta$ , blue: DAPI) of 3-month-old fORG<sup>N1411</sup>, scale bars: 250 $\mu$ m. (B) Composite images (red: AT8, green: TUBB3, blue: DAPI) of 3-month-old fORG<sup>N1411</sup>, scale bars: 250 $\mu$ m. (C) A $\beta$ 40 (left), A $\beta$ 42 (middle), and pTau-181 (right) protein levels in fORG<sup>N1411</sup> lysates from 2- to 4-months. Each point represents a lysate sample of a combined 3-5 organoids. One-way ANOVA with Tukey's multiple comparison test. 2-month-old fORG<sup>N1411</sup> vs 4-month-old fORG<sup>N1411</sup>, p-value < 0.05. 3-month-old fORG<sup>N1411</sup> vs 4-month-old fORG<sup>N1411</sup>, p-value < 0.05. (D) Quantified SYN1 fluorescence intensity. One-way ANOVA with Tukey's multiple comparison test. Data are mean  $\pm$  SD.

## Discussion

One might think neuroinflammation is on an unwavering increase in the aging diseased brain, but it is a much more convoluted series of likely co-existing cell states that are differentially responding to immune challenge. A $\beta$  and hyperphosphorylated pathological tau both activate microglia, but there is evidence for diverse responses, such as an over-exaggerated “primed” response,<sup>335</sup> a dampened, tolerant response,<sup>101</sup> or even the initiation of cellular senescence.<sup>103–107</sup> At the transcriptomic level, there is even more appreciation for the diversity of unique microglial states,<sup>310–312</sup> but how these translate to their dysfunction is not completely understood. Here, we have demonstrated a dynamic immune milieu in a human cerebral organoid model as a consequence of the familial AD PSEN2 N141I mutation, and, importantly, there are key differences between organoids generated from a male hiPSC line and another from a female cell line. The mORG<sup>N141I</sup> exhibited a gradually decreasing cytokine signature over months in culture, whereas the fORG<sup>N141I</sup> demonstrated a distinct profile that consisted of both increasing and decreasing levels in age. These signatures uniquely reflected the underlying pathology. Early in mORG<sup>N141I</sup> culture, increased cytokines correlated with microglia-sensitive pTau levels, as revealed by microglia depletion studies, whereas the later near-complete decrease in cytokines coincided with a decrease in synapse density that was prevented with microglial depletion. In fORG<sup>N141I</sup>, the amplified cytokine profile of 4-month organoids coincided with an increase of pTau levels. Surprisingly, levels of A $\beta$ 40 and A $\beta$ 42 did not change over time in either model; however, A $\beta$  immunostaining exhibited concentrated signal as opposed to mORG<sup>iso</sup> where A $\beta$  staining was primarily diffuse. Importantly, the regions with the most apparent A $\beta$  deposition in the fORG<sup>N141I</sup> were much more exaggerated than those of mORG<sup>N141I</sup>, with concentrated A $\beta$  appearing along atrophied areas and surrounded cell nuclei in the absence of neuron projections. On the other hand, mORG<sup>N141I</sup> also displayed large, concentrated regions of A $\beta$ , but these areas were still intermingled with neuronal microtubules. It appreciated that there is a greater degree of neuroinflammation and neuropathology in females,<sup>357,358</sup> and while our results are consistent with known

sex-differences, this study's comparison of one male and one female cell line cannot inform sex effects. Further investigation with organoids derived from more iPSC lines from unique individuals is needed.

Microglia are thought to sequester A $\beta$  in the form of plaques and plaque-associated microglia display an altered immune profile,<sup>120,121,336</sup> and, as such, the differences in the deposition of A $\beta$  may be a result of the altered immune signaling rather than an increase in the levels of A $\beta$ . Consistent with our findings, even in the absence of inflammatory stimuli, the microglia of N141I carrying mice secrete more inflammatory cytokines and demonstrate increased engulfment of A $\beta$ .<sup>318</sup> iPSC-derived microglia carrying the N141I mutation exhibited a primed phenotype, with increased secretion of pro-inflammatory cytokines, but, importantly, the three N141I-carrying iPSC lines were all derived from females.<sup>320</sup>

The specific signatures of mORG<sup>N141I</sup> and fORG<sup>N141I</sup> highlighted key cytokines that have previously been identified in AD research. IL-4, which was up-regulated in 2-month-old mORG<sup>N141I</sup> and 4-month-old fORG<sup>N141I</sup>, is traditionally regarded as an anti-inflammatory cytokine that can signal to microglia to adopt a phagocytic phenotype,<sup>334</sup> and IL-4 treatment ameliorates AD pathology in AD mouse models.<sup>337</sup> The down-regulation of G-CSF was uniquely involved in aged mORG<sup>N141I</sup>. G-CSF mobilizes microglia, and, consistently, microglia in AD exhibit impaired motility.<sup>338,339</sup> G-CSF treatment has been shown to rescue cognitive impairment in AD mouse models.<sup>340,341</sup> Fractalkine, or CX3CL1, is a transmembrane protein that is constitutively expressed by neurons.<sup>342</sup> Temporal recruitment of microglia by fractalkine signaling directs homeostatic synapse pruning and network maturation,<sup>343</sup> and injured neurons also cleave fractalkine from their cell membrane to recruit microglia, resulting in their death.<sup>344</sup> Fractalkine was decreased in both 4-month-old mORG<sup>N141I</sup> and fORG<sup>N141I</sup>, but increased at earlier time points. GRO (CXCL1), up-regulated in early mORG<sup>N141I</sup>, has been linked to the phosphorylation of tau and the production of reactive oxygen species.<sup>345,346</sup> 2- and 3-month mORG<sup>N141I</sup> also exhibited increased FGF-2, which was subsequently down-regulated at 4-months. FGF-2 is secreted by injured neurons to initiate protective microglial phenotypes.<sup>347</sup> Most notably, the PLS-DA models differentiating the cytokine profiles of mORG<sup>N141I</sup> and mORG<sup>iso</sup> showed key contribution of the up-regulation of VEGF in the AD organoids in the 3-month model and the sole up-

regulation of VEGF in 4-month-old mORG<sup>N141I</sup>. VEGF has previously been identified through PLS modeling in Alzheimer's disease patient data by our group and was demonstrated to decrease neuron viability in the presence of A $\beta$ .<sup>348</sup> The makeup of the cytokine signatures convey a complicated depiction of the overall immune state with simultaneous protective and detrimental activities; however, it is correlated with a larger picture of decreasing synapse density, accumulation of concentrated A $\beta$  and some increase in pTau.

Synapse loss is one of the earliest alterations in AD and is closely associated with microglia activation in human imaging studies.<sup>349–351</sup> AD mouse models have demonstrated microglia's involvement thorough their direct engulfment of synapses,<sup>80,81</sup> and synapse loss is observed before plaque deposition.<sup>352,353</sup> The prevention of synapse loss in mORG<sup>N141I</sup> with the depletion of microglia, support their direct role in aberrant synapse engulfment, and, importantly, this occurred prior to the chronic immune insult of substantial pathology accumulation. Although Tmem119 signal intensity increased in both the mORG<sup>N141I</sup> and mORG<sup>iso</sup>, suggesting an increasing microglial population, only increasing Tmem119 signal in the AD organoids coincided with decreasing synaptic density, implicating the dysregulated immune response of mORG<sup>N141I</sup>. The very mild, if any, change in the A $\beta$  and pTau levels over time in the organoids is quite remarkable, given the known numerous microglial drivers of A $\beta$  and pTau pathology.<sup>306</sup> This could suggest that the microglia are driving the observed changes, i.e A $\beta$  deposition and synapse loss, independently of pathology. Others have also suggested a larger role of microglia in neurodegeneration, including one study that determined microglia-mediated neuronal damage, rather than tau-dependent mechanisms, was the primary contributor of neurodegeneration in a tauopathy mouse model.<sup>32</sup> It has also been shown that activated microglia alone can initiate neurodegeneration.<sup>307</sup>

It has been demonstrated that the N141I mutation results in the exaggeration of the glial immune response, which resembles a “primed” phenotype commonly observed in age and with chronic A $\beta$  insult.<sup>94</sup> This heightened immune response is largely observable after immune challenge, where A $\beta$ -stimulation or LPS treatment causes an increase in the cytokine secretion of N141I-expressing glial cells compared to

controls.<sup>318,319</sup> We did not observe an increase of A $\beta$  over the experimental timeline but observed an amplified immune milieu in aged female and early male organoids. With the normal accumulation of A $\beta$  in age and insult,<sup>28,354</sup> the early observed phenotypes from the N141I mutation may evolve over time. The events observed over the experimental timeline may be more reminiscent of early events in disease and could inform how glial dysfunction would contribute to the eventual development of AD.

Following treatment with 5 $\mu$ M PLX5622, we observed more than 50% reduction in Tmem119 signal. It has been previously demonstrated that 1 $\mu$ M PLX5622 can achieve nearly 99% reduction of microglia in organotypic slice culture.<sup>355</sup> This discrepancy may be due to the size of the organoids if the compound cannot penetrate far enough into the organoid to deplete persistent microglia populations. Also, because of the immaturity of the cells and heterogeneous expression of microglia specific genes including CSF1R,<sup>299</sup> the cells may not be as sensitive to PLX5622 treatment. However, in our organoids, increasing the concentration to 10 $\mu$ M and 20 $\mu$ M PLX5622 resulted in the organoids falling apart, although concentrations less than 20 $\mu$ M did not previously demonstrate negative effects on viability.<sup>355</sup> Other strategies may have to be employed to achieve full microglia knockout in the organoids, such as a drug antibody conjugates. It is worth noting that we used the expression of Tmem119 to quantify the reduction in the microglia population. Tmem119, thought to be involved in the regulation of the microglial immune response, is differentially expressed in homeostatic and reactive states.<sup>325</sup> Thus, a reduction in the associated fluorescence intensity does not directly correspond to an equal reduction in the microglial population, though this would also be the case of IBA1 as it is regarded as a marker of microglial activation.

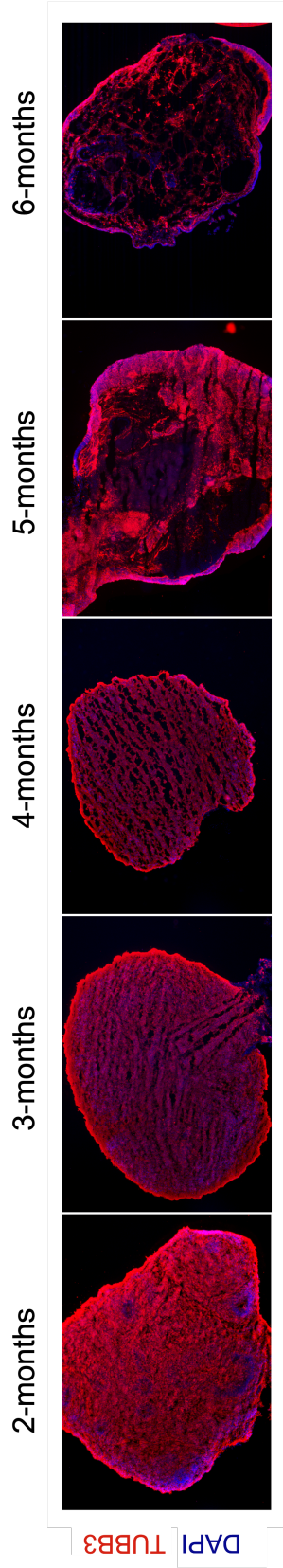
In sporadic disease, AD develops in the absence of disease-causing mutations from a variety of genetic and environmental factors. Primed microglia, which exhibit exaggerated immune responses, contribute to disease in a variety of ways including the accumulation of A $\beta$  and tau pathology and by directly engulfing synapses and injuring neurons through the production of reactive oxygen species.<sup>94</sup> N141I-expressing microglia resemble a primed phenotype, but it is not known if the events of this familial AD-causing mutation and others resemble those of sporadic AD. Human cerebral organoid models offer

the potential to investigate the parallels between familial and sporadic AD, as both patient iPSC-derived models develop some degree of A $\beta$  and pTau pathology, which would allow for the identification of shared therapeutic targets or the recognition of unique mechanisms that would require different disruptions. A caveat to iPSC models, however, are the cells' immaturity. Alzheimer's disease is a disease of aging, and the impact of age on progressing disease cannot be studied in organoids and the confounding effect of cellular maturation are not known. As with all imperfect disease models, the results must be viewed within the lens of its limitations. Correspondingly, we recognize that the comparison of the organoids from two cell lines cannot be taken to wholly reflect sex differences, but the results support previous findings and stress the need for further investigation. With the use of genetically modifiable human cells, the organoid model will be particularly critical in the discovery of the unique roles of AD-specific mutations and risk factors in early disease events through the activities of specific cell-types and their cell-to-cell communication.

We have previously identified an A $\beta$ -specific cytokine signature in 5xFAD mice that reduces neuronal mitochondrial metabolism, capable of predisposing neurons to injury in the absence of A $\beta$  and pTau pathology.<sup>323</sup> In this study, the dynamic cytokine signature of human organoids corresponds to reduced synaptic density and the changes to the deposition of A $\beta$ . Our studies and those of others are highlighting the importance of early glial involvement that may drive neuronal injury to a greater extent than the accumulation of proteinopathy.<sup>307,356</sup> However, preventing dysfunctional immune responses is made more complicated by their diversity and dynamic nature. In this study, over a relatively short culture period, there were numerous dynamic changes in AD organoids, including variable cytokine regulation, the initial increase and subsequent decrease of synaptic density, and microglia-sensitive changes in pathology. Over the course of human disease spanning decades, the magnitude and diversity of changes is imaginably quite impressive, and further investigation will be needed to determine what initiates these changes and when and how is best to modulate them to ameliorate disease.

## Conclusion

In this study of human iPSC-derived Alzheimer's disease cerebral organoids carrying the PSEN2 mutation N141I, we demonstrated dynamic immune signatures that were distinct between organoids derived from a male and female iPSC line and corresponded to underlying changes in pathology. The N141I mutation is observed to alter glial immune activation, which was supported in the organoid model. However, only the organoids derived from the female N141I-carrying iPSC line exhibited persistent amplified responses, whereas the organoids derived from the male N141I-carrying iPSC line demonstrated a dampened response with time that uniquely coincided with synapse loss. The organoid microglia, while not driving the accumulation of A $\beta$  and pTau, decreased synapse density in male AD organoids, which could be prevented with microglial depletion. Significant reduction in synapse density was not observed in female organoids, although they displayed more prominent A $\beta$  deposition and tissue atrophy corresponding to an increase in inflammatory cytokines. Through the use of human patient-derived models, gene-specific changes capable of driving disease will identify early disease-causing mechanisms, likely unobservable in mouse models.



**Supplementary Figure 3-1: Female PSEN2 N141I organoids exhibit robust tissue atrophy after 5-months in culture. TUBB3 (red) and DAPI (blue) immunostaining of 2-, 3-, 4-, 5-, and 6-month-old organoids (left to right),**

scale bars: 500µm

## Chapter 4

### Summary of Research, Implications, And Future Research Directions

#### Summary of Research

A growing appreciation for neuroinflammation, especially the role of microglia, in the early events of disease progression has suggested restoring homeostatic immune function to be a worthwhile therapeutic target. However, the diversity and dynamic nature of microglia responses in AD have not been completely characterized to identify modulation strategies that would offer beneficial effects without worsening detrimental function. In this dissertation, I have taken two views of approaching dysregulated immune response. In Chapter 2, we used a 5xFAD mouse model for a tissue-level characterization of the immune milieu in the hippocampus to gain an understanding for the overall dysregulation of immune cues that resident cells would be experiencing. We investigated how healthy neurons in the absence of pathology respond to key cytokines of the progressing A $\beta$ -predictive signature of IFN- $\gamma$ , IP-10, and IL-9. The cytokine treatment reduced the expression of mitochondrial respiration chain complex subunits, which translated to the functional reduction of mitochondrial respiration in primary neurons at both the basal level (decreased basal respiration upon cytokine treatment,  $p$ -val < 0.05) and under a simulated energy demand (decreased maximal respiration upon cytokine treatment,  $p$ -val = 0.01). Without the presence of pathology, dysregulated immune signaling negatively affects neurons and could predispose them to further injury. In Chapter 3, we used an AD cerebral organoid model to look at microglia-specific function related to the immune milieu that affects pathology and neuronal viability. Organoids derived from a male or female iPSC line exhibit drastically different cytokine signatures over time, with the male organoids demonstrating an overall reduction in cytokine secretion after an initial amplified immune response and the female organoids exhibiting a persistent heightened immune response over time, despite less levels of A $\beta$  and tau.

The male organoids demonstrated a significant reduction in synapse density (SYN1 signal intensity decrease,  $p\text{-val}<0.05$ ), whereas the female organoids displayed larger deposition of amyloid and tissue atrophy. There were not large changes to the levels of pathological proteins over the experimental timeline, and the effect on amyloid presentation in accumulated deposits and the loss of synapses were associated with altered microglial responses not initiated by a substantial accumulation pathology. In these studies, we identified how the overall immune milieu, likely made up of a large diversity of different activation patterns and response, independently affects neurons and the cell-specific contribution of microglia.

## **Implications**

There is a growing number of studies characterizing the diversity of microglial transcriptomic states and the effect of the dysfunction of microglial risk genes on pathology. However, there had not yet been an overall characterization of the neuroinflammatory state over time and how the great diversity of immune activation signatures converges to produce changes in AD pathology. In our studies, we leverage a systems biology approach to take an unbiased survey of evolving neuroinflammation to identify key dysregulated cytokine signaling and study their effects in combination with each other rather than in isolation to better reflect the physiological environment of the brain. Additionally, the use of a human organoid model to study the effects of microglia in Alzheimer's disease has not been previously demonstrated, and, importantly, we identified the differential dysregulation of immune signaling in organoids carrying the familial PSEN2 N141I mutation from either a male or female iPSC line, previously only appreciated to result in an amplified, persisted immune response. It is my hope that our use of iPSC-derived models further demonstrates their unique advantages to others in the field and that smaller labs are encouraged to venture into iPSC work.

## Future Research Directions

Both the 5xFAD and AD organoid studies were newly started in the first couple years of the Proctor, and I'm excited to have created a foundation that incoming students can work off of for years to come. Especially in the 5xFAD study, there is future possibilities of identifying the mechanism by which cytokine signaling affects neuronal mitochondrial metabolism. We have identified potential regulation by PGC-1 $\alpha$  signaling, which is known to control mitochondrial bioenergetics and the expression of electron transport chain complex genes. PGC-1 $\alpha$  can be differentially regulated by cytokines in other tissues, such as the heart, kidney, and liver. Notably, PGC-1 $\alpha$  activation is downstream of GLP-1 signaling, which in recent months has been studied in drugs like Ozempic for their positive effects on dementia. Immunometabolism, which marries two critical early alterations in the AD brain: neuroinflammation and dysregulated metabolism, is an additional research "arm" of the Proctor lab that that will continue building from this work.

In the organoid work, there are vast emerging possibilities to explore since the model's development less than 10 years ago. Stemming directly from the work presented in this dissertation, I envision future investigations to involve many patient-derived iPSC lines from both males and females. In Chapter 3, we saw parallels of dysregulated immune signaling by the PSEN2 N141I mutation and that of primed microglia in sporadic disease. With the capacity of iPSC-derived models to develop pathology from patients of sporadic disease, there is an opportunity for the characterization of etiological differences in familial and sporadic disease, unachievable using AD mouse models. The identification of early disease events will likely be pivotal in the discovery of therapeutic interventions, as downstream AD is driven by a relentless multifaceted feedback loop of increasing neuroinflammation, proteinopathy, and neurodegeneration. Our upcoming single-cell RNA sequencing studies of the AD and isogenic control organoids will allow us to dissect the overall neuroinflammatory profiles we observed with cell-type

specific transcriptomic differences. This work will inform the future identification of modulation strategies to disrupt detrimental immune signaling that can be easily explored in the organoid model.

In the combination of these two studies, I envision new investigation of the region-specific effects of microglia. This dissertation has stressed the importance of dynamic regulation of diverse immune states, particularly in its temporal changes. But, there is another critical factor in its spatial information. Microglia display region-specific transcriptomes and immune function,<sup>111,172</sup> and there is evidence to suggest that these differences contribute to the regional spread and sensitivity to AD pathology in the brain.<sup>173</sup> Tau pathology spread that does not occur along the connections of synapses has been attributed to microglia.<sup>137,138</sup> In our 5xFAD and other mouse model work, we have also observed region-specific effects on cytokine signaling. In light of our previous investigation of how the combination of dysregulated immune cues converge to contribute disease, it is likely that regional differences in immune signaling contribute to the differential regional sensitivity and spread of AD pathology. The nature of this work may be restricted to mouse models; however, there are differentiation strategies to develop region-specific identities in cerebral organoids, such as hippocampal, ventral, and cortical identities.<sup>296,297</sup>

## **Conclusions**

The work presented in this dissertation aimed to characterize dynamic neuroinflammatory signatures that uniquely contribute to pathology accumulation and neuronal vulnerability in Alzheimer's disease. There is vast diversity in the microglia activation states that underly the overall immune milieu of the brain, and I sought to better understand how they converge at the tissue-level to translate to functional changes and ultimately the progression of disease. This work demonstrates the first use of microglia-containing organoids in Alzheimer's disease research, which allowed us to identify dysregulated immune signaling that was specific to a disease-causing mutation. Future work will expand on microglia-specific

contributions to disease and their temporal and spatial diversity and aim to identify modulations in early disease events capable of disrupting or preventing the multifaceted, synergistic drivers of Alzheimer's disease.

## REFERENCES

1. Stelzmann, R. A., Norman Schnitzlein, H. & Reed Murtagh, F. An english translation of alzheimer's 1907 paper, "über eine eigenartige erkankung der hirnrinde". *Clinical Anatomy* **8**, 429–431 (1995).
2. Rajan, K. B. *et al.* Population estimate of people with clinical Alzheimer's disease and mild cognitive impairment in the United States (2020–2060). *Alzheimer's & Dementia* **17**, 1966–1975 (2021).
3. Heppner, F. L., Ransohoff, R. M. & Becher, B. Immune attack: The role of inflammation in Alzheimer disease. *Nature Reviews Neuroscience* vol. 16 358–372 Preprint at <https://doi.org/10.1038/nrn3880> (2015).
4. Hemonnot, A. L., Hua, J., Ulmann, L. & Hirbec, H. Microglia in Alzheimer disease: Well-known targets and new opportunities. *Frontiers in Cellular and Infection Microbiology* vol. 9 233 Preprint at <https://doi.org/10.3389/fnagi.2019.00233> (2019).
5. Tarkowski, E., Andreasen, N., Tarkowski, A. & Blennow, K. Intrathecal inflammation precedes development of Alzheimer's disease. *J Neurol Neurosurg Psychiatry* **74**, 1200–1205 (2003).
6. Brosseron, F., Krauthausen, M., Kummer, M. & Heneka, M. T. Body fluid cytokine levels in mild cognitive impairment and Alzheimer's disease: a comparative overview. *Mol Neurobiol* **50**, 534–544 (2014).
7. Hansen, D. V., Hanson, J. E. & Sheng, M. Microglia in Alzheimer's disease. *Journal of Cell Biology* vol. 217 459–472 Preprint at <https://doi.org/10.1083/jcb.201709069> (2018).
8. Yoshiyama, Y. *et al.* Synapse Loss and Microglial Activation Precede Tangles in a P301S Tauopathy Mouse Model. *Neuron* **53**, 337–351 (2007).
9. Minhas, P. S. *et al.* Restoring metabolism of myeloid cells reverses cognitive decline in ageing. *Nature* 2021 590:7844 **590**, 122–128 (2021).

10. Fakhoury, M. Microglia and astrocytes in Alzheimer's disease: implications for therapy. *Curr Neuropharmacol* **15**, (2017).
11. Sheffield, L. G., Marquis, J. G. & Berman, N. E. J. Regional distribution of cortical microglia parallels that of neurofibrillary tangles in Alzheimer's disease. *Neurosci Lett* **285**, 165–168 (2000).
12. Serrano-Pozo, A. *et al.* Reactive glia not only associates with plaques but also parallels tangles in Alzheimer's disease. *American Journal of Pathology* **179**, 1373–1384 (2011).
13. Pimenova, A. A., Raj, T. & Goate, A. M. Untangling Genetic Risk for Alzheimer's Disease. *Biological Psychiatry* vol. 83 300–310 Preprint at <https://doi.org/10.1016/j.biopsych.2017.05.014> (2018).
14. Wolf, S. A., Boddeke, H. W. G. M. & Kettenmann, H. Microglia in Physiology and Disease. *Annual Review of Physiology* vol. 79 619–643 Preprint at <https://doi.org/10.1146/annurev-physiol-022516-034406> (2017).
15. EC, K., LD, M. & RM, R. Old Maids: Aging and Its Impact on Microglia Function. *Int J Mol Sci* **18**, (2017).
16. Sarlus, H. & Heneka, M. T. Microglia in Alzheimer's disease. *Journal of Clinical Investigation* vol. 127 3240–3249 Preprint at <https://doi.org/10.1172/JCI90606> (2017).
17. Paolicelli, R. C. *et al.* Microglia states and nomenclature: A field at its crossroads. *Neuron* vol. 110 Preprint at <https://doi.org/10.1016/j.neuron.2022.10.020> (2022).
18. Mhatre, S. D., Tsai, C. A., Rubin, A. J., James, M. L. & Andreasson, K. I. Microglial Malfunction: The Third Rail in the Development of Alzheimer's Disease. *Trends in Neurosciences* vol. 38 621–636 Preprint at <https://doi.org/10.1016/j.tins.2015.08.006> (2015).
19. Baik, S. H. *et al.* A Breakdown in Metabolic Reprogramming Causes Microglia Dysfunction in Alzheimer's Disease. *Cell Metab* **30**, 493–507 (2019).

20. Block, M. L., Zecca, L. & Hong, J. S. Microglia-mediated neurotoxicity: Uncovering the molecular mechanisms. *Nature Reviews Neuroscience* vol. 8 57–69 Preprint at <https://doi.org/10.1038/nrn2038> (2007).
21. Mathys, H. *et al.* Temporal Tracking of Microglia Activation in Neurodegeneration at Single-Cell Resolution. *Cell Rep* **21**, (2017).
22. Perez-Nievas, B. G. *et al.* Dissecting phenotypic traits linked to human resilience to Alzheimer's pathology. *Brain* **136**, 2510–26 (2013).
23. Braak, H. & Del Tredici, K. The pathological process underlying Alzheimer's disease in individuals under thirty. *Acta Neuropathol* **121**, 171–181 (2011).
24. Vojtechova, I., Machacek, T., Kristofikova, Z., Stuchlik, A. & Petrasek, T. Infectious origin of Alzheimer's disease: Amyloid beta as a component of brain antimicrobial immunity. *PLoS Pathogens* vol. 18 Preprint at <https://doi.org/10.1371/journal.ppat.1010929> (2022).
25. Bowirrat, A. Immunosenescence and Aging: Neuroinflammation Is a Prominent Feature of Alzheimer's Disease and Is a Likely Contributor to Neurodegenerative Disease Pathogenesis. *Journal of Personalized Medicine* vol. 12 Preprint at <https://doi.org/10.3390/jpm12111817> (2022).
26. McFarland, K. N. & Chakrabarty, P. Microglia in Alzheimer's Disease: a Key Player in the Transition Between Homeostasis and Pathogenesis. *Neurotherapeutics* vol. 19 Preprint at <https://doi.org/10.1007/s13311-021-01179-3> (2022).
27. MR, D. *et al.* Age-related alterations in the dynamic behavior of microglia. *Aging Cell* **10**, 263–276 (2011).
28. Rodrigue, K. M. *et al.*  $\beta$ -amyloid burden in healthy aging: Regional distribution and cognitive consequences. *Neurology* **78**, (2012).
29. Johnson, V. E., Stewart, W. & Smith, D. H. Traumatic brain injury and amyloid- $\beta$  pathology: A link to alzheimer's disease? *Nat Rev Neurosci* **11**, (2010).

30. Pascoal, T. A. *et al.* Microglial activation and tau propagate jointly across Braak stages. doi:10.1038/s41591-021-01456-w.
31. Shi, Y. & Holtzman, D. M. Interplay between innate immunity and Alzheimer disease: APOE and TREM2 in the spotlight. *Nature Reviews Immunology* vol. 18 759–772 Preprint at <https://doi.org/10.1038/s41577-018-0051-1> (2018).
32. Shi, Y. *et al.* Microglia drive APOE-dependent neurodegeneration in a tauopathy mouse model. *Journal of Experimental Medicine* **216**, (2019).
33. Esquerda-Canals, G., Montoliu-Gaya, L., Güell-Bosch, J. & Villegas, S. Mouse Models of Alzheimer's Disease. *Journal of Alzheimer's Disease* **57**, 1171–1183 (2017).
34. Sasaguri, H. *et al.* APP mouse models for Alzheimer's disease preclinical studies. *EMBO J* **36**, 2473–2487 (2017).
35. Elder, G. A., Gama Sosa, M. A. & De Gasperi, R. Transgenic Mouse Models of Alzheimer's Disease. *Mount Sinai Journal of Medicine: A Journal of Translational and Personalized Medicine* **77**, 69–81 (2010).
36. Myers, A. & McGonigle, P. Overview of Transgenic Mouse Models for Alzheimer's Disease. *Curr Protoc Neurosci* **89**, e81 (2019).
37. Schwab, C., Hosokawa, M. & McGeer, P. L. Transgenic mice overexpressing amyloid beta protein are an incomplete model of Alzheimer disease. *Exp Neurol* **188**, 52–64 (2004).
38. De Strooper, B. & Karran, E. The Cellular Phase of Alzheimer's Disease. *Cell* vol. 164 603–615 Preprint at <https://doi.org/10.1016/j.cell.2015.12.056> (2016).
39. Irizarry, M. C. *et al.* A $\beta$  deposition is associated with neuropil changes, but not with overt neuronal loss in the human amyloid precursor protein V717F (PDAPP) transgenic mouse. *Journal of Neuroscience* **17**, (1997).

40. Irizarry, M. C., McNamara, M., Fedorchak, K., Hsiao, K. & Hyman, B. T. APP(Sw) transgenic mice develop age-related A $\beta$  deposits and neuropil abnormalities, but no neuronal loss in CA1. *J Neuropathol Exp Neurol* **56**, (1997).
41. Cruchaga, C. *et al.* Rare variants in APP, PSEN1 and PSEN2 increase risk for AD in late-onset Alzheimer's disease families. *PLoS One* **7**, (2012).
42. Galatro, T. F. *et al.* Transcriptomic analysis of purified human cortical microglia reveals age-associated changes. *Nat Neurosci* **20**, 1162–1171 (2017).
43. Gosselin, D. *et al.* An environment-dependent transcriptional network specifies human microglia identity. *Science (1979)* **356**, 1248–1259 (2017).
44. BA, F. *et al.* Diverse Brain Myeloid Expression Profiles Reveal Distinct Microglial Activation States and Aspects of Alzheimer's Disease Not Evident in Mouse Models. *Cell Rep* **22**, 832–847 (2018).
45. Zerbino, D. R. *et al.* Ensembl 2018. *Nucleic Acids Res* **46**, D754–D761 (2018).
46. Penney, J., Ralvenius, W. T. & Tsai, L.-H. Modeling Alzheimer's disease with iPSC-derived brain cells. *Molecular Psychiatry* 2019 25:1 **25**, 148–167 (2019).
47. Lee, D. C. *et al.* Review: Experimental manipulations of microglia in mouse models of Alzheimer's pathology: Activation reduces amyloid but hastens tau pathology. *Neuropathol Appl Neurobiol* **39**, 69–85 (2013).
48. Sessa, G. *et al.* Distribution and signaling of TREM2/DAP12, the receptor system mutated in human polycystic lipomembraneous osteodysplasia with sclerosing leukoencephalopathy dementia. *European Journal of Neuroscience* **20**, (2004).
49. Neumann, H. & Takahashi, K. Essential role of the microglial triggering receptor expressed on myeloid cells-2 (TREM2) for central nervous tissue immune homeostasis. *Journal of Neuroimmunology* vol. 184 Preprint at <https://doi.org/10.1016/j.jneuroim.2006.11.032> (2007).

50. Takahashi, K., Prinz, M., Stagi, M., Chechneva, O. & Neumann, H. TREM2-transduced myeloid precursors mediate nervous tissue debris clearance and facilitate recovery in an animal model of multiple sclerosis. *PLoS Med* **4**, (2007).
51. K, T., CD, R. & H, N. Clearance of apoptotic neurons without inflammation by microglial triggering receptor expressed on myeloid cells-2. *J Exp Med* **201**, 647–657 (2005).
52. Nguyen, M. D., Julien, J. P. & Rivest, S. Innate immunity: The missing link in neuroprotection and neurodegeneration? *Nat Rev Neurosci* **3**, (2002).
53. C, C. *et al.* GWAS of cerebrospinal fluid tau levels identifies risk variants for Alzheimer's disease. *Neuron* **78**, 256–268 (2013).
54. LF, L. *et al.* TREM2 Protein Expression Changes Correlate with Alzheimer's Disease Neurodegenerative Pathologies in Post-Mortem Temporal Cortices. *Brain Pathol* **25**, 469–480 (2015).
55. Jay, T. R. *et al.* TREM2 deficiency eliminates TREM2+ inflammatory macrophages and ameliorates pathology in Alzheimer's disease mouse models. *Journal of Experimental Medicine* **212**, (2015).
56. T, J. *et al.* Upregulation of TREM2 ameliorates neuropathology and rescues spatial cognitive impairment in a transgenic mouse model of Alzheimer's disease. *Neuropsychopharmacology* **39**, 2949–2962 (2014).
57. Melchior, B. *et al.* Dual induction of TREM2 and tolerance-related transcript, Tmem176b, in amyloid transgenic mice: Implications for vaccine-based therapies for Alzheimer's disease. *ASN Neuro* **2**, (2010).
58. Wang, Y. *et al.* TREM2 lipid sensing sustains the microglial response in an Alzheimer's disease model. *Cell* **160**, (2015).
59. Frank, S. *et al.* TREM2 is upregulated in amyloid plaque-associated microglia in aged APP23 transgenic mice. *Glia* **56**, (2008).

60. Ulrich, J. D. *et al.* Altered microglial response to A $\beta$  plaques in APPPS1-21 mice heterozygous for TREM2. *Mol Neurodegener* **9**, (2014).
61. Y, W. *et al.* TREM2-mediated early microglial response limits diffusion and toxicity of amyloid plaques. *J Exp Med* **213**, 667–675 (2016).
62. Jiang, T. *et al.* Silencing of TREM2 exacerbates tau pathology, neurodegenerative changes, and spatial learning deficits in P301S tau transgenic mice. *Neurobiol Aging* **36**, 3176–3186 (2015).
63. Yoshiyama, Y. *et al.* Synapse Loss and Microglial Activation Precede Tangles in a P301S Tauopathy Mouse Model. *Neuron* **53**, 337–351 (2007).
64. Quintanilla, R. A., Orellana, D. I., González-Billault, C. & Maccioni, R. B. Interleukin-6 induces Alzheimer-type phosphorylation of tau protein by deregulating the cdk5/p35 pathway. *Exp Cell Res* **295**, 245–257 (2004).
65. Gorlovoy, P., Larionov, S., Pham, T. T. H. & Neumann, H. Accumulation of tau induced in neurites by microglial proinflammatory mediators. *The FASEB Journal* **23**, 2502–2513 (2009).
66. Lee, D. C. *et al.* LPS- induced inflammation exacerbates phospho-tau pathology in rTg4510 mice. *J Neuroinflammation* **7**, 56 (2010).
67. Maphis, N. *et al.* Reactive microglia drive tau pathology and contribute to the spreading of pathological tau in the brain. *Brain* **138**, 1738–1755 (2015).
68. Jiang, T. *et al.* TREM2 Ameliorates Neuronal Tau Pathology Through Suppression of Microglial Inflammatory Response. *Inflammation* **41**, 811–823 (2018).
69. Bemiller, S. M. *et al.* TREM2 deficiency exacerbates tau pathology through dysregulated kinase signaling in a mouse model of tauopathy. *Molecular Neurodegeneration* **12**, 1–12 (2017).
70. Leyns, C. E. G. *et al.* TREM2 deficiency attenuates neuroinflammation and protects against neurodegeneration in a mouse model of tauopathy. *Proceedings of the National Academy of Sciences* **114**, 11524–11529 (2017).

71. Hansen, D. V., Hanson, J. E. & Sheng, M. Microglia in Alzheimer's disease. *Journal of Cell Biology* vol. 217 459–472 Preprint at <https://doi.org/10.1083/jcb.201709069> (2018).
72. Brown, G. C. & Neher, J. J. Microglial phagocytosis of live neurons. *Nat Rev Neurosci* **15**, (2014).
73. Arnoux, I. & Audinat, E. Fractalkine signaling and microglia functions in the developing brain. *Neural Plasticity* vol. 2015 Preprint at <https://doi.org/10.1155/2015/689404> (2015).
74. Paolicelli, R. C., Bisht, K. & Tremblay, M. È. Fractalkine regulation of microglial physiology and consequences on the brain and behavior. *Frontiers in Cellular Neuroscience* vol. 8 Preprint at <https://doi.org/10.3389/fncel.2014.00129> (2014).
75. Lee, S. *et al.* CX3CR1 deficiency alters microglial activation and reduces beta-amyloid deposition in two Alzheimer's disease mouse models. *American Journal of Pathology* **177**, 2549–2562 (2010).
76. Fuhrmann, M. *et al.* Microglial Cx3cr1 knockout prevents neuron loss in a mouse model of Alzheimer's disease. *Nat Neurosci* **13**, 411–413 (2010).
77. Nash, K. R. *et al.* Fractalkine overexpression suppresses tau pathology in a mouse model of tauopathy. *Neurobiol Aging* **34**, 1540–1548 (2013).
78. Z, L., C, C., A, S., R, H. & J, G. CX3CR1 in microglia regulates brain amyloid deposition through selective protofibrillar amyloid- $\beta$  phagocytosis. *J Neurosci* **30**, 17091–17101 (2010).
79. Bhaskar, K. *et al.* Regulation of tau pathology by the microglial fractalkine receptor. *Neuron* **68**, 19–31 (2010).
80. Stephan, A. H., Barres, B. A. & Stevens, B. The complement system: An unexpected role in synaptic pruning during development and disease. *Annual Review of Neuroscience* vol. 35 Preprint at <https://doi.org/10.1146/annurev-neuro-061010-113810> (2012).
81. Y, W., L, D.-O., BA, M. & B, S. Microglia: Dynamic Mediators of Synapse Development and Plasticity. *Trends Immunol* **36**, 605–613 (2015).

82. Zanjani, H. *et al.* Complement activation in very early Alzheimer disease. *Alzheimer Dis Assoc Disord* **19**, (2005).
83. Alexander, J. J., Anderson, A. J., Barnum, S. R., Stevens, B. & Tenner, A. J. The complement cascade: Yin-Yang in neuroinflammation - Neuro-protection and -degeneration. *Journal of Neurochemistry* vol. 107 Preprint at <https://doi.org/10.1111/j.1471-4159.2008.05668.x> (2008).
84. Hong, S. *et al.* Complement and microglia mediate early synapse loss in Alzheimer mouse models. *Science (1979)* **352**, (2016).
85. Shi, Q. *et al.* Complement C3 deficiency protects against neurodegeneration in aged plaque-rich APP/PS1 mice. *Sci Transl Med* **9**, (2017).
86. M, M. *et al.* Complement C3 deficiency leads to accelerated amyloid beta plaque deposition and neurodegeneration and modulation of the microglia/macrophage phenotype in amyloid precursor protein transgenic mice. *J Neurosci* **28**, 6333–6341 (2008).
87. T, W.-C. *et al.* Prominent neurodegeneration and increased plaque formation in complement-inhibited Alzheimer's mice. *Proc Natl Acad Sci U S A* **99**, 10837–10842 (2002).
88. MI, F. *et al.* Treatment with a C5aR antagonist decreases pathology and enhances behavioral performance in murine models of Alzheimer's disease. *J Immunol* **183**, 1375–1383 (2009).
89. MI, F. *et al.* Contribution of complement activation pathways to neuropathology differs among mouse models of Alzheimer's disease. *J Neuroinflammation* **8**, (2011).
90. MI, F., J, Z., M, B. & AJ, T. Absence of C1q leads to less neuropathology in transgenic mouse models of Alzheimer's disease. *J Neurosci* **24**, 6457–6465 (2004).
91. Reichwald, J., Danner, S., Wiederhold, K. H. & Staufenbiel, M. Expression of complement system components during aging and amyloid deposition in APP transgenic mice. *J Neuroinflammation* **6**, (2009).
92. M, B. *et al.* Deficiency of terminal complement pathway inhibitor promotes neuronal tau pathology and degeneration in mice. *J Neuroinflammation* **9**, (2012).

93. Franceschi, C., Garagnani, P., Parini, P., Giuliani, C. & Santoro, A. Inflammaging: a new immune–metabolic viewpoint for age-related diseases. *Nature Reviews Endocrinology* vol. 14 576–590 Preprint at <https://doi.org/10.1038/s41574-018-0059-4> (2018).
94. Li, J.-W., Zong, Y., Cao, X.-P., Tan, L. & Tan, L. Microglial priming in Alzheimer’s disease. *Ann Transl Med* **6**, (2018).
95. Norden, D. M. & Godbout, J. P. Review: Microglia of the aged brain: Primed to be activated and resistant to regulation. *Neuropathology and Applied Neurobiology* vol. 39 Preprint at <https://doi.org/10.1111/j.1365-2990.2012.01306.x> (2013).
96. Hickman, S. E., Allison, E. K. & El Khoury, J. Microglial dysfunction and defective  $\beta$ -amyloid clearance pathways in aging alzheimer’s disease mice. *Journal of Neuroscience* **28**, (2008).
97. A, D. *et al.* Young microglia restore amyloid plaque clearance of aged microglia. *EMBO J* **36**, 583–603 (2017).
98. Hellwig, S. *et al.* Forebrain microglia from wild-type but not adult 5xFAD mice prevent amyloid- $\beta$  plaque formation in organotypic hippocampal slice cultures. *Sci Rep* **5**, (2015).
99. Radde, R. *et al.* Abeta42-driven cerebral amyloidosis in transgenic mice reveals early and robust pathology. *EMBO Rep* **7**, 940–946 (2006).
100. Oakley, H. *et al.* Intraneuronal  $\beta$ -amyloid aggregates, neurodegeneration, and neuron loss in transgenic mice with five familial Alzheimer’s disease mutations: Potential factors in amyloid plaque formation. *Journal of Neuroscience* **26**, 10129–10140 (2006).
101. Baik, S. H. *et al.* A Breakdown in Metabolic Reprogramming Causes Microglia Dysfunction in Alzheimer’s Disease. *Cell Metab* **30**, 493–507 (2019).
102. Chen, X. *et al.* Microglia-mediated T cell infiltration drives neurodegeneration in tauopathy. *Nature* **615**, (2023).
103. Karabag, D. *et al.* Characterizing microglial senescence: Tau as a key player. *J Neurochem* (2023) doi:10.1111/jnc.15866.

104. Bussian, T. J. *et al.* Clearance of senescent glial cells prevents tau-dependent pathology and cognitive decline. *Nature* **562**, 578–582 (2018).
105. Musi, N. *et al.* Tau protein aggregation is associated with cellular senescence in the brain. *Aging Cell* **17**, (2018).
106. Brelstaff, J. H. *et al.* Microglia become hypofunctional and release metalloproteases and tau seeds when phagocytosing live neurons with P301S tau aggregates. *Sci Adv* **7**, (2021).
107. Streit, W. J., Braak, H., Xue, Q. S. & Bechmann, I. Dystrophic (senescent) rather than activated microglial cells are associated with tau pathology and likely precede neurodegeneration in Alzheimer's disease. *Acta Neuropathol* **118**, 475–485 (2009).
108. Greenwood, E. K. & Brown, D. R. Senescent microglia: The key to the ageing brain? *International Journal of Molecular Sciences* vol. 22 Preprint at <https://doi.org/10.3390/ijms22094402> (2021).
109. Muñoz-Espín, D. & Serrano, M. Cellular senescence: From physiology to pathology. *Nature Reviews Molecular Cell Biology* vol. 15 Preprint at <https://doi.org/10.1038/nrm3823> (2014).
110. Masuda, T. *et al.* Spatial and temporal heterogeneity of mouse and human microglia at single-cell resolution. *Nature* **566**, (2019).
111. Grabert, K. *et al.* Microglial brain region–dependent diversity and selective regional sensitivities to aging. *Nature Neuroscience* **2016 19:3 19**, 504–516 (2016).
112. H, M. *et al.* Single-cell transcriptomic analysis of Alzheimer's disease. *Nature* **570**, 332–337 (2019).
113. Alsema, A. M. *et al.* Profiling Microglia From Alzheimer's Disease Donors and Non-demented Elderly in Acute Human Postmortem Cortical Tissue. *Front Mol Neurosci* **13**, (2020).
114. Keren-Shaul, H. *et al.* A Unique Microglia Type Associated with Restricting Development of Alzheimer's Disease. *Cell* **169**, 1276-1290.e17 (2017).

115. Krasemann, S. *et al.* The TREM2-APOE Pathway Drives the Transcriptional Phenotype of Dysfunctional Microglia in Neurodegenerative Diseases. *Immunity* **47**, 566-581.e9 (2017).
116. Frautschy, S. A., Baird, A. & Coleo, G. M. *Effects of injected Alzheimer f3-amyloid cores in rat brain. Proc. Natl. Acad. Sci. USA* vol. 88 (1991).
117. Ard, M. D., Cole, G. M., Wei, J., Mehrle, A. P. & Fratkin, J. D. Scavenging of Alzheimer's amyloid  $\beta$ -protein by microglia in culture. *J Neurosci Res* **43**, 190–202 (1996).
118. Weldon, D. T. *et al.* Fibrillar  $\beta$ -amyloid induces microglial phagocytosis, expression of inducible nitric oxide synthase, and loss of a select population of neurons in the rat CNS in vivo. *Journal of Neuroscience* **18**, 2161–2173 (1998).
119. Lee, M., McGeer, E. & McGeer, P. L. Activated human microglia stimulate neuroblastoma cells to upregulate production of beta amyloid protein and tau: Implications for Alzheimer's disease pathogenesis. *Neurobiol Aging* **36**, 42–52 (2015).
120. Huang, Y. *et al.* Microglia use TAM receptors to detect and engulf amyloid  $\beta$  plaques. *Nat Immunol* **22**, (2021).
121. Lee, H. G. *et al.* Challenging the amyloid cascade hypothesis: Senile plaques and amyloid- $\beta$  as protective adaptations to Alzheimer disease. in *Annals of the New York Academy of Sciences* vol. 1019 (2004).
122. Villemagne, V. L. *et al.* Amyloid  $\beta$  deposition, neurodegeneration, and cognitive decline in sporadic Alzheimer's disease: A prospective cohort study. *Lancet Neurol* **12**, 357–367 (2013).
123. Jack, C. R. *et al.* BRAIN A JOURNAL OF NEUROLOGY Serial PIB and MRI in normal, mild cognitive impairment and Alzheimer's disease: implications for sequence of pathological events in Alzheimer's disease. doi:10.1093/brain/awp062.
124. Sperling, R., Mormino, E. & Johnson, K. The evolution of preclinical Alzheimer's disease: Implications for prevention trials. *Neuron* vol. 84 Preprint at <https://doi.org/10.1016/j.neuron.2014.10.038> (2014).

125. Su, Y. & Chang, P. T. Acidic pH promotes the formation of toxic fibrils from  $\beta$ -amyloid peptide. *Brain Res* **893**, (2001).
126. Tseng, B. P. *et al.* Deposition of monomeric, not oligomeric, A $\beta$  mediates growth of Alzheimer's disease amyloid plaques in human brain preparations. *Biochemistry* **38**, (1999).
127. Spangenberg, E. *et al.* Sustained microglial depletion with CSF1R inhibitor impairs parenchymal plaque development in an Alzheimer's disease model. *Nat Commun* **10**, 1–21 (2019).
128. Oddo, S. *et al.* Triple-transgenic model of Alzheimer's Disease with plaques and tangles: Intracellular A $\beta$  and synaptic dysfunction. *Neuron* **39**, 409–421 (2003).
129. Condello, C., Yuan, P., Schain, A. & Grutzendler, J. Microglia constitute a barrier that prevents neurotoxic protofibrillar A $\beta$ 42 hotspots around plaques. *Nature Communications* **2015 6:1 6**, 1–14 (2015).
130. Hsia, A. Y. *et al.* Plaque-independent disruption of neural circuits in Alzheimer's disease mouse models. *Proc Natl Acad Sci U S A* **96**, (1999).
131. Sengupta, U., Nilson, A. N. & Kaye, R. The Role of Amyloid- $\beta$  Oligomers in Toxicity, Propagation, and Immunotherapy. *EBioMedicine* vol. 6 Preprint at <https://doi.org/10.1016/j.ebiom.2016.03.035> (2016).
132. El Hajj, H. *et al.* Ultrastructural evidence of microglial heterogeneity in Alzheimer's disease amyloid pathology. *J Neuroinflammation* **16**, (2019).
133. d'Errico, P. *et al.* Microglia contribute to the propagation of A $\beta$  into unaffected brain tissue. *Nat Neurosci* **25**, (2022).
134. Hopp, S. C. *et al.* The role of microglia in processing and spreading of bioactive tau seeds in Alzheimer's disease 11 Medical and Health Sciences 1109 Neurosciences. *J Neuroinflammation* **15**, (2018).
135. Asai, H. *et al.* Depletion of microglia and inhibition of exosome synthesis halt tau propagation. *Nat Neurosci* **18**, 1584–1593 (2015).

136. Bolós, M. *et al.* Direct Evidence of Internalization of Tau by Microglia in Vitro and in Vivo. *Journal of Alzheimer's Disease* **50**, 77–87 (2016).
137. De Calignon, A. *et al.* Propagation of Tau Pathology in a Model of Early Alzheimer's Disease. *Neuron* **73**, (2012).
138. Braak, H. & Braak, E. Neuropathological staging of Alzheimer-related changes. *Acta Neuropathologica* vol. 82 239–259 Preprint at <https://doi.org/10.1007/BF00308809> (1991).
139. De Felice, F. G. *et al.* Alzheimer's disease-type neuronal tau hyperphosphorylation induced by A $\beta$  oligomers. *Neurobiol Aging* **29**, 1334–1347 (2008).
140. Zhang, F. *et al.*  $\beta$ -amyloid redirects norepinephrine signaling to activate the pathogenic GSK3 $\beta$ /tau cascade. *Sci Transl Med* **12**, (2020).
141. Clavaguera, F., Hench, J., Goedert, M. & Tolnay, M. Invited review: Prion-like transmission and spreading of tau pathology. *Neuropathol Appl Neurobiol* **41**, 47–58 (2015).
142. Spires-Jones, T. L. & Hyman, B. T. The Intersection of Amyloid Beta and Tau at Synapses in Alzheimer's Disease. *Neuron* vol. 82 756–771 Preprint at <https://doi.org/10.1016/j.neuron.2014.05.004> (2014).
143. M, I. *et al.* Synthetic tau fibrils mediate transmission of neurofibrillary tangles in a transgenic mouse model of Alzheimer's-like tauopathy. *J Neurosci* **33**, 1024–1037 (2013).
144. Dagher, N. N. *et al.* Colony-stimulating factor 1 receptor inhibition prevents microglial plaque association and improves cognition in 3xTg-AD mice. *J Neuroinflammation* **12**, (2015).
145. Elmore, M. R. P. *et al.* Colony-stimulating factor 1 receptor signaling is necessary for microglia viability, unmasking a microglia progenitor cell in the adult brain. *Neuron* **82**, (2014).
146. Y, L. *et al.* Concentration-dependent effects of CSF1R inhibitors on oligodendrocyte progenitor cells ex vivo and in vivo. *Exp Neurol* **318**, 32–41 (2019).
147. Bennett, R. E. *et al.* Partial reduction of microglia does not affect tau pathology in aged mice 11 Medical and Health Sciences 1109 Neurosciences. *J Neuroinflammation* **15**, (2018).

148. Sosna, J. *et al.* Early long-term administration of the CSF1R inhibitor PLX3397 ablates microglia and reduces accumulation of intraneuronal amyloid, neuritic plaque deposition and pre-fibrillar oligomers in 5XFAD mouse model of Alzheimer's disease. *Mol Neurodegener* **13**, (2018).
149. Casali, B. T., MacPherson, K. P., Reed-Geaghan, E. G. & Landreth, G. E. Microglia depletion rapidly and reversibly alters amyloid pathology by modification of plaque compaction and morphologies. *Neurobiol Dis* **142**, (2020).
150. Spangenberg, E. E. *et al.* Eliminating microglia in Alzheimer's mice prevents neuronal loss without modulating amyloid- $\beta$  pathology. *Brain* **139**, 1265–1281 (2016).
151. Poon, A. *et al.* Modeling neurodegenerative diseases with patient-derived induced pluripotent cells: Possibilities and challenges. *N Biotechnol* **39**, 190–198 (2017).
152. Choi, S. H. *et al.* A three-dimensional human neural cell culture model of Alzheimer's disease. *Nature* **515**, 274–278 (2014).
153. Gonzalez, C. *et al.* Modeling amyloid beta and tau pathology in human cerebral organoids. *Mol Psychiatry* **23**, 2363–2374 (2018).
154. Muffat, J. *et al.* Efficient derivation of microglia-like cells from human pluripotent stem cells. *Nat Med* **22**, 1358–1367 (2016).
155. Abud, E. M. *et al.* iPSC-Derived Human Microglia-like Cells to Study Neurological Diseases. *Neuron* **94**, 278-293.e9 (2017).
156. Haenseler, W. *et al.* A Highly Efficient Human Pluripotent Stem Cell Microglia Model Displays a Neuronal-Co-culture-Specific Expression Profile and Inflammatory Response. *Stem Cell Reports* **8**, 1727–1742 (2017).
157. Douvaras, P. *et al.* Directed Differentiation of Human Pluripotent Stem Cells to Microglia. *Stem Cell Reports* **8**, 1516–1524 (2017).
158. Konttinen, H. *et al.* PSEN1 $\Delta$ E9, APP<sup>sw</sup>, and APOE4 Confer Disparate Phenotypes in Human iPSC-Derived Microglia. *Stem Cell Reports* **13**, 669–683 (2019).

159. Lin, Y. *et al.* APOE4 Causes Widespread Molecular and Cellular Alterations Associated with Alzheimer ' s Disease Article APOE4 Causes Widespread Molecular and Cellular Alterations Associated with Alzheimer ' s Disease Phenotypes in Human iPSC-Derived Brain Cell Types. *Neuron* **98**, 1141-1154.e7 (2018).
160. Garcia-Reitboeck, P. *et al.* Human Induced Pluripotent Stem Cell-Derived Microglia-Like Cells Harboring TREM2 Missense Mutations Show Specific Deficits in Phagocytosis. *Cell Rep* **24**, 2300–2311 (2018).
161. Piers, T. M. *et al.* A locked immunometabolic switch underlies TREM2 R47H loss of function in human iPSC-derived microglia. *The FASEB Journal* **34**, 2436–2450 (2020).
162. Ormel, P. R. *et al.* Microglia innately develop within cerebral organoids. doi:10.1038/s41467-018-06684-2.
163. Guttikonda, S. R. *et al.* Fully defined human pluripotent stem cell-derived microglia and tri-culture system model C3 production in Alzheimer's disease. *Nat Neurosci* **24**, 343–354 (2021).
164. Grubman, A. *et al.* A CX3CR1 Reporter hESC Line Facilitates Integrative Analysis of In-Vitro-Derived Microglia and Improved Microglia Identity upon Neuron-Glia Co-culture. *Stem Cell Reports* **14**, 1018–1032 (2020).
165. Choi, S. H., Kim, Y. H., Quinti, L., Tanzi, R. E. & Kim, D. Y. 3D culture models of Alzheimer ' s disease : a road map to a “ cure-in-a-dish ”. *Mol Neurodegener* 1–11 (2016) doi:10.1186/s13024-016-0139-7.
166. Raja, W. K. *et al.* Self-Organizing 3D Human Neural Tissue Derived from Induced Pluripotent Stem Cells Recapitulate Alzheimer ' s Disease Phenotypes. 1–18 (2016) doi:10.1371/journal.pone.0161969.
167. Lee, H. *et al.* Three Dimensional Human Neuro-Spheroid Model of Alzheimer ' s Disease Based on Differentiated Induced Pluripotent Stem Cells. 1–23 (2016) doi:10.1371/journal.pone.0163072.

168. Park, J. C. *et al.* A logical network-based drug-screening platform for Alzheimer's disease representing pathological features of human brain organoids. *Nat Commun* **12**, (2021).
169. Lancaster, M. A. & Knoblich, J. A. Generation of cerebral organoids from human pluripotent stem cells. *Nat Protoc* **9**, 2329–2340 (2014).
170. Giandomenico, S. L., Sutcliffe, M. & Lancaster, M. A. Generation and long-term culture of advanced cerebral organoids for studying later stages of neural development. *Nature Protocols* **2020 16:2 16**, 579–602 (2020).
171. Song, L. *et al.* Functionalization of Brain Region-specific Spheroids with Isogenic Microglia-like Cells. *Scientific Reports* **2019 9:1 9**, 1–18 (2019).
172. Furube, E., Kawai, S., Inagaki, H., Takagi, S. & Miyata, S. Brain Region-dependent Heterogeneity and Dose-dependent Difference in Transient Microglia Population Increase during Lipopolysaccharide-induced Inflammation. *Scientific Reports* **2018 8:1 8**, 1–15 (2018).
173. Prokop, S. *et al.* Impact of TREM2 risk variants on brain region-specific immune activation and plaque microenvironment in Alzheimer's disease patient brain samples. *Acta Neuropathol* **138**, (2019).
174. Casano, A. M. & Peri, F. Microglia: Multitasking specialists of the brain. *Developmental Cell* vol. 32 469–477 Preprint at <https://doi.org/10.1016/j.devcel.2015.01.018> (2015).
175. Xu, R. *et al.* Developing human pluripotent stem cell-based cerebral organoids with a controllable microglia ratio for modeling brain development and pathology. *Stem Cell Reports* **16**, 1923–1937 (2021).
176. Xu, R. *et al.* Human iPSC-derived mature microglia retain their identity and functionally integrate in the chimeric mouse brain. *Nature Communications* **2020 11:1 11**, 1–16 (2020).
177. Mansour, A. A. *et al.* An in vivo model of functional and vascularized human brain organoids. *Nature Biotechnology* **2018 36:5 36**, 432–441 (2018).

178. Bubnys, A. & Tsai, L. H. Harnessing cerebral organoids for Alzheimer's disease research. *Curr Opin Neurobiol* **72**, 120–130 (2022).
179. Zhao, J. *et al.* APOE4 exacerbates synapse loss and neurodegeneration in Alzheimer's disease patient iPSC-derived cerebral organoids. *Nature Communications* **2020 11:1** **11**, 1–14 (2020).
180. Ghatak, S. *et al.* Mechanisms of hyperexcitability in alzheimer's disease hiPSC-derived neurons and cerebral organoids vs. Isogenic control. *Elife* **8**, (2019).
181. Yin, J. & Vandongen, A. M. Enhanced Neuronal Activity and Asynchronous Calcium Transients Revealed in a 3D Organoid Model of Alzheimer's Disease. *ACS Biomater Sci Eng* **7**, 254–264 (2021).
182. Cairns, D. M. *et al.* A 3D human brain-like tissue model of herpes-induced Alzheimer's disease. *Sci. Adv* **6**, (2020).
183. Chen, X. *et al.* Modeling Sporadic Alzheimer's Disease in Human Brain Organoids under Serum Exposure. *Advanced Science* **8**, (2021).
184. 2022 Alzheimer's disease facts and figures. *Alzheimer's and Dementia* **18**, 700–789 (2022).
185. Cagnin, A. *et al.* In-vivo measurement of activated microglia in dementia. *Lancet* **358**, 461–467 (2001).
186. Heneka, M. T. *et al.* Neuroinflammation in Alzheimer's disease. *The Lancet Neurology* vol. 14 388–405 Preprint at [https://doi.org/10.1016/S1474-4422\(15\)70016-5](https://doi.org/10.1016/S1474-4422(15)70016-5) (2015).
187. Welikovitch, L. A. *et al.* Early intraneuronal amyloid triggers neuron-derived inflammatory signaling in APP transgenic rats and human brain. *Proc Natl Acad Sci U S A* **117**, 6844–6854 (2020).
188. Rao, Y. L. *et al.* Hippocampus and its involvement in Alzheimer's disease: a review. *3 Biotech* vol. 12 55 Preprint at <https://doi.org/10.1007/s13205-022-03123-4> (2022).

189. Gilhus, N. E. & Deuschl, G. Neuroinflammation — a common thread in neurological disorders. *Nature Reviews Neurology* vol. 15 429–430 Preprint at <https://doi.org/10.1038/s41582-019-0227-8> (2019).
190. van Horssen, J., van Schaik, P. & Witte, M. Inflammation and mitochondrial dysfunction: A vicious circle in neurodegenerative disorders? *Neuroscience Letters* vol. 710 Preprint at <https://doi.org/10.1016/j.neulet.2017.06.050> (2019).
191. Swerdlow, R. H. Mitochondria and Mitochondrial Cascades in Alzheimer's Disease. *Journal of Alzheimer's Disease* vol. 62 1403–1416 Preprint at <https://doi.org/10.3233/JAD-170585> (2018).
192. Chen, Z. & Zhong, C. Decoding Alzheimer's disease from perturbed cerebral glucose metabolism: Implications for diagnostic and therapeutic strategies. *Progress in Neurobiology* vol. 108 21–43 Preprint at <https://doi.org/10.1016/j.pneurobio.2013.06.004> (2013).
193. Zhang, J. M. & An, J. Cytokines, inflammation, and pain. *International Anesthesiology Clinics* vol. 45 27–37 Preprint at <https://doi.org/10.1097/AIA.0b013e318034194e> (2007).
194. Becher, B., Spath, S. & Goverman, J. Cytokine networks in neuroinflammation. *Nat Rev Immunol* **17**, 49–59 (2016).
195. Wold, S., Ruhe, A., Wold, H. & Dunn, III, W. J. The Collinearity Problem in Linear Regression. The Partial Least Squares (PLS) Approach to Generalized Inverses. *SIAM Journal on Scientific and Statistical Computing* **5**, 735–743 (1984).
196. Geladi, P. & Kowalski, B. R. Partial least-squares regression: a tutorial. *Anal Chim Acta* **185**, 1–17 (1986).
197. Thévenot, E. A., Roux, A., Xu, Y., Ezan, E. & Junot, C. Analysis of the Human Adult Urinary Metabolome Variations with Age, Body Mass Index, and Gender by Implementing a Comprehensive Workflow for Univariate and OPLS Statistical Analyses. *J Proteome Res* **14**, 3322–3335 (2015).

198. Trygg, J. & Wold, S. Orthogonal projections to latent structures (O-PLS). *J Chemom* **16**, 119–128 (2002).
199. Galindo-Prieto, B., Eriksson, L. & Trygg, J. Variable influence on projection (VIP) for orthogonal projections to latent structures (OPLS). *J Chemom* **28**, 623–632 (2014).
200. Donninelli, G. *et al.* Interleukin-9 regulates macrophage activation in the progressive multiple sclerosis brain. *J Neuroinflammation* **17**, 1–14 (2020).
201. Wang, K. *et al.* IP-10 promotes blood-brain barrier damage by inducing tumor necrosis factor alpha production in Japanese encephalitis. *Front Immunol* **9**, (2018).
202. Szklarczyk, D. *et al.* The STRING database in 2021: Customizable protein-protein networks, and functional characterization of user-uploaded gene/measurement sets. *Nucleic Acids Res* **49**, D605–D612 (2021).
203. Doncheva, N. T., Morris, J. H., Gorodkin, J. & Jensen, L. J. Cytoscape StringApp: Network Analysis and Visualization of Proteomics Data. *J Proteome Res* **18**, 623–632 (2019).
204. Morris, J. H., Kuchinsky, A., Ferrin, T. E. & Pico, A. R. EnhancedGraphics: A Cytoscape app for enhanced node graphics. *FI000Res* **3**, (2014).
205. Nicholas, D. *et al.* Advances in the quantification of mitochondrial function in primary human immune cells through extracellular flux analysis. *PLoS One* **12**, (2017).
206. Monteiro, S., Roque, S., Marques, F., Correia-Neves, M. & Cerqueira, J. J. Brain interference: Revisiting the role of IFN $\gamma$  in the central nervous system. *Progress in Neurobiology* vol. 156 149–163 Preprint at <https://doi.org/10.1016/j.pneurobio.2017.05.003> (2017).
207. Kim, I. J., Beck, H. N., Lein, P. J. & Higgins, D. Interferon  $\gamma$  Induces Retrograde Dendritic Retraction and Inhibits Synapse Formation. *Journal of Neuroscience* **22**, 4530–4539 (2002).
208. Monteiro, S. *et al.* Absence of IFN $\gamma$  promotes hippocampal plasticity and enhances cognitive performance. *Transl Psychiatry* **5**, e707 (2015).

209. Andres, D. A., Shi, G. X., Bruun, D., Barnhart, C. & Lein, P. J. Rit signaling contributes to interferon- $\gamma$ -induced dendritic retraction via p38 mitogen-activated protein kinase activation. *J Neurochem* **107**, 1436–1447 (2008).
210. Vlkolinský, R., Siggins, G. R., Campbell, I. L. & Krucker, T. Acute exposure to CXC chemokine ligand 10, but not its chronic astroglial production, alters synaptic plasticity in mouse hippocampal slices. *J Neuroimmunol* **150**, 37–47 (2004).
211. Sui, Y. *et al.* CXCL10-induced cell death in neurons: Role of calcium dysregulation. *European Journal of Neuroscience* **23**, 957–964 (2006).
212. Sui, Y. *et al.* Neuronal Apoptosis Is Mediated by CXCL10 Overexpression in Simian Human Immunodeficiency Virus Encephalitis. *American Journal of Pathology* **164**, 1557–1566 (2004).
213. Yshii, L. *et al.* Astrocyte-targeted gene delivery of interleukin 2 specifically increases brain-resident regulatory T cell numbers and protects against pathological neuroinflammation. *Nat Immunol* **23**, 878–891 (2022).
214. Salmeron, K. E. *et al.* Interleukin 1 alpha administration is neuroprotective and neuro-restorative following experimental ischemic stroke. *J Neuroinflammation* **16**, 1–14 (2019).
215. Rothwell, N. J. & Luheshi, G. N. Interleukin 1 in the brain: Biology, pathology and therapeutic target. *Trends in Neurosciences* vol. 23 618–625 Preprint at [https://doi.org/10.1016/S0166-2236\(00\)01661-1](https://doi.org/10.1016/S0166-2236(00)01661-1) (2000).
216. Chakrabarty, P. *et al.* IFN- $\gamma$  Promotes Complement Expression and Attenuates Amyloid Plaque Deposition in Amyloid  $\beta$  Precursor Protein Transgenic Mice. *The Journal of Immunology* **184**, 5333–5343 (2010).
217. Butovsky, O., Talpalar, A. E., Ben-Yaakov, K. & Schwartz, M. Activation of microglia by aggregated  $\beta$ -amyloid or lipopolysaccharide impairs MHC-II expression and renders them cytotoxic whereas IFN- $\gamma$  and IL-4 render them protective. *Molecular and Cellular Neuroscience* **29**, 381–393 (2005).

218. Wilhelm, C., Turner, J. E., Van Snick, J. & Stockinger, B. The many lives of IL-9: A question of survival? *Nature Immunology* vol. 13 637–641 Preprint at <https://doi.org/10.1038/ni.2303> (2012).
219. Murray, K. N., Parry-Jones, A. R. & Allan, S. M. Interleukin-1 and acute brain injury. *Front Cell Neurosci* **9**, 18 (2015).
220. Castro, F., Cardoso, A. P., Gonçalves, R. M., Serre, K. & Oliveira, M. J. Interferon-gamma at the crossroads of tumor immune surveillance or evasion. *Frontiers in Immunology* vol. 9 847 Preprint at <https://doi.org/10.3389/fimmu.2018.00847> (2018).
221. Monteiro, S., Roque, S., Marques, F., Correia-Neves, M. & Cerqueira, J. J. Brain interference: Revisiting the role of IFN $\gamma$  in the central nervous system. *Progress in Neurobiology* vol. 156 149–163 Preprint at <https://doi.org/10.1016/j.pneurobio.2017.05.003> (2017).
222. Chakrabarty, P. *et al.* IFN- $\gamma$  Promotes Complement Expression and Attenuates Amyloid Plaque Deposition in Amyloid  $\beta$  Precursor Protein Transgenic Mice. *The Journal of Immunology* **184**, 5333–5343 (2010).
223. Butovsky, O., Talpalar, A. E., Ben-Yaakov, K. & Schwartz, M. Activation of microglia by aggregated  $\beta$ -amyloid or lipopolysaccharide impairs MHC-II expression and renders them cytotoxic whereas IFN- $\gamma$  and IL-4 render them protective. *Molecular and Cellular Neuroscience* **29**, 381–393 (2005).
224. Andres, D. A., Shi, G. X., Bruun, D., Barnhart, C. & Lein, P. J. Rit signaling contributes to interferon- $\gamma$ -induced dendritic retraction via p38 mitogen-activated protein kinase activation. *J Neurochem* **107**, 1436–1447 (2008).
225. Kim, I. J., Beck, H. N., Lein, P. J. & Higgins, D. Interferon  $\gamma$  Induces Retrograde Dendritic Retraction and Inhibits Synapse Formation. *Journal of Neuroscience* **22**, 4530–4539 (2002).
226. Monteiro, S. *et al.* Absence of IFN $\gamma$  promotes hippocampal plasticity and enhances cognitive performance. *Transl Psychiatry* **5**, e707 (2015).

227. Mizuno, T. *et al.* Interferon- $\gamma$  directly induces neurotoxicity through a neuron specific, calcium-permeable complex of IFN- $\gamma$  receptor and AMPA GluR1 receptor. *The FASEB Journal* **22**, 1797–1806 (2008).
228. Cho, J., Nelson, T. E., Bajova, H. & Gruol, D. L. Chronic CXCL10 alters neuronal properties in rat hippocampal culture. *J Neuroimmunol* **207**, 92–100 (2009).
229. Nelson, T. E. & Gruol, D. L. The chemokine CXCL10 modulates excitatory activity and intracellular calcium signaling in cultured hippocampal neurons. *J Neuroimmunol* **156**, 74–87 (2004).
230. Xia, M. Q., Bacskai, B. J., Knowles, R. B., Qin, S. X. & Hyman, B. T. Expression of the chemokine receptor CXCR3 on neurons and the elevated expression of its ligand IP-10 in reactive astrocytes: In vitro ERK1/2 activation and role in Alzheimer's disease. *J Neuroimmunol* **108**, 227–235 (2000).
231. Vlkolinský, R., Siggins, G. R., Campbell, I. L. & Krucker, T. Acute exposure to CXC chemokine ligand 10, but not its chronic astroglial production, alters synaptic plasticity in mouse hippocampal slices. *J Neuroimmunol* **150**, 37–47 (2004).
232. Sui, Y. *et al.* Neuronal Apoptosis Is Mediated by CXCL10 Overexpression in Simian Human Immunodeficiency Virus Encephalitis. *American Journal of Pathology* **164**, 1557–1566 (2004).
233. Sui, Y. *et al.* CXCL10-induced cell death in neurons: Role of calcium dysregulation. *European Journal of Neuroscience* **23**, 957–964 (2006).
234. Wilhelm, C., Turner, J. E., Van Snick, J. & Stockinger, B. The many lives of IL-9: A question of survival? *Nature Immunology* vol. 13 637–641 Preprint at <https://doi.org/10.1038/ni.2303> (2012).
235. Fontaine, R. H. *et al.* IL-9/IL-9 receptor signaling selectively protects cortical neurons against developmental apoptosis. *Cell Death Differ* **15**, 1542–1552 (2008).
236. Bharath, L. P. *et al.* Metformin Enhances Autophagy and Normalizes Mitochondrial Function to Alleviate Aging-Associated Inflammation. *Cell Metab* **32**, 44-55.e6 (2020).

237. Franceschi, C. *et al.* Inflamm-aging. An evolutionary perspective on immunosenescence. in *Annals of the New York Academy of Sciences* vol. 908 244–254 (2000).
238. Xia, X., Jiang, Q., McDermott, J. & Han, J. D. J. Aging and Alzheimer's disease: Comparison and associations from molecular to system level. *Aging Cell* vol. 17 Preprint at <https://doi.org/10.1111/ace1.12802> (2018).
239. Perez-Nievas, B. G. *et al.* Astrocytic C-X-C motif chemokine ligand-1 mediates  $\beta$ -amyloid-induced synaptotoxicity. *J Neuroinflammation* **18**, 1–17 (2021).
240. Zhang, K. *et al.* CXCL1 Contributes to  $\beta$ -Amyloid-Induced Transendothelial Migration of Monocytes in Alzheimer's Disease. *PLoS One* **8**, e72744 (2013).
241. Xia, M. Q. & Hyman, B. T. GRO $\alpha$ /KC, a chemokine receptor CXCR2 ligand, can be a potent trigger for neuronal ERK1/2 and PI-3 kinase pathways and for tau hyperphosphorylation - A role in Alzheimer's disease? *J Neuroimmunol* **122**, 55–64 (2002).
242. Mohd Hasni, D. S. *et al.* Peripheral cytokines, C-X-C motif ligand10 and interleukin-13, are associated with Malaysian Alzheimer's disease. *Geriatr Gerontol Int* **17**, 839–846 (2017).
243. Friedberg, J. S. *et al.* Associations between brain inflammatory profiles and human neuropathology are altered based on apolipoprotein E  $\epsilon$ 4 genotype. *Sci Rep* **10**, 1–10 (2020).
244. Bélanger, M., Allaman, I. & Magistretti, P. J. Brain energy metabolism: Focus on Astrocyte-neuron metabolic cooperation. *Cell Metabolism* vol. 14 724–738 Preprint at <https://doi.org/10.1016/j.cmet.2011.08.016> (2011).
245. Magistretti, P. J. Neuron-glia metabolic coupling and plasticity. *Journal of Experimental Biology* vol. 209 2304–2311 Preprint at <https://doi.org/10.1242/jeb.02208> (2006).
246. De Cárcer, G., Manning, G. & Malumbres, M. From Plk1 to Plk5: Functional evolution of Polo-like kinases. *Cell Cycle* vol. 10 2255–2262 Preprint at <https://doi.org/10.4161/cc.10.14.16494> (2011).

247. Kim, A. H. *et al.* A Centrosomal Cdc20-APC Pathway Controls Dendrite Morphogenesis in Postmitotic Neurons. *Cell* **136**, 322–336 (2009).
248. Zheng, R. *et al.* KIF2C regulates synaptic plasticity and cognition in mice through dynamic microtubule depolymerization. *Elife* **11**, (2022).
249. Ranjan, A. *et al.* Targeting cdk9 for the treatment of glioblastoma. *Cancers* vol. 13 Preprint at <https://doi.org/10.3390/cancers13123039> (2021).
250. Padmanabhan, J., Brown, K. R., Padilla, A. & Shelanski, M. L. Functional role of RNA polymerase II and P70 S6 kinase in KCl withdrawal-induced cerebellar granule neuron apoptosis. *Journal of Biological Chemistry* **290**, 5267–5279 (2015).
251. Marquez-Lona, E. M., Tan, Z. & Schreiber, S. S. Nucleolar stress characterized by downregulation of nucleophosmin: A novel cause of neuronal degeneration. *Biochem Biophys Res Commun* **417**, 514–520 (2012).
252. Pfister, J. A. & D’Mello, S. R. Regulation of neuronal survival by nucleophosmin 1 (NPM1) is dependent on its expression level, subcellular localization, and oligomerization status. *Journal of Biological Chemistry* **291**, 20787–20797 (2016).
253. Xu, S. *et al.* The p53/miRNAs/Ccna2 pathway serves as a novel regulator of cellular senescence: Complement of the canonical p53/p21 pathway. *Aging Cell* **18**, (2019).
254. Alves, M. J. *et al.* CCNA2 Ablation in Aged Mice Results in Abnormal rRNA Granule Accumulation in Hippocampus. *American Journal of Pathology* **189**, 426–439 (2019).
255. Gygli, P. E. *et al.* Cyclin A2 promotes DNA repair in the brain during both development and aging. *Aging* **8**, 1540–1570 (2016).
256. Pellerin, L. & Magistretti, P. J. Glutamate uptake into astrocytes stimulates aerobic glycolysis: A mechanism coupling neuronal activity to glucose utilization. *Proc Natl Acad Sci U S A* **91**, 10625–10629 (1994).

257. Afridi, R., Kim, J. H., Rahman, M. H. & Suk, K. Metabolic Regulation of Glial Phenotypes: Implications in Neuron–Glia Interactions and Neurological Disorders. *Frontiers in Cellular Neuroscience* vol. 14 Preprint at <https://doi.org/10.3389/fncel.2020.00020> (2020).
258. Jansen, A. H. P., Reits, E. A. J. & Hol, E. M. The ubiquitin proteasome system in glia and its role in neurodegenerative diseases. *Frontiers in Molecular Neuroscience* vol. 7 Preprint at <https://doi.org/10.3389/fnmol.2014.00073> (2014).
259. Hong, L., Huang, H. C. & Jiang, Z. F. Relationship between amyloid-beta and the ubiquitin-proteasome system in alzheimer's disease. *Neurological Research* vol. 36 276–282 Preprint at <https://doi.org/10.1179/1743132813Y.0000000288> (2014).
260. Lopez Salon, M., Pasquini, L., Besio Moreno, M., Pasquini, J. M. & Soto, E. Relationship between  $\beta$ -amyloid degradation and the 26S proteasome in neural cells. *Exp Neurol* **180**, 131–143 (2003).
261. Wharton, W. *et al.* Interleukin 9 alterations linked to alzheimer disease in african americans. *Ann Neurol* **86**, 407–418 (2019).
262. Belkhef, M. *et al.* IFN- $\gamma$  and TNF- $\alpha$  are involved during Alzheimer disease progression and correlate with nitric oxide production: A study in Algerian patients. *Journal of Interferon and Cytokine Research* **34**, 839–847 (2014).
263. Asselineau, D. *et al.* Interleukin-10 Production in Response to Amyloid- $\beta$  Differs between Slow and Fast Decliners in Patients with Alzheimer's Disease. *Journal of Alzheimer's Disease* **46**, 837–842 (2015).
264. Galimberti, D. *et al.* Intrathecal chemokine synthesis in mild cognitive impairment and Alzheimer disease. *Arch Neurol* **63**, 538–543 (2006).
265. Fontaine, R. H. *et al.* IL-9/IL-9 receptor signaling selectively protects cortical neurons against developmental apoptosis. *Cell Death Differ* **15**, 1542–1552 (2008).

266. Xia, M. Q., Bacsikai, B. J., Knowles, R. B., Qin, S. X. & Hyman, B. T. Expression of the chemokine receptor CXCR3 on neurons and the elevated expression of its ligand IP-10 in reactive astrocytes: In vitro ERK1/2 activation and role in Alzheimer's disease. *J Neuroimmunol* **108**, 227–235 (2000).
267. Tran, P. B., Banisadr, G., Ren, D., Chenn, A. & Miller, R. J. Chemokine receptor expression by neural progenitor cells in neurogenic regions of mouse brain. *Journal of Comparative Neurology* **500**, 1007–1034 (2007).
268. Mizuno, T. *et al.* Interferon- $\gamma$  directly induces neurotoxicity through a neuron specific, calcium-permeable complex of IFN- $\gamma$  receptor and AMPA GluR1 receptor. *The FASEB Journal* **22**, 1797–1806 (2008).
269. Zhou, Y. *et al.* IL-9 Promotes Th17 Cell Migration into the Central Nervous System via CC Chemokine Ligand-20 Produced by Astrocytes. *The Journal of Immunology* **186**, 4415–4421 (2011).
270. Flynn, G., Maru, S., Loughlin, J., Romero, I. A. & Male, D. Regulation of chemokine receptor expression in human microglia and astrocytes. *J Neuroimmunol* **136**, 84–93 (2003).
271. Biber, K. *et al.* Functional expression of CXCR3 in cultured mouse and human astrocytes and microglia. *Neuroscience* **112**, 487–497 (2002).
272. Fleeman, R. M. *et al.* Predictive link between systemic metabolism and cytokine signatures in the brain of apolipoprotein E  $\epsilon$ 4 mice. *Neurobiol Aging* **123**, 154–169 (2023).
273. Wood, L. B. *et al.* Identification of neurotoxic cytokines by profiling Alzheimer's disease tissues and neuron culture viability screening. *Sci Rep* **5**, (2015).
274. Nicholas, D. A. *et al.* Fatty Acid Metabolites Combine with Reduced  $\beta$  Oxidation to Activate Th17 Inflammation in Human Type 2 Diabetes. *Cell Metab* **30**, 447-461.e5 (2019).

275. Makowski, L., Chaib, M. & Rathmell, J. C. Immunometabolism: From basic mechanisms to translation. *Immunological Reviews* vol. 295 5–14 Preprint at <https://doi.org/10.1111/imr.12858> (2020).
276. de Felice, F. G. & Lourenco, M. V. Brain metabolic stress and neuroinflammation at the basis of cognitive impairment in Alzheimer's disease. *Frontiers in Aging Neuroscience* vol. 7 94 Preprint at <https://doi.org/10.3389/fnagi.2015.00094> (2015).
277. Shoffner, J. M. Oxidative phosphorylation defects and Alzheimer's disease. *Neurogenetics* vol. 1 13–19 Preprint at <https://doi.org/10.1007/s100480050002> (1997).
278. Parker, W. D., Parks, J., Filley, C. M. & Kleinschmidt-Demasters, B. K. Electron transport chain defects in alzheimer's disease brain. *Neurology* **44**, 1090–1096 (1994).
279. Reichmann, H., Fhirke, S., Hebenstreit, G., Schrubar, H. & Riederer, P. Analyses of energy metabolism and mitochondrial genome in post-mortem brain from patients with Alzheimer's disease. *J Neurol* **240**, 377–380 (1993).
280. Schägger, H. & Ohm, T. G. Human Diseases with Defects in Oxidative Phosphorylation: 2. F1F0 ATP-Synthase Defects in Alzheimer Disease Revealed by Blue Native Polyacrylamide Gel Electrophoresis. *Eur J Biochem* **227**, 916–921 (1995).
281. Mukherjee, S. *et al.* Systems biology approach to late-onset Alzheimer's disease genome-wide association study identifies novel candidate genes validated using brain expression data and *Caenorhabditis elegans* experiments. *Alzheimer's and Dementia* **13**, 1133–1142 (2017).
282. Adav, S. S., Park, J. E. & Sze, S. K. Quantitative profiling brain proteomes revealed mitochondrial dysfunction in Alzheimer's disease. *Mol Brain* **12**, (2019).
283. Manczak, M., Park, B. S., Jung, Y. & Reddy, P. H. Differential Expression of Oxidative Phosphorylation Genes in Patients with Alzheimer's Disease: Implications for Early Mitochondrial Dysfunction and Oxidative Damage. *Neuromolecular Med* **5**, 147–162 (2004).

284. Węgrzyn, P. *et al.* A search for genes modulated by interleukin-6 alone or with interleukin-1 $\beta$  in HepG2 cells using differential display analysis. *Biochim Biophys Acta Mol Basis Dis* **1762**, 319–328 (2006).
285. Jura, J., Węgrzyn, P., Zarębski, A., Władyka, B. & Koj, A. Identification of changes in the transcriptome profile of human hepatoma HepG2 cells stimulated with interleukin-1 beta. *Biochim Biophys Acta Mol Basis Dis* **1689**, 120–133 (2004).
286. Zell, R., Geck, P., Werdan, K. & Boekstegers, P. TNF- $\alpha$  and IL-1 $\alpha$  inhibit both pyruvate dehydrogenase activity and mitochondrial function in cardiomyocytes: Evidence for primary impairment of mitochondrial function. *Mol Cell Biochem* **177**, 61–67 (1997).
287. Kitade, H. *et al.* Regulation of energy metabolism by interleukin-1 $\beta$ , but not by interleukin-6, is mediated by nitric oxide in primary cultured rat hepatocytes. *Biochim Biophys Acta Mol Cell Res* **1311**, 20–26 (1996).
288. Berthiaume, F., MacDonald, A. D., Kang, Y. H. & Yarmush, M. L. Control analysis of mitochondrial metabolism in intact hepatocytes: Effect of interleukin-1 $\beta$  and interleukin-6. *Metab Eng* **5**, 108–123 (2003).
289. Morris, R., Kershaw, N. J. & Babon, J. J. The molecular details of cytokine signaling via the JAK/STAT pathway. *Protein Science* vol. 27 Preprint at <https://doi.org/10.1002/pro.3519> (2018).
290. Rius-Pérez, S. *et al.* PGC-1  $\alpha$ , Inflammation, and Oxidative Stress: An Integrative View in Metabolism. *Oxid Med Cell Longev* **2020**, (2020).
291. Evans, M. J. & Scarpulla, R. C. NRF-1: A trans-activator of nuclear-encoded respiratory genes in animal cells. *Genes Dev* **4**, (1990).
292. Kelly, D. P. & Scarpulla, R. C. Transcriptional regulatory circuits controlling mitochondrial biogenesis and function. *Genes and Development* vol. 18 357–368 Preprint at <https://doi.org/10.1101/gad.1177604> (2004).

293. Bennett, J. P. & Keeney, P. M. Alzheimer's and Parkinson's brain tissues have reduced expression of genes for mtDNA OXPHOS Proteins, mitobiogenesis regulator PGC-1 $\alpha$  protein and mtRNA stabilizing protein LRPPRC (LRP130). *Mitochondrion* **53**, 154–157 (2020).
294. Qin, W. *et al.* PGC-1 $\alpha$  expression decreases in the Alzheimer disease brain as a function of dementia. *Arch Neurol* **66**, 352–361 (2009).
295. Penney, J., Ralvenius, W. T. & Tsai, L.-H. Modeling Alzheimer's disease with iPSC-derived brain cells. *Molecular Psychiatry* 2019 25:1 **25**, 148–167 (2019).
296. Barak, M. *et al.* Human iPSC-Derived Neural Models for Studying Alzheimer's Disease: from Neural Stem Cells to Cerebral Organoids. *Stem Cell Rev Rep* **18**, (2022).
297. Bubnys, A. & Tsai, L. H. Harnessing cerebral organoids for Alzheimer's disease research. *Curr Opin Neurobiol* **72**, 120–130 (2022).
298. Muffat, J. *et al.* Efficient derivation of microglia-like cells from human pluripotent stem cells. *Nat Med* **22**, 1358–1367 (2016).
299. Ormel, P. R. *et al.* Microglia innately develop within cerebral organoids. doi:10.1038/s41467-018-06684-2.
300. Xu, R. *et al.* Developing human pluripotent stem cell-based cerebral organoids with a controllable microglia ratio for modeling brain development and pathology. *Stem Cell Reports* **16**, 1923–1937 (2021).
301. Park, J. C. *et al.* A logical network-based drug-screening platform for Alzheimer's disease representing pathological features of human brain organoids. *Nat Commun* **12**, (2021).
302. Yin, J. & Vandongen, A. M. Enhanced Neuronal Activity and Asynchronous Calcium Transients Revealed in a 3D Organoid Model of Alzheimer's Disease. *ACS Biomater Sci Eng* **7**, 254–264 (2021).
303. Ghatak, S. *et al.* Mechanisms of hyperexcitability in alzheimer's disease hiPSC-derived neurons and cerebral organoids vs. Isogenic control. *Elife* **8**, (2019).

304. Zhao, J. *et al.* APOE4 exacerbates synapse loss and neurodegeneration in Alzheimer's disease patient iPSC-derived cerebral organoids. *Nature Communications* 2020 11:1 **11**, 1–14 (2020).
305. Gonzalez, C. *et al.* Modeling amyloid beta and tau pathology in human cerebral organoids. *Mol Psychiatry* **23**, 2363–2374 (2018).
306. Leng, F. & Edison, P. Neuroinflammation and microglial activation in Alzheimer disease: where do we go from here? *Nature Reviews Neurology* vol. 17 Preprint at <https://doi.org/10.1038/s41582-020-00435-y> (2021).
307. Socodato, R. *et al.* Microglia dysfunction caused by the loss of Rhoa disrupts neuronal physiology and leads to neurodegeneration. *Cell Reports* 218107 Preprint at <https://doi.org/10.1101/218107> (2020).
308. Hansen, D. V., Hanson, J. E. & Sheng, M. Microglia in Alzheimer's disease. *Journal of Cell Biology* vol. 217 459–472 Preprint at <https://doi.org/10.1083/jcb.201709069> (2018).
309. McFarland, K. N. & Chakrabarty, P. Microglia in Alzheimer's Disease: a Key Player in the Transition Between Homeostasis and Pathogenesis. *Neurotherapeutics* vol. 19 Preprint at <https://doi.org/10.1007/s13311-021-01179-3> (2022).
310. H, M. *et al.* Single-cell transcriptomic analysis of Alzheimer's disease. *Nature* **570**, 332–337 (2019).
311. Masuda, T. *et al.* Spatial and temporal heterogeneity of mouse and human microglia at single-cell resolution. *Nature* **566**, (2019).
312. Grabert, K. *et al.* Microglial brain region-dependent diversity and selective regional sensitivities to aging. *Nature Neuroscience* 2016 19:3 **19**, 504–516 (2016).
313. Penney, J., Ralvenius, W. T. & Tsai, L. H. Modeling Alzheimer's disease with iPSC-derived brain cells. *Molecular Psychiatry* vol. 25 148–167 Preprint at <https://doi.org/10.1038/s41380-019-0468-3> (2020).

314. Poon, A. *et al.* Modeling neurodegenerative diseases with patient-derived induced pluripotent cells: Possibilities and challenges. *N Biotechnol* **39**, 190–198 (2017).
315. Choi, S. H. *et al.* A three-dimensional human neural cell culture model of Alzheimer's disease. *Nature* **515**, 274–278 (2014).
316. C, G. *et al.* Modeling amyloid beta and tau pathology in human cerebral organoids. *Mol Psychiatry* **23**, 2363–2374 (2018).
317. Lancaster, M. A. & Knoblich, J. A. Generation of cerebral organoids from human pluripotent stem cells. *Nat Protoc* **9**, 2329–2340 (2014).
318. Fung, S. *et al.* Early-Onset Familial Alzheimer Disease Variant PSEN2 N141I Heterozygosity is Associated with Altered Microglia Phenotype. *Journal of Alzheimer's Disease* **77**, (2020).
319. Nam, H. *et al.* Presenilin 2 N141I mutation induces hyperactive immune response through the epigenetic repression of REV-ERB $\alpha$ . *Nat Commun* **13**, (2022).
320. Sullivan, M. A. *et al.* iPSC-Derived PSEN2 (N141I) Astrocytes and Microglia Exhibit a Primed Inflammatory Phenotype. *bioRxiv* 2022.12.05.518134 (2022) doi:10.1101/2022.12.05.518134.
321. Pantazis, C. B. *et al.* A reference human induced pluripotent stem cell line for large-scale collaborative studies. *Cell Stem Cell* **29**, (2022).
322. Giandomenico, S. L., Sutcliffe, M. & Lancaster, M. A. Generation and long-term culture of advanced cerebral organoids for studying later stages of neural development. *Nature Protocols* **2020 16:2 16**, 579–602 (2020).
323. Kuhn, M. K. *et al.* Cellular and Molecular Bioengineering SI: 2023 CMBE YOUNG INNOVATORS Amyloid- $\beta$  Pathology-Specific Cytokine Secretion Suppresses Neuronal Mitochondrial Metabolism. **1**, 3.
324. Heppner, F. L., Ransohoff, R. M. & Becher, B. Immune attack: The role of inflammation in Alzheimer disease. *Nature Reviews Neuroscience* vol. 16 358–372 Preprint at <https://doi.org/10.1038/nrn3880> (2015).

325. Ruan, C. & Elyaman, W. A New Understanding of TMEM119 as a Marker of Microglia. *Frontiers in Cellular Neuroscience* vol. 16 Preprint at <https://doi.org/10.3389/fncel.2022.902372> (2022).
326. Abud, E. M. *et al.* iPSC-Derived Human Microglia-like Cells to Study Neurological Diseases. *Neuron* **94**, 278-293.e9 (2017).
327. Song, L. *et al.* Functionalization of Brain Region-specific Spheroids with Isogenic Microglia-like Cells. *Scientific Reports* 2019 9:1 **9**, 1–18 (2019).
328. Pandya, H. *et al.* Differentiation of human and murine induced pluripotent stem cells to microglia-like cells. *Nat Neurosci* **20**, 753–759 (2017).
329. M, X. *et al.* Pathological Changes in Alzheimer’s Disease Analyzed Using Induced Pluripotent Stem Cell-Derived Human Microglia-Like Cells. *J Alzheimers Dis* **67**, 357–368 (2019).
330. Sosna, J. *et al.* Early long-term administration of the CSF1R inhibitor PLX3397 ablates microglia and reduces accumulation of intraneuronal amyloid, neuritic plaque deposition and pre-fibrillar oligomers in 5XFAD mouse model of Alzheimer’s disease. *Mol Neurodegener* **13**, (2018).
331. Noble, W., Hanger, D. P., Miller, C. C. J. & Lovestone, S. The importance of tau phosphorylation for neurodegenerative diseases. *Frontiers in Neurology* vol. 4 JUL Preprint at <https://doi.org/10.3389/fneur.2013.00083> (2013).
332. Hirota, Y. *et al.* Distinct brain pathologies associated with Alzheimer’s disease biomarker-related phospho-tau 181 and phospho-tau 217 in App knock-in mouse models of amyloid- $\beta$  amyloidosis. *Brain Commun* **4**, (2022).
333. Dolan, P. J. & Johnson, G. V. W. The role of tau kinases in Alzheimer’s disease. *Current Opinion in Drug Discovery and Development* vol. 13 Preprint at (2010).
334. Guo, S., Wang, H. & Yin, Y. Microglia Polarization From M1 to M2 in Neurodegenerative Diseases. *Frontiers in Aging Neuroscience* vol. 14 Preprint at <https://doi.org/10.3389/fnagi.2022.815347> (2022).

335. Li, J.-W., Zong, Y., Cao, X.-P., Tan, L. & Tan, L. Microglial priming in Alzheimer's disease. *Ann Transl Med* **6**, (2018).
336. Schwab, C., Hosokawa, M. & McGeer, P. L. Transgenic mice overexpressing amyloid beta protein are an incomplete model of Alzheimer disease. *Exp Neurol* **188**, 52–64 (2004).
337. Kiyota, T. *et al.* CNS expression of anti-inflammatory cytokine interleukin-4 attenuates Alzheimer's disease-like pathogenesis in APP+PS1 bigenic mice. *The FASEB Journal* **24**, (2010).
338. Galatro, T. F. *et al.* Transcriptomic analysis of purified human cortical microglia reveals age-associated changes. *Nat Neurosci* **20**, 1162–1171 (2017).
339. Greenwood, E. K. & Brown, D. R. Senescent microglia: The key to the ageing brain? *International Journal of Molecular Sciences* vol. 22 Preprint at <https://doi.org/10.3390/ijms22094402> (2021).
340. Tsai, K. J., Tsai, Y. C. & Shen, C. K. J. G-CSF rescues the memory impairment of animal models of Alzheimer's disease. *Journal of Experimental Medicine* **204**, (2007).
341. Sanchez-Ramos, J. *et al.* Granulocyte colony stimulating factor decreases brain amyloid burden and reverses cognitive impairment in Alzheimer's mice. *Neuroscience* **163**, (2009).
342. Hemonnot, A. L., Hua, J., Ulmann, L. & Hirbec, H. Microglia in Alzheimer disease: Well-known targets and new opportunities. *Frontiers in Cellular and Infection Microbiology* vol. 9 233 Preprint at <https://doi.org/10.3389/fnagi.2019.00233> (2019).
343. Arnoux, I. & Audinat, E. Fractalkine signaling and microglia functions in the developing brain. *Neural Plasticity* vol. 2015 Preprint at <https://doi.org/10.1155/2015/689404> (2015).
344. Chapman, G. A. *et al.* Fractalkine cleavage from neuronal membranes represents an acute event in the inflammatory response to excitotoxic brain damage. *J Neurosci* **20**, (2000).
345. Shang, Y. *et al.* CXCL1 promotes the proliferation of neural stem cells by stimulating the generation of reactive oxygen species in APP/PS1 mice. *Biochem Biophys Res Commun* **515**, (2019).

346. Zhang, X. F. *et al.* CXCL1 triggers caspase-3 dependent tau cleavage in long-term neuronal cultures and in the hippocampus of aged mice: Implications in Alzheimer's disease. *Journal of Alzheimer's Disease* **48**, (2015).
347. Noda, M. *et al.* FGF-2 released from degenerating neurons exerts microglial-induced neuroprotection via FGFR3-ERK signaling pathway. *J Neuroinflammation* **11**, (2014).
348. Wood, L. B. *et al.* Identification of neurotoxic cytokines by profiling Alzheimer's disease tissues and neuron culture viability screening. *Sci Rep* **5**, (2015).
349. Knobloch, M. & Mansuy, I. M. Dendritic spine loss and synaptic alterations in Alzheimer's disease. *Molecular Neurobiology* vol. 37 Preprint at <https://doi.org/10.1007/s12035-008-8018-z> (2008).
350. Scheff, S. W., Price, D. A., Schmitt, F. A. & Mufson, E. J. Hippocampal synaptic loss in early Alzheimer's disease and mild cognitive impairment. *Neurobiol Aging* **27**, (2006).
351. Subramanian, J., Savage, J. C. & Tremblay, M. È. Synaptic Loss in Alzheimer's Disease: Mechanistic Insights Provided by Two-Photon in vivo Imaging of Transgenic Mouse Models. *Frontiers in Cellular Neuroscience* vol. 14 Preprint at <https://doi.org/10.3389/fncel.2020.592607> (2020).
352. Jacobsen, J. S. *et al.* Early-onset behavioral and synaptic deficits in a mouse model of Alzheimer's disease. *Proc Natl Acad Sci U S A* **103**, (2006).
353. Hsia, A. Y. *et al.* Plaque-independent disruption of neural circuits in Alzheimer's disease mouse models. *Proc Natl Acad Sci U S A* **96**, (1999).
354. Vojtechova, I., Machacek, T., Kristofikova, Z., Stuchlik, A. & Petrasek, T. Infectious origin of Alzheimer's disease: Amyloid beta as a component of brain antimicrobial immunity. *PLoS Pathogens* vol. 18 Preprint at <https://doi.org/10.1371/journal.ppat.1010929> (2022).
355. Y, L. *et al.* Concentration-dependent effects of CSF1R inhibitors on oligodendrocyte progenitor cells ex vivo and in vivo. *Exp Neurol* **318**, 32–41 (2019).

356. Shi, Y. *et al.* Microglia drive APOE-dependent neurodegeneration in a tauopathy mouse model.

*Journal of Experimental Medicine* **216**, (2019).

## APPENDIX

**Supplementary Table 2-1: Significantly differentially expressed genes of cytokine-treated neurons compared to vehicle-treated neurons**

Gene	log2FC	P-value
A2m	-0.91	0.043
Acaa2	-0.8	0.003
Acadl	0.2	0.001
Acox1	-0.44	0.004
Ak1	-0.19	0.028
Ak3	-0.37	0.040
Aldh2	-0.43	0.015
Apoe	-0.52	0.030
Ar	0.64	0.043
Atf4	0.3	0.021
Atf7ip	0.37	0.004
Atp5d	-0.26	0.010
Birc3	1.01	0.021
Brip1	1.03	0.016
Bub1	-0.47	0.007
Cacng2	-0.43	0.026
Cat	-0.23	0.014
Cel19	1.56	0.001
Cel2	3.44	0.001
Ccl4	-2.75	0.011
Ccl5	5.18	0.001
Ccna2	-0.68	0.009
Cd14	-2.32	0.002
Cd274	4.94	0.001
Cd36	4.36	0.000
Cdc20	-0.39	0.048
Cdk9	0.09	0.006
Cenpa	-0.56	0.015
Ctsl	-0.62	0.035
Cxcl9	5.13	0.004
Cyp1b1	-0.17	0.033
Dck	0.3	0.040
Dguok	0.34	0.020
Epc1	0.33	0.006
Fcfl	0.35	0.031
Fcgr4	2.71	0.015
Fcrls	-3.06	0.013
Fdx1	0.39	0.012
Fgf1	-1.05	0.002
Fnip1	0.18	0.031
Foxm1	-0.6	0.005
Fpr1	1.68	0.011
Gad1	-0.52	0.044
Gclc	-0.26	0.024
Glxr	0.71	0.011
Glul	-0.86	0.016
Gmpr	-0.69	0.008
Gng12	0.24	0.021
Gpx1	0.89	0.006
Gusb	-0.81	0.042
H2-Aa	9.43	0.001
H2-D1	2.74	0.019

Gene	log2FC	P-value
H2-DMa	4.32	0.000
H2-Eb1	7.61	0.001
H2-M3	2.13	0.024
H2-T23	4.42	0.014
Hacd2	-0.5	0.017
Hadh	-0.18	0.004
Hdc	1.75	0.002
Hk2	0.72	0.011
Hk3	2.25	0.014
Hsd11b1	-1.16	0.032
Hspe1	0.26	0.010
Idh3g	-0.23	0.048
Idnk	1.3	0.000
Irf1	5.15	0.000
Itch	0.18	0.030
Itga1	-0.64	0.021
Jak2	0.97	0.000
Keap1	0.51	0.002
Kif2c	-0.46	0.028
Klrl1	5.22	0.002
Kmt2a	0.41	0.050
Kyat1	-0.39	0.014
Lamc1	0.55	0.035
Lamtor2	0.13	0.001
Lck	1.24	0.020
Ldha	-0.41	0.036
Ldha	-0.37	0.000
Map11c3b	-0.37	0.002
Map2k2	0.21	0.010
Mki67	-0.86	0.005
Msrb2	-0.6	0.009
Mtfl	-0.16	0.032
Myb	-0.65	0.007
Myd88	1.2	0.007
Nadk	0.35	0.023
Ncoa2	0.33	0.021
Ndufa1	-0.15	0.005
Ndufa4	-0.37	0.032
Nfs1	-0.13	0.042
Nme2	0.21	0.020
Npm1	0.2	0.010
Nqo1	-1.05	0.008
Nras	0.31	0.027
Pclaf	-0.5	0.029
Pgk1	-0.38	0.017
Pik3cb	-0.26	0.040
Pik3r3	0.54	0.008
Plk1	-0.87	0.005
Pole	-0.58	0.037
Prdx5	0.38	0.001
Prim2	-0.22	0.016
Prkag1	-0.22	0.009

Gene	log2FC	P-value
Psat1	-0.34	0.030
Psma3	0.49	0.001
Psma7	0.72	0.003
Psmb10	3.27	0.004
Psmb3	0.34	0.001
Psmc1	0.14	0.014
Psmc13	0.15	0.046
Psme2	2.2	0.002
Psph	-0.16	0.015
Ptger4	-0.54	0.022
Ptges	1.22	0.001
Rgn	0.81	0.046
Rplp0	0.28	0.027
Rps6kb1	0.3	0.014
Rrm1	-0.26	0.006
Rrm2	-0.69	0.006
Scd1	-0.44	0.001
Sdhb	0.49	0.006
Sdhc	-0.05	0.012
Sec13	0.12	0.035
Slc16a1	0.19	0.027
Slc16a2	-0.46	0.001
Slc16a3	-0.5	0.001
Slc1a5	-1.14	0.002
Slc25a1	0.1	0.010
Slc7a5	-0.36	0.007
Smad4	0.17	0.022
Sox2	0.29	0.011
Sqstm1	0.31	0.001
Stat1	4.05	0.006
Stat3	0.76	0.001
Stat5a	0.46	0.020
Tbk1	0.37	0.020
Tkt	-0.2	0.022
Tlr1	0.76	0.023
Tnf	1.76	0.023
Tpr	0.22	0.025
Traf1	1.02	0.001
Traf6	0.17	0.023
Trf	-0.82	0.045
Trp53	0.4	0.016
Trp63	-0.83	0.017
Txn1	0.81	0.002
Ubb	0.38	0.003
Upp1	0.79	0.008
Uqcr11	-0.32	0.045
Usp39	0.35	0.011
Usp8	0.39	0.006
Washc4	0.4	0.020
Wrn	1.06	0.001
Zfp65	0.31	0.005
Zfp869	0.44	0.006

**Supplementary Table 2-2: Significantly differentially expressed genes of cytokine-treated astrocytes compared to vehicle-treated astrocytes**

Gene	log2FC	P-value
Ada	0.73	0.049
Akt3	0.48	0.002
Cab39	-0.22	0.025
Ccl2	2.88	0.037
Ccl5	3.55	0.016
Cd180	0.7	0.020
Cd274	5.36	0.000
Ctss	1.63	0.003
Cxcl9	3.21	0.017
Cybb	1.2	0.002
Dnajc14	-0.15	0.043
Fcgr4	2.02	0.001
Fgfl	-0.85	0.003
Gns	0.23	0.040
Gsk3b	-0.29	0.020
H2-Aa	8.65	0.001
H2-D1	5.79	0.000
H2-DMa	5.32	0.000
H2-Eb1	6.87	0.001
H2-M3	4.61	0.000
H2-T23	4	0.003
Hexa	0.27	0.003
Hk3	2.07	0.008
Hspa2	0.52	0.011
Hspa4	-0.39	0.001
Idh2	-0.49	0.036
Idnk	1.31	0.007
Irf1	4.39	0.001
Itgb2	0.91	0.041
Ldha	-0.46	0.025
Ly86	0.54	0.045
Map2k1	0.1	0.028
Mlst8	-0.39	0.026
Mycn	-0.5	0.021
Ndufa3	0.17	0.028
Pik3r1	-0.4	0.035
Prkcg	-0.63	0.032
Psma3	0.46	0.008
Psma7	0.55	0.009

Gene	log2FC	P-value
Psmb10	3.73	0.000
Psmb3	0.35	0.006
Psmc1	0.17	0.013
Psmc13	0.16	0.042
Psmc2	2.17	0.000
Ptk2	-0.25	0.015
Pycr1	0.59	0.021
Rbks	-0.34	0.025
Sdha	-0.25	0.050
Slc25a1	0.23	0.014
Sqstm1	0.29	0.044
Stat1	5.3	0.000
Tyms	-0.44	0.033
Washc4	0.3	0.000
Wrm	0.53	0.048
Xdh	1.67	0.006
Zfp457	-0.67	0.001

## CURRICULUM VITA

**Madison Kathryn Kuhn**

### EDUCATION

**Ph.D. Biomedical Engineering**, Pennsylvania State University 2023  
**B.S. Biomedical Engineering**, Brown University 2018

### HONORS AND ACTIVITIES

Penn State College of Medicine Fall Travel Award Recipient 2023  
T32 Cross Disciplinary Neural Engineering Training Program 2021-2023  
Faculty Opinions Associate Faculty Member 2021  
Penn State College of Medicine Summer Undergraduate Research Internship Program Mentor 2020-2023  
Trustee Prize for highest cumulative grade point average, Lancaster Country Day School, Lancaster, PA 2013

### TALKS

1. Biomedical Engineering Society Annual Meeting, Seattle, Washington (October 2023)
2. NINDS T32 Workshop, Philadelphia, Pennsylvania (June 2023)
3. Biomedical Engineering Society Annual Meeting, Virtual (October 2020)

### FUNDING

T32 Cross Disciplinary Neural Engineering Training Program Fellow 2022-2023

### SELECTED PEER-REVIEWED PUBLICATIONS

1. M. K. Kuhn, R. M. Fleeman, L. M. Beidler, A. M. Snyder, D. C. Chan, E. A. Proctor. "Amyloid- $\beta$  pathology-specific cytokine secretion suppresses neuronal mitochondrial metabolism," Cellular and Molecular Bioengineering, in press. doi:10.1107/s12195-023-00782-y (2023).
2. E. Zukowski, M. Sannella, J. Donato Rockhold, G. Pugh, J. Yu, M. K. Kuhn, N. Hah, L. Ouyang, T.-W. Wang, M. Drummond, E. A. Proctor, H. Hasturk, B. S. Nikolajczyk, L. P. Bharath. "STAT3 Modulates CD4<sup>+</sup> Mitochondrial Dynamics and Function in Aging," accepted, Aging Cell (2023).
3. R. M. Fleeman, M. K. Kuhn, D. C. Chan, E. A. Proctor. "Apolipoprotein E4 modulates astrocyte neuronal support functions in the presence of amyloid- $\beta$ ," Journal of Neurochemistry 165:536-549 (2023).
4. R. M. Fleeman, A. M. Snyder, M. K. Kuhn, D. C. Chan, G. C. Smith, N. A. Crowley, A. C. Arnold, E. A. Proctor. "Predictive link between systemic metabolism and cytokine signatures in the brain of apolipoprotein E  $\epsilon$ 4 mice," Neurobiology of Aging 123:154-169 (2023).
6. E. A. Proctor, S. M. Dineen, S. C. Van Nostrand, M. K. Kuhn, C. D. Barrett, D. K. Brubaker, M. B. Yaffe, D. A. Lauffenburger, L. R. Leon. "Coagulopathy signature precedes and predicts severity of end-organ heat stroke pathology in a mouse model," Journal of Thrombosis and Haemostasis 18:1900-1910 (2020).